





**UNIVERSITY PABLO DE OLAVIDE**

Experimental Sciences Faculty

Department of Physiology, Anatomy and Cell Biology

Neuroscience Division

Samuel Hernández González

**MOTOR AND PREFRONTAL CORTICES MECHANISMS  
UNDERLYING ASSOCIATIVE LEARNING IN RODENTS**

Doctoral thesis directed by:

José María Delgado García

Seville, 2017

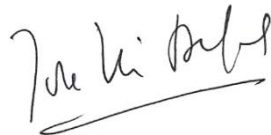


D. José María Delgado García, Catedrático de Fisiología en el Departamento de Fisiología, Anatomía y Biología Celular de la Facultad de Ciencias Experimentales de la Universidad Pablo de Olavide:

CERTIFICA:

Que el presente trabajo titulado “**Motor and Prefrontal cortices mechanisms underlying associative learning in rodents**” ha sido realizado bajo su dirección y supervisión por D. Samuel Hernández González, Licenciado en Ciencias Biológicas por la Universidad de Valencia y consideran que reúne las condiciones y el rigor científico para ser presentado y defendido como Tesis Doctoral.

Sevilla, 24 de Mayo de 2017

A handwritten signature in black ink, appearing to read 'José María Delgado García', with a horizontal line underneath.

Fdo: José María Delgado García







## RESUMEN

Entender qué fenómenos funcionales ocurren en las poblaciones neuronales durante el aprendizaje y la memoria de nuevas experiencias resulta crucial para comprender el funcionamiento del cerebro. Esta Tesis Doctoral aporta nuevos datos sobre dichos fenómenos empleando para ello la corteza cerebral como sustrato experimental. En concreto, se han utilizado las cortezas motora y prefrontal como representativas del procesamiento de información motora y cognitiva. Con el fin de estudiar los cambios corticales funcionales, se utilizaron paradigmas básicos de aprendizaje como el condicionamiento clásico de traza entre dos estímulos, el cual requiere la participación de la corteza motora, el cerebelo y el hipocampo, y el condicionamiento operante (o instrumental) entre un estímulo y una respuesta, en el cual está involucrado activamente la corteza prefrontal. Para este último, se utilizó una versión sencilla de la jaula de Skinner, equipada con una palanca o con una pantalla táctil como elemento sobre el que los animales debían responder, así como una versión compleja en la que se llevó a cabo un condicionamiento neuronal por medio de interfaces cerebro-computadora. Tales paradigmas de aprendizaje fueron llevados a cabo por dos especies de roedores en función de la dificultad de los mismos: ratones, de los cuales se generó un grupo que carecía de la subunidad NR1 del receptor de NMDA y ratas tratadas farmacológicamente con lidocaína.

Un estudio comparativo inicial entre ratones control y ratones “knockout” para el gen de la subunidad NR1 del receptor de NMDA en la corteza motora primaria (M1) reveló la importancia del receptor y dicha región en el proceso de aprendizaje asociativo entre dos estímulos durante un condicionamiento clásico y también la asociación tipo estímulo-respuesta de un condicionamiento instrumental complejo.

En una segunda fase experimental, se examinó la participación del área prelímbica (PrL) de la corteza prefrontal (PFC) en ratas durante un aprendizaje instrumental simple advirtiéndose una activa participación del área PrL en las primeras fases del aprendizaje así como cierta relación funcional entre las vías talamocortical y mesocortical tanto en la actividad sináptica inducida por el proceso de aprendizaje como en la potenciación a largo plazo inducida en ambas sinapsis.



En un siguiente experimento, utilizando actividad neural del área PrL, se demostró la posibilidad de controlar una interfaz cerebro-computadora por medio de las características contenidas en los potenciales de campo locales de dicha región relacionada con el procesamiento de información de comportamientos dirigidos a un objetivo. Las características de la actividad neural fueron suficientemente estables para controlar a largo plazo dicha interfaz. Además, se produjo el condicionamiento de poblaciones neuronales inferido a partir del aumento de la tasa de generación de dicha actividad y la disminución de la potencia de determinadas frecuencias oscilatorias que mejoraron el control de dicha interfaz.

## List of Abbreviations

Abbreviation	Description
<b>AC</b>	Anterior cingulate cortex
<b>Acb</b>	Nucleus accumbens
<b>AI</b>	Agranular insular cortex
<b>ANOVA</b>	Analysis of variance
<b>BCI</b>	Brain computer interface
<b>BLA</b>	Basolateral nucleus of amygdala
<b>BMA</b>	Basomedial nucleus of amygdala
<b>CA1</b>	Cornu ammonis, area 1
<b>Cg1</b>	Cingulate cortex, area 1
<b>Cl</b>	Clastrum
<b>CR</b>	Conditioned response
<b>CS</b>	Conditioned stimulus
<b>CS-US</b>	Conditioned-unconditioned paired stimuli
<b>DR</b>	Dorsal raphe nucleus
<b>EBC</b>	Eyeblink conditioning
<b>EEG</b>	Electroencephalographic
<b>EMG</b>	Electromyography
<b>fPSP</b>	Field postsynaptic potential
<b>HFS</b>	High frequency stimulation
<b>IL</b>	Infralimbic cortex
<b>LFP</b>	Local field potential
<b>LTD</b>	Long-term depression
<b>LTP</b>	Long-term potentiation
<b>LO</b>	Lateral orbital cortex
<b>MO</b>	Medial orbital cortex
<b>M1</b>	Primary motor cortex
<b>M2</b>	Secondary motor cortex
<b>PFC</b>	Prefrontal cortex
<b>PV</b>	Paraventricular nucleus of thalamus
<b>PrCm</b>	Precentral cortex
<b>PrL</b>	Prelimbic cortex
<b>Re</b>	Nucleus reuniens of thalamus
<b>S1</b>	Primary somatosensorial cortex
<b>MDTh</b>	Mediodorsal nucleus of thalamus
<b>US</b>	Unconditioned stimulus
<b>VLO</b>	Ventralateral orbital cortex
<b>VO</b>	Ventrorbital cortex
<b>VTA</b>	Ventral tegmental area



# INDEX



---

<b>1. INTRODUCTION .....</b>	<b>3</b>
<b>1.1. LEARNING AND MEMORY .....</b>	<b>3</b>
1.1.1. Classical conditioning: eyeblink conditioning paradigm .....	4
1.1.2. Operant conditioning learning.....	6
<b>1.2 SYNAPTIC TRANSMISSION .....</b>	<b>7</b>
1.2.1 Short-term synaptic plasticity: depression and facilitation .....	8
1.2.2 Long-term synaptic plasticity: long-term depression and potentiation.....	10
<b>1.3. CEREBRAL CORTEX .....</b>	<b>11</b>
1.3.1. Primary motor cortex .....	11
1.3.2. Prefrontal cortex. ....	12
1.3.3. The prefrontal cortex in rats: Prelimbic cortex. ....	13
<b>1.4. BRAIN COMPUTER INTERFACES.....</b>	<b>16</b>
1.4.2. Neuronal operant conditioning in BCIs.....	18
<b>2. OBJECTIVES AND HYPOTHESYS.....</b>	<b>23</b>
<b>3. MATERIAL AND METHODS.....</b>	<b>27</b>
<b>3.1. ANIMALS.....</b>	<b>27</b>
<b>3.2. MOTOR CORTEX-SPECIFIC GRIN1 GENE KNOCKOUT .....</b>	<b>27</b>
<b>3.3. SURGERY FOR CHRONIC-RECORDING EXPERIMENTS.....</b>	<b>29</b>
<b>3.4. STIMULATION AND RECORDING PROCEDURES .....</b>	<b>31</b>
3.4.1. Electrical disruption of the PrL cortex.....	31
<b>3.5. CLASSICAL CONDITIONING: EYEBLINK CONDITIONING .....</b>	<b>32</b>
<b>3.6. INTRACRANIAL DRUG INFUSION .....</b>	<b>33</b>
<b>3.7. INSTRUMENTAL CONDITIONING. ....</b>	<b>34</b>
3.7.1. Light/dark instrumental conditioning protocol.....	34
3.7.2. Brain activity closed-loop training. ....	35

---

<b>3.8. PERFUSION AND HISTOLOGY .....</b>	<b>38</b>
<b>3.9. ACQUISITION AND DATA ANALYSIS .....</b>	<b>39</b>
<b>4. RESULTS .....</b>	<b>43</b>
<b>4.1. EFFECT OF FUNCTIONAL LOSS OF THE NMDA RECEPTOR IN M1 .....</b>	<b>43</b>
4.1.1. In vivo LTP measurements .....	43
4.1.2. Synaptic plasticity and the conditioned response .....	45
4.1.3. Instrumental learning .....	47
<b>4.2. CONTRIBUTION OF PrL CORTEX IN EARLY PHASES OF INSTRUMENTAL LEARNING .....</b>	<b>49</b>
4.2.1. Validation of a Skinner box with touch-screen. ....	49
4.2.2. Input/output curves and paired pulse stimulation test.....	50
4.2.3. PrL inactivation with lidocaine and HFS on thalamocortical and mesocortical pathways .....	51
4.2.4. Lidocaine inactivation of PrL cortex during an instrumental learning .....	53
<b>4.3. NEURAL ACTIVITY CHANGES DURING AN ASSOCIATIVE LEARNING WITH BCIs.....</b>	<b>57</b>
4.3.1. Validation of a wireless recording system. ....	57
4.3.2. Properties of the transition pattern .....	58
4.3.3. Learning curves for instrumental conditioning tasks. ....	61
4.3.4. Changes in duration and power ratio index $[\theta/(\beta+\gamma)]$ after the use of the pattern in a BCI .....	63
4.3.5. Changes in spectral power property of the pattern used as a trigger in a BCI.....	64
4.3.6. Coherence between different regions and the PrL cortex.....	65
4.3.7. Unitary activity in the PrL cortex in presence of the oscillatory transition pattern .....	67
4.3.8. Vibrissal muscles activity and pattern correlation.....	68
4.3.9. The electrical stimulation of the PrL cortex prevented the proper performance of the operant conditioning task .....	69
<b>5. DISCUSSION .....</b>	<b>73</b>

---

<b>5.1. EXPERIMENT 1: EFFECT OF FUNCTIONAL LOSS OF THE NMDA RECEPTOR IN M1 .....</b>	<b>73</b>
<b>5.2. EXPERIMENT 2: CONTRIBUTION OF PrL CORTEX IN EARLY PHASES OF INSTRUMENTAL LEARNING .....</b>	<b>75</b>
5.2.1. Electrophysiological characteristics of the thalamocortical and mesocortical synapses .....	75
5.2.2. Involvement of PrL cortex in early stages of associative learning.....	77
<b>5.3. EXPERIMENT 3: NEURAL ACTIVITY CHANGES DURING AN ASSOCIATIVE LEARNING WITH BCIS .....</b>	<b>78</b>
5.3.1. The PrL cortex related to goal-directed behaviors .....	78
5.3.2. Neural correlates between behavior and the oscillatory activity pattern .....	78
5.3.4. Distribution of the oscillatory activity pattern in the brain .....	80
<b>6. CONCLUSIONS .....</b>	<b>85</b>
<b>7. REFERENCES.....</b>	<b>89</b>
<b>8. ANNEXES .....</b>	<b>105</b>





# 1. INTRODUCTION



## 1. INTRODUCTION

### 1.1. LEARNING AND MEMORY

We refer to learning as the process whereby the experience modifies our nervous system for the purpose of developing new behaviors adapted to a continuously modified environment. Subsequently to the process of learning, information can be encoded, stored and retrieved through memory processes. Memory can be classified along two dimensions: (1) the time course of storage and (2) the nature of the information stored. Considering both factors we can find:

- **Short term memory:** its duration is from seconds to minutes and can be selectively transferred to long-term memory. For example, to hold in mind a new number of telephone. An important type of short term memory is the **working memory** which maintains current, albeit transient, representations of goal-relevant knowledge.
- **Long term memory:** it can last from minutes to years. Long term memory can be classified as **explicit** or **implicit** (Squire and Zola-Morgan, 1991).
  - The **explicit memory** (or declarative memory) is the *deliberate or conscious* retrieval of previous experiences as well as conscious recall of factual knowledge about people, places and things. Explicit memory is highly flexible; multiple pieces of information can be associated under different circumstances.
  - The **implicit memory** (also referred to as non-declarative or procedural memory) is typically manifested in an automatic manner, with unconscious processing on the part of the subject during the performance of a task. Some examples of this type of memory are **priming, skill learning, habit memory, and conditioning**. Implicit memory is tightly connected to the original conditions under which the learning occurred. Nonhuman animal studies have distinguished two types of implicit memory: **non-associative** and **associative**, that are generated by their respective kinds of learning (non-associative and associative):
    - **Non-associative learning:** an animal learns about the properties of a single stimulus.
    - **Associative learning:** the animal learns about the relationship between two stimuli (**classical conditioning**) or between a stimulus and its consequences (**operant conditioning**).

In addition to these forms of learning defined above, it has been described other compatible classification of learning based on the nature of the involved information. In this classification, there are known four basic learning forms: **perceptual**, to learn to recognize stimuli that have been perceived before; **motor**, learning to carry out a new behavioral response; **stimulus-response**, the ability to learn to perform a particular behavior when a certain stimulus is present and **relational learning**, relationships among individual stimuli. On the basis of these four learning forms, it has been described other types of complex learning as spatial, episodic and observational whereby it is necessary the use of more than one sensory modality.

#### *1.1.1. Classical conditioning: eyeblink conditioning paradigm*

Classical conditioning was first described by the physiologist Ivan Pavlov in 1903 by means of his well-known research in associative learning in animals (dogs). In these experiments, Pavlov and his assistant observed the process of association between two stimuli when they were presented next in time. Pavlov assistant used to feed the dogs that were employed in their experiment. During these experimental sessions, Pavlov noticed an increase of salivation in the animal when his assistant acceded to the room despite not carrying any food. This observation led Pavlov to utilize a bell every time they fed the dogs and finally he checked for any increase in salivation exclusively related to the use of the bell. The increase of salivation was confirmed. Pavlov called **unconditioned stimulus (US)**; the food in this experiment) to the stimulus that produced a strong and consistent response (**unconditioned response (UR)**; salivation) and considered of innate nature (generated without learning). The stimulus that initially did not produce any response (the sound of the bell) or a weak response different to the UR but subsequently was paired with the food (US) was called **conditioned stimulus (CS)**. And finally, the response elicited by the CS was named **conditioned response (CR)**; salivation produced by the CS). After repeated (and paired) ringing and food presentation, the process of association between the two stimuli could be interpreted as a “transference of meaning” from the second stimulus (food) to the first in time (bell ringing). Thus, classical conditioning depends on the order of appearance of the stimulus, wherein the CS (ringing) must precede, in order to predict, the US (food) appearance. Finally, it is necessary a good degree of correlation between the two stimuli. Generally, the conditioned stimulus must be followed by an unconditioned stimulus after a short period of time, wherein 200 to

500 ms seems an optimal time interval (Thomson, 1989; Caro-Martín et al., 2015) for creating a good association between stimuli. The prolonged absence of unconditioned (food) stimulus may eliminate the association between the CS-US pair (ringing-food), which is termed **extinction** of the associative learning.

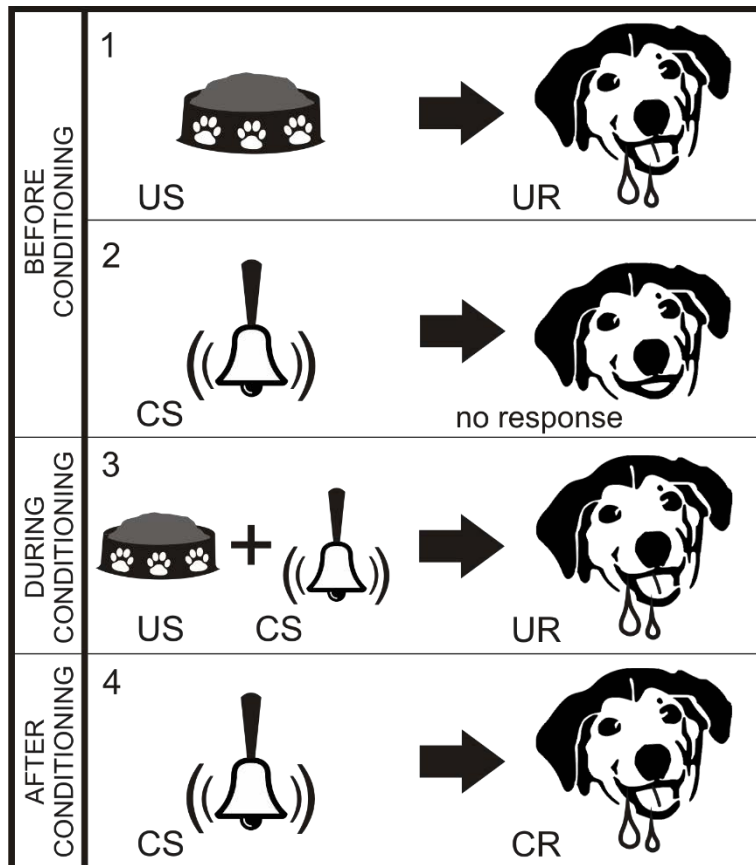


**Figure 1.1. Classical conditioning paradigm based in Pavlov's experiment.** (1) Before conditioning the food (unconditioned stimulus (US)) produces a reflex response in the dog (salivation; unconditioned response (UR)) and (2) the ringing of the bell (conditioned stimulus (CS)) does not generate any response. (3) During conditioning the bell (CS) and the food (US) are presented in this order and the first CS-US pairings induce salivation (UR) that depends on the food presence (4) but after several CS-US pairings the ringing of the bell (CS) elicits salivation too (conditioned response (CR)).

### *Eyeblink conditioning paradigm*

Eyeblink conditioning (EBC) is a form of classical conditioning that is well suited to dissect the cellular and molecular mechanisms of learning and memory consolidation. In EBC, for CS-US pairing, the conditioned stimulus (CS; a tone), generally is presented 500 milliseconds in advance of the unconditioned stimulus (US; a mild shock to the eyelid). In untrained animals, the US alone elicits an eyeblink as the unconditioned response (UR). However, after repetitive CS–US pairings, the CS alone is sufficient to elicit an eyeblink, or the conditioned response (CR). In the delayed EBC, the CS is presented before the US and the two stimuli end together. In the trace EBC, however, there is a stimulus-free period (trace interval) between the CS and the US. While both of these conditioning paradigms require the cerebellum (McCormick & Thompson, 1984), the trace EBC also requires the participation of the hippocampus (Gruart et al., 2006; Moyer et al., 1996) and different cortical areas (Troncoso et al., 2007; Weible et al., 2000).

### *1.1.2. Operant conditioning learning*

This second major paradigm of associative learning was discovered by Edgar Thorndike and initially named as **instrumental learning** (which it is considered synonym for **operant learning**). This type of associative learning was systematically studied by Burrhus Frederic Skinner and others, who baptized it with the term **operant conditioning** (also called **trial-and-error learning**). Thorndike employed a methodology based in the use of a box equipped with a pedal or lever (“puzzle box”) that a cat must to press in order to escape from it. He observed that after a short period of time the cat achieved the ability of pressing the lever and leave the box. The cat was returned several times to the box and Thorndike detected a decrease in the time that it took it to escape again. Every time he introduced the animal into the box it pressed the lever and escaped faster and faster. Skinner followed up on Thorndike’s work, studying primarily pigeons and rats in a wide variety of conditions for which invented the operant conditioning chamber or Skinner’s Box. Operant conditioning implicates the association between a motor response (to press the lever) and a stimulus detection (to see the lever) meanwhile classical conditioning implied the association between two stimuli. At the beginning of this learning process the animal through a random activity perform the action (for example, press lever) that produces an outcome (open door, release food). But subsequently and according to the **law of effect** enunciated by Thorndike, if the outcome is favorable (**reinforcement**; to obtain

food) then the animal will try to repeat the action (press lever). In contrast, if the outcome is an aversive consequence (**punishment**; electric shock) the animal will tend to avoid it (not pressing the lever). Operant conditioning can be considered as the formation of a predictive relationship between an action (press a lever) and an outcome (obtain food). So, it is important the outcome happens after the response in a short time, in a similar way to the interval of time between the two stimuli in classical conditioning

A great contribution to the study of the operant conditioning by Skinner and his colleague C. B. Ferster (1957) was the definition of different types of schedules or ways of providing reinforcement depending on the type of response:

- **Continuous reinforcement (CRF)**: in which every response emitted is reinforced.
- **Intermittent reinforcement (IR)**: only some responses emitted are reinforced.
  - **Ratio Schedules**: based on the ratio of responses to reinforcements.
    - **Fixed Ratio (FR)**: the reinforcement is provided upon completion of a fixed number of responses. For example, in FR 10, after ten responses a reinforcement is offered.
    - **Variable Ratio (VR)**: reinforcements are provided according to a random number of responses (a real case, slot machines).
  - **Interval Schedules**: based on the time interval between reinforcements.
    - **Fixed Interval (FI)**: reinforcements are delivered after a fixed time period from the response. For example, FI 5 (where the number is considered in seconds) means that the reinforcement will take 5 seconds to be delivered from the moment the response was made by the animal.
    - **Variable Interval (VI)**: the behavior is reinforced after changing and random time periods.

## 1.2 SYNAPTIC TRANSMISSION

Some cerebral functions as learning and memory are thought to emerge from the elementary properties of chemical synapses (Sutton and Shuman, 2006). These synapses are complex because they participate in several mechanisms that contribute to experience-dependent modifications of brain functions. It is generally assumed that one of the most important properties of the brain is the so-called **neuronal plasticity**, which can be defined as the ability of neuronal cells to react



with adaptive changes (at functional, molecular and structural levels) to relevant intrinsic or extrinsic inputs. Into this molecular and structural changes the synapse plays an essential role in several mechanistic forms of **short** and **long-term synaptic plasticity**.

### *1.2.1 Short-term synaptic plasticity: depression and facilitation*

This type of plasticity refers to synaptic properties and mechanisms having an effect on synaptic efficacy which occur on the tens of milliseconds to several minutes time scale. Many important functional roles have been described for short-term synaptic plasticity, such as sensory adaptation (Chung et al., 2002), directional selectivity (Carver et al., 2008) and some forms of short-lasting memory (Citri and Malenka, 2008). It depends on factors following the action potential invasion of the presynaptic terminal but preceding secretion of neurotransmitter. Particularly, the **residual calcium** remaining into the presynaptic bouton. When an action potential reaches the presynaptic bouton, it opens voltage-gated calcium channels that increase calcium levels into this space. Calcium binds vesicles that contain the neurotransmitter and trigger the fusion with the membrane of the presynaptic bouton. The calcium that did not bind these vesicles (residual calcium) will increase calcium reserves with the arrival of a new action potential which will increase the probability of vesicle release. This is known as the **residual calcium hypothesis** that is responsible of some forms of short-term plasticity (Katz and Miledi, 1967). Another important factor in short-term plasticity is the distribution of the vesicles containing neurotransmitter into functional pools: a reserve pool, a recycling pool and a **readily releasable pool (RRP)** (**Fig. 1.2b**). The availability of a large pool of readily releasable vesicles (or RRP) increase the probability of neurotransmitter discharge (Schneggenburger et al. 2002). Postsynaptic mechanisms such as **saturation** and **desensitization** of postsynaptic receptors can also mediate short-term plasticity (Foster et al., 2002; Chen et al., 2002). They are factors to take into account when estimating correctly the effect of presynaptic mechanisms.

Classical methods such as the **paired pulse test** have been used to check for the presence of short-term plasticity. Paired-pulse is based on the comparison of the synaptic efficacy, represented by the amplitude of the postsynaptic potential ( $A_1$  and  $A_2$  in **Fig. 1.2a**), between two electric pulses separated by an interval of time. Two basic forms of short-term synaptic plasticity have been described in laboratory: **facilitation** and **depression**. Facilitation is an enhancement in synaptic

efficacy, as amplitude increase of the second pulse in paired-pulse test, due to the effect of residual calcium after a first pulse that contributes to the neurotransmitter release of an additional second pulse (red trace in **Fig. 1.2a**). On the other hand, depression most probably results from a transient depletion of the readily releasable pool of vesicles docked at the presynaptic terminal (depletion model of depression), from inactivation of voltage-dependent sodium or calcium channels or inactivation of release sites after fusion of a vesicle at an active zone.

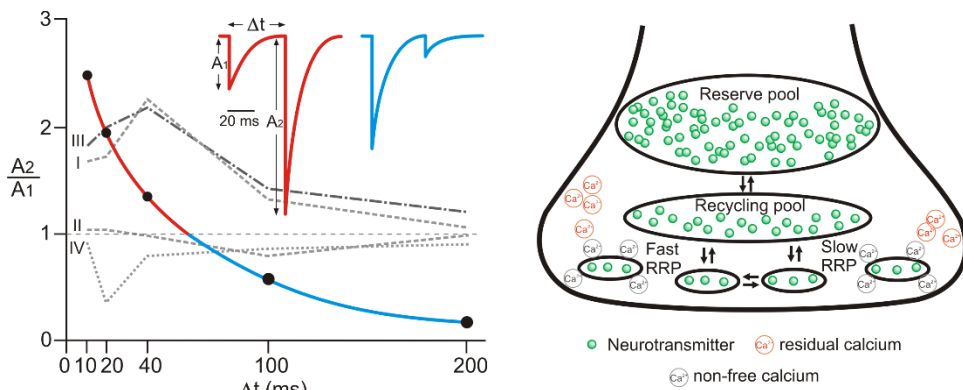


**Figure 1.2. Simulated paired-pulse test curve and diagram of different pools of vesicles in a presynaptic bouton. a.** As shown in the red trace inset, activation with pairs of electrical stimuli separated by time  $\Delta t$  evokes synaptic currents with the second response ( $A_2$ ) larger than the first ( $A_1$ ) that represents a paired-pulse facilitation. The blue trace inset represents an example of depression in which the second response is smaller than the first. As shown in the plot of  $A_2/A_1$  versus  $\Delta t$ , the magnitude of facilitation (plotted in red) decreases as the interpulse interval is increased. (Modified from Zucker and Regehr, 2002) In gray dashed line different real examples of (I) CA3-CA1, (II) S1-M1, (III) MDTh-PrL and (IV) VTA-PrL synapses paired-pulse tests. (Madroñal et al, 2009; Hassan et al, 2012). **b.** Schematic representation of the different functional pools containing neurotransmitter into a postsynaptic terminal.

Most synapses possess multiple forms of presynaptic plasticity but the relative prominence of one of them is controlled by the initial release probability of neurotransmitter. Thereby, synapses with a high initial probability of release tend to depress, whereas those with a low initial probability of release usually facilitate (Madroñal et al., 2009).

Indeed, most synapses can show either facilitation or depression depending on the initial probability of release (see Regehr, 2012 for review).

### 1.2.2 Long-term synaptic plasticity: long-term depression and potentiation

This type of plasticity has an effect lasting minute to hours or even weeks and it is considered to be involved in long-lasting storage of the memory. There are different forms of long-term synaptic plasticity depending on the duration and whether it has a potentiating or depressing effect on the synapse: early and late **long-term potentiation (LTP)** and **long-term depression (LTD)** (see Lisman, 2017 for review). Many experiments have shown that long-term synaptic plasticity may follow or not the Hebb principle, in which is postulated that the strengthening of the synapses is due to the correlation between presynaptic activity and postsynaptic firing (Hebb, 1949). So, this is a first criteria of classifying, in which **Hebbian LTP** needs correlation between depolarization of pre- and postsynaptic cells but **non-Hebbian LTP** does not requires it.

#### *Long-term potentiation*

The first work in LTP began at 1970's with the studies conducted by Timothy Bliss and Terje Lømo in the hippocampus of rabbits. They and their colleagues discovered that a few seconds of **high frequency electrical stimulation (HFS)** enhanced synaptic transmission for days or even weeks (Bliss and Gardner-Medwin, 1971; Bliss and Lømo, 1973): this persistent synaptic increase following HFS has been called the **LTP**.

LTP exhibits some properties, such as **input specificity**: when LTP is induced by the stimulation of one synapse, it is not propagated to other, inactive synapses that contact the same neuron; **associativity**: if one pathway is activated with a weak stimulation that will not by itself trigger LTP and at the same time a neighboring pathway is strongly activated onto the same postsynaptic cell, both synaptic pathways undergo LTP; and **cooperativity**: if two or more pathways that converge on the same postsynaptic neuron are weakly activated it can induce LTP.

In the molecular mechanisms involved in the generation of LTP participates two major types of ionotropic glutamate receptor:  $\alpha$ -amino-3-hydroxy-5-methyl-4-isoxazole- propionic acid (AMPA) and N-methyl-D-aspartate (NMDA) receptors.

After high frequency stimulation, a first phase called **early LTP**, which lasts about 30 minutes, can be induced. This phase is characterized by the increase in activity and number of the AMPA receptors (AMPA) within the postsynaptic membrane but without protein synthesis. The next phase is the **late LTP** that requires gene transcription and protein synthesis whose purpose is to enlarge the

synapse both pre- and postsynaptically with the incorporation of new AMPAR (Meyer et al., 2014) as well as generating new synaptic contact (Bosch et al., 2014).

During basal synaptic activity, AMPAR are responsible for postsynaptic responses allowing  $\text{Na}^+$  and  $\text{K}^+$  ions to be transferred through the postsynaptic membrane. When presynaptic cells are active and there is strong postsynaptic depolarization, the ion channel (voltage-dependent) attached to NMDA receptor is unlocked and permits the  $\text{Na}^+$  and  $\text{Ca}^{2+}$  transfer into the postsynaptic dendritic spine.  $\text{Ca}^{2+}$  binds to calmodulin, which activates many enzymes, most notably calcium/calmodulin-dependent protein kinase II (CaMKII) (Lisman et al., 2012) and protein kinase C (PKC).

### *Long-term depression*

The general concept of LTD is defined by a persistent decrease in strength of synaptic transmission following the application of a low frequency stimulation protocol. Nevertheless, there is a multitude of different forms of LTD elicited by various protocols of stimulation. Two fundamental forms are **homosynaptic LTD** that occurs when there is a persisting low-frequency input to a synapse and **heterosynaptic LTD** that occurs to pathways or inputs that were not stimulated when other path or input was strongly stimulated (Staubli and Ji, 1996; Chistiakova et al., 2014). In addition, LTD has been described in several brain regions such as hippocampus, cerebellum, striatum of the basal ganglia (dorsal striatum and nucleus accumbens), visual cortex and perirhinal cortex showing different mechanisms that supports the function of these regions (Massey and Bashir, 2007; Jurado-Parras et al., 2012). LTP and LTD are not unitary phenomena and their mechanisms vary depending on the synapses and circuits in which they operate (Malenka and Bear, 2004)

## **1.3. CEREBRAL CORTEX**

### *1.3.1. Primary motor cortex*

The primary motor cortex (M1) is pivotal for sensorimotor integration and precise control of voluntary movements (Sanes and Donoghue, 2000). Sensory signals in the cortex are represented as activity maps, with active neurons organized as functional clusters or modules (Hubel and Wiesel, 1959; Mountcastle, 1957) which are continuously re-shaped by experience and learning (Margolis et al., 2012; Huber et al., 2012). However, there are also dynamic interactions between widely

distributed functional modules in different cortical and subcortical regions. These interactions, by way of ‘putative’ overlapping functional neuronal assemblies (Hebb, 1949), are thought to form the necessary neural substrates for multimodal processing, and learning and memory consolidation (Buzsaki, 2010). At a connectivity level, cortical excitatory neurons, with their elaborate basal and apical dendrites, receive synaptic input from distantly located excitatory neurons, and local excitatory as well as inhibitory neurons. Reciprocal corticocortical connections (Aronoff et al 2010) and functional interactions between M1 and the primary somatosensory cortex (S1) (Huber et al 2012; Ferezou et al., 2007)—possibly involving mechanisms of synaptic integration in different dendritic compartments (Xu et al., 2012) with recruitment of NMDAR channels (Larkum et al., 2009)—are thus hypothesized to have an important role, for example, in organizing an animal’s motor activity plan to changes in the sensory experiences.

It has been hypothesized that cue–response associations occur in the M1 cortex, which enables an animal to make a correct sensory-guided behavioral response. During motor learning, sensory signals are transmitted to the M1 cortex, inducing morphological and functional plasticity on multiple timescales (Karni et al., 1998; Kleim et al., 2004)

Dynamic changes in neuronal activity (Komikaya et al., 2010) and activation of immediate-early genes (Kleim et al 2004) in the M1 cortex call into action cellular and molecular processes to strengthen preexisting sensorimotor synaptic connections and to form new synapses (Xu et al., 2009; Kleim et al., 2002). The M1 cortex has the capacity for LTP (Hess and Donoghue, 1994) a candidate cellular model for learning and memory consolidation, and, importantly, LTP can be induced in this region by learning (Rioul-Pedotti et al., 1998).

### *1.3.2. Prefrontal cortex.*

The prefrontal cortex (PFC) is localized in the rostral margin of the frontal lobe and constitutes the highest level of cortical hierarchy devoted to the representation and execution of selected actions. In general, the PFC is connected with the brainstem, the thalamus, the basal ganglia, and the limbic system. Much of that connectivity with subcortical structures is reciprocal. Especially well organized topologically are the connections between the PFC and the thalamus. Prefrontal connections with the mediodorsal thalamic nucleus have been used as a criterion for identifying the PFC in a wide variety of species (Fuster, 1997). This wide interconnection among the PFC and other cortical and subcortical regions can be

observed between the different PFC subregions too. The PFC can be subdivided in three major regions: orbital, medial, and lateral. The orbital and medial regions are involved in emotional behavior. The lateral region, which is maximally developed in the human, provides the cognitive support to the temporal organization of behavior, speech, and reasoning.

### 1.3.3. The prefrontal cortex in rats: Prelimbic cortex.

The presence of a PFC in the rat has been largely discussed in several studies concluding the existence of anatomic and functional correlates among some areas of the PFC of rodents and primates (Uylings, 2003; Tsuitsui, 2016). Some of the early criteria taken into account to define the existence of a PFC in the rat has been the reciprocal connections with thalamic nuclei in which the mediodorsal nucleus (MD) show the higher number of projecting neurons and density of terminal. The cytoarchitecture of the prefrontal cortex of rats presents an absence of granular layer IV that is exhibited in the primate species but we have to take into account that the criteria of cytoarchitecture among distant species seems to be untenable.

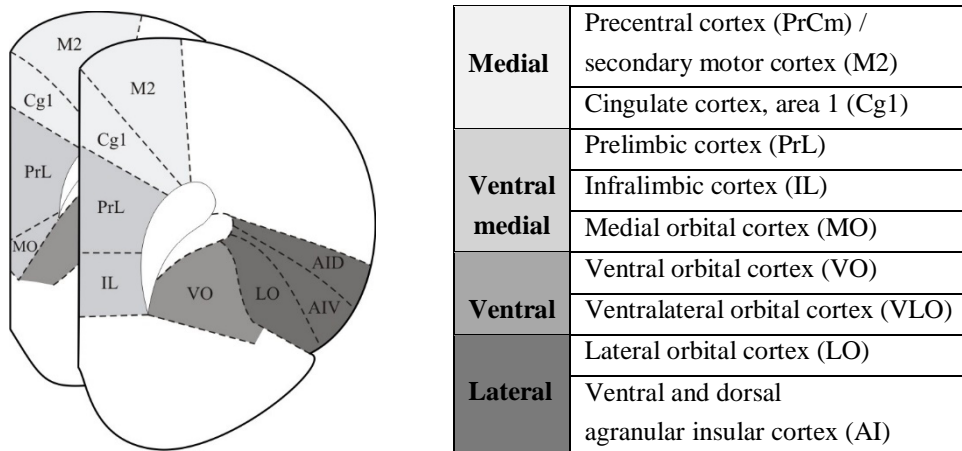


**Figure 1.3. Illustrative diagrams of the rat prefrontal cortex.** (adapted from Paxinos & Watson, 1998). Unilateral coronal sections, 3.7 mm (bottom) and 3.2 mm (front) forward of bregma. The different shadings represent the four major subdivisions of the prefrontal cortex (medial, ventral-medial, ventral and lateral).

From an architectonic and connectivity point of view, subregions of the PFC in the rat can be organized according to the schema proposed by Groenewegen and Uylings (2000) and Uylings and van Eden (1990) (**Fig. 1.3**). These subregions

include the **medial, ventral-medial, ventral** and **lateral** PFC (Kesner & Churchwell, 2011). The ventral-medial prefrontal cortex is divided into two areas, the **prelimbic** (PrL) and the infralimbic cortex (IL).

### *Connectivity*

The main sources of afferent projections to PL and IL are from the orbitomedial prefrontal, agranular insular, perirhinal and entorhinal cortices, the hippocampus, the claustrum, the medial basal forebrain, the basal nuclei of amygdala, the midline thalamus and monoaminergic nuclei of the brainstem (Hoover et al., 2007) (**Fig 1.4**). The most significant difference in distribution of connections to PrL (and IL) from those to dorsal areas of the medial subregion is a progressively decrease of projections from sensory, somatosensory and motor cortical regions to ventral-medial PFC cortex. Nevertheless, PL receives dense projections from other areas of the PFC [MO, VO, anterior cingulate cortex (AC), IL, AI] as well as other formations: subiculum and area 1 of cornu ammonis of hippocampus (CA1), midline and mediodorsal thalamic (MD) nuclei, ventral tegmental area (VTA), the claustrum (Cl), nucleus accumbens (Acb) (via thalamic nuclei) and nucleus reuniens of thalamus (Re).

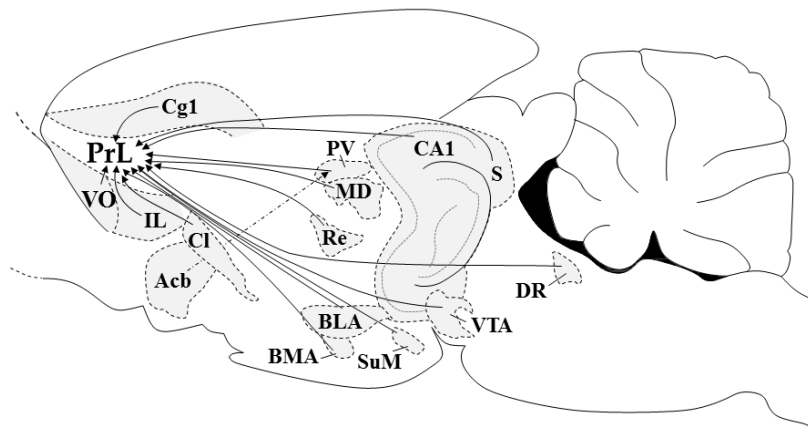


**Figure 1.4. Summary of main sources of afferent projections to PL:** from the cortex (VO, Cg1, IL), basal forebrain (Cl), amygdala (basolateral nucleus (BLA), basomedial nucleus (BMA)), thalamus (MD, paraventricular nucleus (PV), Re), hypothalamus (supramammillary nucleus (SuM)), midbrain (VTA), and pons/medulla (dorsal raphe nucleus (DR)). The arrows with continuous line represent direct projections among regions (grey color areas). Arrow with dashed line represents indirect projection to PrL. Sagittal diagram 0.9 mm lateral (modified from Paxinos & Watson, 1998)

### *Function*

All prefrontal areas are strongly interconnected, meaning that information about actions, emotions, and stimuli is directly or indirectly available to all prefrontal areas. From a functional point of view, as Fuster (2001) point out, it is important to remember that these functions rely closely on the PFC connections (among prefrontal areas as well as PFC with other regions) and sometimes it will be difficult to localized any of them within a discrete portion of PFC. The rodent PFC is involved in a multitude of processes that make animals capable of many complex behaviors. These processes include working memory, temporal processing, planning (prospective coding), oculomotor control (frontal eye fields), visceromotor activity, goal directed behavior, attention, flexibility, and decision making.

Complementarily to this integrative approach, multitude of studies have reported some specific functions associated to these areas of PFC. The PrL cortex of rodents seems to be homologous to the dorsolateral PFC of primates (related to cognitive processing) since it was observed functional similarities between these two regions based on behavioral experiments (Delatour and Guisquet-Verrier, 2000; Groenewegen and Uylings, 2000), as well as in connectivity (Hoover et al., 2007) and cellular activity in working memory assays (Baeg et al., 2003; Funahashi, 2006). More specifically, based on behavioral and electrophysiological data the ventral-medial subregion (PrL and IL areas) appears to play an important role in working memory for visual object and spatial location information (Di Pietro, 2004; Horst & Laubach, 2009; Yang et al., 2014; Baeg et al., 2003), temporal order memory (for a list of objects or locations) (Hannesson et al., 2004a; Hannesson et al., 2004b), prospective coding (defined as the ability to code and later retrieve and execute an action plan) (Goto & Grace, 2007;), object-place association learning (Kesner & Ragozzino, 2003; Lee and Solivan, 2008), cross-modal reversal learning (Ragozzino et al., 2003; Floresco et al., 2008), and decision making (St. Onge & Floresco, 2010) (for more information see review: Kesner & Churchwell, 2011). Within this subregion (the ventral medial cortex) it has been shown rodent prelimbic cortex (PrL), regulates the expression of conditioned fear and behaviors interpreted as reward seeking. Meanwhile, the ventral-medial PFC, namely the infralimbic cortex (IL), is essential to extinction conditioning in both appetitive and aversive domains (Gourlley, 2016).



#### 1.4. BRAIN COMPUTER INTERFACES

Brain-computer interfaces (BCI), sometimes called brain-machine interfaces (BMI), are electronic systems that translate the neural brain activity into commands for controlling external devices. The activity generated by ensembles of neurons is recorded by means of electrodes strategically placed on the surface of the scalp or intracranially implanted on the surface of the cortex or deeply placed in some regions of the brain. Thus, depending on the type of electrode that is employed in these systems it is possible to create a preliminary classification of the different types of BCI commonly used during the last decades. As Lebedev and Nicholelis point out in a review on general aspect of these interfaces (2006) we can find systems based in **non-invasive** recordings of the electroencephalographic (**EEG**) activity of the cerebral cortex and functional near infrared spectroscopy (**fNIRS**) as well as **invasive** methods which are based on implanting electrodes either to record single units, ensembles of cells [with multiunitary arrays (**MUA**) electrodes] or the joint activity of multiple neurons [multi-units recording of local field potentials (**LFPs**) from cortical and subcortical brain regions and electrocorticogram (**ECoG**) activity with subdurally implanted electrodes].

Although unitary recordings present the highest spatial resolution among the different acquisition types of brain activity they are very susceptible to signal degradation due to tissue encapsulation (Shain et al., 2003) and to small displacements of the electrodes sensors. An alternative to solve this handicap is the use of electrodes with a lower impedance to register the activity of neuronal populations which generate local field potentials (LFPs). It has been shown that LFPs possess features which are equivalent and even better than those observed in single cells during working memory and inferring motor processes (Pesaran et al., 2002; Mehring et al., 2003) and that they are appropriate to be employed into brain-machine interfaces (Flint et al., 2013; So et al., 2014). These LFPs electrodes have higher spatial resolution (tenths of millimeters) than electrodes used for EEG activity (centimeters) as well as broader bandwidth (0-500 Hz) than electrocorticographic (ECoG; 0-40 Hz) and EEG (0-40 Hz) activity and higher signal amplitude (Freeman et al., 2003).

Brain computer interfaces have used multiple electrophysiological activity signals to control external devices (Birbaumer et al., 2006).

- **Visual evoked potentials (VEP)**: recorded over the visual cortex to determine, for example, direction in which a user wants to move a cursor.
- **Slow cortical potentials (SCP)**: are very low frequency oscillations generated on the cortex and occur over a timescale of 0.5-10.0 seconds of duration. Negative SCPs are typically associated with movement and other functions involving cortical activation, while positive SCPs are usually associated with reduced cortical activation (Rockstroh et al., 1989; Van Boxtel, 1997). Several studies demonstrate prefrontal and frontal cortex are good candidates to generate SCPs under voluntary control compared to posterior parietal cortices
- **P300** evoked potentials.
- **Sensorimotor rhythm (SMR)**: Mu and Beta rhythms associated with movement execution or imagination.
- **Movement related potentials (MRP)**.
- **Oscillatory activity** (EEG or LFPs) augmentation and reduction of oscillatory waves of specific frequency ( $\theta$ ,  $\alpha$ ,  $\beta$  and  $\gamma$ ) bands.
- **Cortical neuronal action potentials** firing rate increase in M1, premotor and posterior parietal cortices.

Many of these electrophysiological signals has been studied in the M1 and/or posterior parietal cortices in different experimental designs including the activation of external devices (Lebedev and Nicolelis, 2006; Bouton et al., 2016) sometimes due to spatial restrictions (for example, EEG recordings are restricted to superficial cortical regions) or to the choice of regions that allow to easily correlate their neural activity with specific functions (motor cortex activity and body movement). But, in the last years, the prefrontal cortex (PFC) and cognitive processed information has become more relevant in brain-machine interfaces (BMIs) from the apparition of new non-invasive techniques like near infrared spectroscopy that allowed to record deep brain regions (Schudlo et al., 2013; Hong et al., 2015).

We finish this section briefly talking about the elements that contain a BCI. The definition of a BCI at the beginning of this section introduce us their components. We told about neural brain activity (from the brain of the **user**) that would be converted into commands by means of an electronic system (the **transducer**) to control an external device [a **computer** (for BCI) or **machine** (for BMI)].

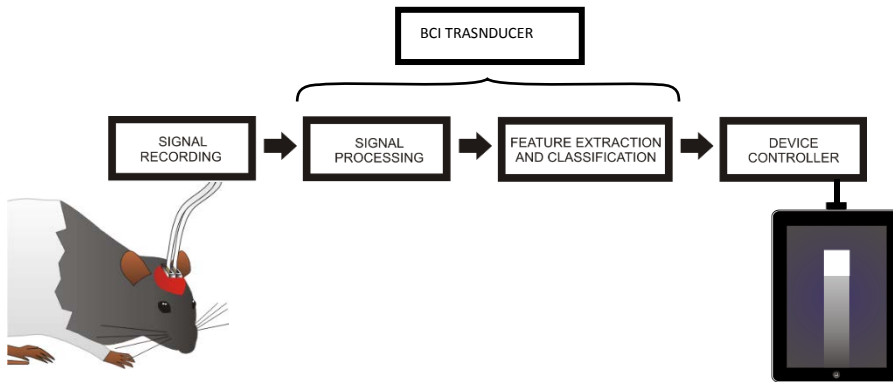


**Figure 1.5. Model of a BCI system illustrating the main components and the order of processes.** In the schematic design the brain activity of a rat is recorded and processed later by means of a transducer which extracts some features or properties of the neural signal. The detection of the proper features (previously defined in the BCI device) sends a command from the device controller that activates some function in the external device (e.g., the activation of a touch-screen tablet).

The most complex component of these interfaces is the transducer that converts the energy contained in a specific brain activity into a signal to be employed in digital electronic circuits. In this point the simplest transducer may carry out various processes (**Fig. 1.5**) as **signal processing** (e.g., enhancement of the signal-to-noise ratio), **feature extraction** (e.g., firing rate, oscillatory frequency synchronization, coherence, etc.) and **feature classification** (into different control signals).

#### *1.4.2. Neuronal operant conditioning in BCIs*

Those BCIs have been exhaustively explored from the point of view of interface design, including algorithms, motor imagery and electronic devices but rarely from an electrophysiological approach. Specifically referred to learning process where two events—a volitional enhancement in neural firing and a subsequent response: a reward or the control of an external device associated to a reward, in the most complex cases—are progressively associated. This intriguing form of learning is named **neuronal operant conditioning**.

The use of neural cortical activity for operant conditioning tasks goes back to the 1970s, with the innovative approaches of Fetz and colleagues (Fetz, 1969; Fetz and Finocchio, 1971, 1972). Fetz's group used awake monkeys to demonstrate the conditioning of single neurons by reinforcing a high rate of neuronal activity, which activated a mechanic arm, with the delivery of a reward. In a similar study, Chapin (1999) trained rats to move a lever with an artificial arm

in a Skinner box for reward with extracellular firing of cortical cells without any actual movement. More recently, a set of BMI studies, replicated these previous findings obtaining similar results of increase of operant-conditioned neurons in medial temporal lobe and M1, prefrontal and motor cortex in humans, monkeys and rats respectively (Cerf et al., 2010; Bouton et al., 2016; Kobayashi et al., 2010; Schafer and Moore, 2011; Arduin et al., 2013).

**Operant conditioning of firing synchrony and oscillations** is an important extension of the neuronal operant conditioning and it is defined as the study of synchronous activity of a population of neurons volitionally controlled. Thereby, some experiments have reported that oscillatory activity of motor cortical neurons in monkeys and hippocampus in rats can be enhanced by operant conditioning (Engelhard et al., 2013; Rouse et al., 2013; Sakurai and Takahashi, 2013).

Some studies have focused on the neural mechanisms underlying motor and cognitive processes using these types of interface. Neural plasticity maybe the most significant aspect induced by the use of BMI (Zacksenhouse et al., 2007; Gangulyetal, 2011). Koralek (2012) investigated alterations of activity in striatal neurons in relation to the progress in learning using BMI and they observed an increase of neurons modulating their activities as learning progressed concluding plasticity in the corticostriatal synapses is necessary for abstract skill learning in BMIs. In a BMI task in humans, it was demonstrated that, although the use of a BCI only required modulation of a local population of neurons in M1 and PFC, a distributed network of diverse cortical areas was involved in the acquisition of BCI proficiency (Wander et al., 2013).

This new field of research provides us with new data on some of the neurophysiological processes related to the actual motor and cognitive learning tasks since it was proposed BMI learning as an analogy to those ones (O'Doherty et al., 2011; Schafer and Moore, 2011; Hiremath et al., 2015).



## 2. OBJECTIVES & HYPOTHESIS



## **2. OBJECTIVES AND HYPOTHESIS**

By means of three different studies carried out in rodents we have examined some synaptic properties and mechanisms of two cerebral cortex regions (M1 and PrL), involved in some types of associative learning. For this purpose, electrophysiological and molecular approaches were used with the aim of achieving the following objectives:

1. To determine the electrophysiological properties of S1–M1 synapses in behaving mice related to synaptic transmission through paired test pulse and HFS protocol for LTP induction.
2. To study whether NMDA receptor in the M1 could act as a coincidence detector for activity-dependent changes in synaptic strength and associative learning.
3. To describe the electrophysiological interrelation of the thalamocortical and mesocortical pathways and their convergent synaptic activity in the PrL cortex.
4. To examine whether the PrL cortex is involved in early stages of the associative learning and its relation with high synaptic strength phases.
5. To test the effect of punctual overstimulation on the PrL cortex and its participation in information processing of cognitive processes related to goal-directed behaviors.
6. To design a simple BCI that could be controlled by rats using LFP activity recorded in PrL cortex in order to demonstrate operant conditioning of oscillatory activity.





### 3. MATERIALS & METHODS



### 3. MATERIAL AND METHODS

#### 3.1. ANIMALS

Experiments were carried out on male C57BL/6 mice (**experiment 1**) or Lister Hooded rats (**experiments 2 and 3**) (3/4 or 5/6 months old respectively) provided by an authorized supplier (Charles River Laboratories, Barcelona, Spain). Upon arrival at the Pablo de Olavide Animal House (Seville, Spain), animals were housed in individual cages until the end of the experiment. Mice and rats were kept on a 12-h light/dark cycle with constant ambient temperature ( $21.5 \pm 1^\circ\text{C}$ ) and humidity ( $55 \pm 8\%$ ), with food and water available ad libitum. All of the experiments were performed in accordance with the guidelines of the European Union Council (2010/276:33-79/EU) and Spanish regulations BOE 34:11370-421, 2013) for the use of laboratory animals in chronic studies, and approved by the local Ethics Committee of the Pablo de Olavide University.

#### 3.2. MOTOR CORTEX-SPECIFIC GRIN1 GENE KNOCKOUT

**Experiment 1.** To investigate whether NMDA receptor in the primary motor cortex could act as a coincidence detector for activity-dependent changes in synaptic strength and associative learning, we developed a combinatorial genetic approach using viruses for conditional Cre recombinase (*Cre*) gene expression (**Fig. 3.1a**) in genetically engineered mice (*Grin1<sup>tm1Rsp</sup>* or *Grin1<sup>2lox</sup>*) (Niewoehner et al., 2007), in which exons of the *Grin1* gene were flanked with *loxP* sites (**Fig. 3.1b**). We developed two recombinant adeno-associated viruses (rAAVs), which were equipped with the doxycycline (Dox)-controlled genetic switches (Zhu et al., 2007; Cambridge et al., 2009). The first virus (*rAAV-hSYN-rtTA*) allowed expression of reverse tetracycline transactivator (*rtTA*) gene under control of the human synapsin promoter (*hSYN*, *Pro* in the **Fig. 3.1a**). The second virus (*rAAV-P<sub>tetbi</sub>-Cre/tdTOM*) was equipped with a bidirectional tet promoter (*P<sub>tetbi</sub>*) to simultaneously express two different genes encoding for the Cre recombinase protein and a red fluorescent protein variant, the tdTomato (tdTOM), for visualizing virus-targeted neurons (**Fig. 3.1a, 3.1c**). The *Cre* and the *tdTOM* genes are expressed when rtTA binds to *P<sub>tetbi</sub>* in the presence of Dox. To increase the spread of virus in the M1 cortex by hyperosmolarity, D-mannitol/virus mixture was injected in the brain (Mastakov et al., 2000) and D-mannitol was also delivered into mice systemically by intraperitoneal injection (Burger et al., 2004) (**Fig. 3.1c**). Viruses were injected in the M1 cortex of age-matched wild-type littermates and *Grin1<sup>2lox</sup>* mice (**Fig. 3.1b**). Three weeks after virus injection, Dox-treated mice

showed robust tdTOM and Cre expression in the M1 cortex (**Fig. 3.1c**). Virus (v)-delivered Cre expression in neurons enabled, by Cre-loxP-mediated gene recombination, the generation of highly specific *Grin1* gene knockout mice, *Grin1-v $\Delta$ <sup>MCx</sup>*, in which the *Grin1* gene is selectively deleted ( $\Delta$ ) in the M1 cortex (MCx) (**Fig. 3.1b**). The virus-injected, age-matched wild-type littermates served as controls (Contr-v<sup>MCx</sup>).

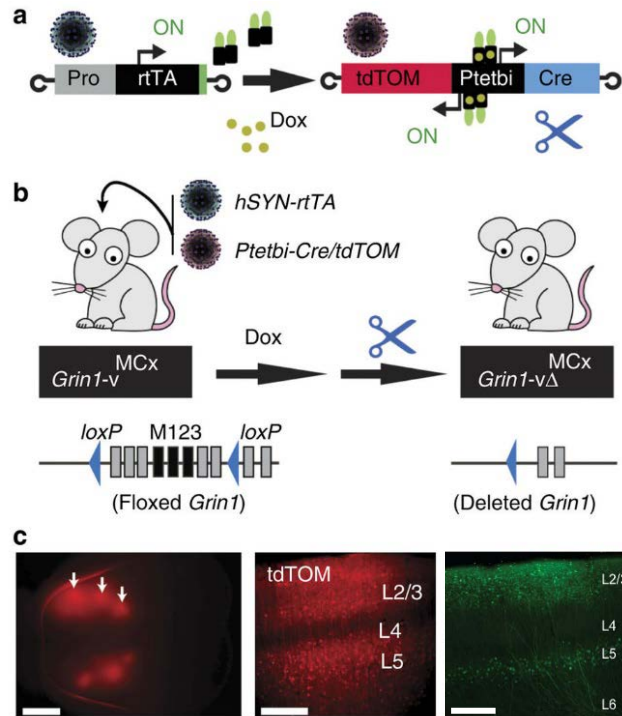


**Figure 3.1. Motor cortex-specific *Grin1* gene knockout.** **a.** Virus-mediated gene transfer for doxycycline (Dox) induced rtTA-dependent expression of tdTomato (tdTOM) and the Cre recombinase. **b.** Cre expression in the brain of *Grin1<sup>tm1Rsp</sup>* mice (*Grin1<sup>2lox</sup>*) activated the excision of *loxP*-flanked exons in the *Grin1* gene, thereby generating mice with neuron-specific *Grin1* gene deletion selectively in the M1 cortex (*Grin1-v $\Delta$ <sup>MCx</sup>*). *LoxP* sites, blue triangles; exons, grey rectangles; exons encoding membrane-inserted segments M1–M3, black rectangles. **c.** Expression of tdTOM detected on both hemispheres with a three-point virus injection in the M1 cortex (scale bar; 3 mm, left). Cellular resolution tdTOM expression (scale bar; 250  $\mu$ m, middle) and Cre (right) expression was specifically detected in cortical L2/3 and L5 (middle and right).

### 3.3. SURGERY FOR CHRONIC-RECORDING EXPERIMENTS.

Animals were anesthetized with 0.8–3 % halothane delivered from a calibrated Fluotec 5 (Fluotec-Ohmeda, Tewksbury, Massachusetts, USA) vaporizer at a flow rate of 1–2 L/min oxygen (AstraZeneca, Madrid, Spain) and delivered by a mouse or rat anesthesia mask (David Kopf Instruments, Tujunga, CA).

**Experiment 1.** Mice were implanted with bipolar stimulating electrodes aimed at the facial area of the right S1 region (1mm posterior to bregma, 2.5mm lateral and 1.2mm from brain surface) and with two recording electrodes aimed at the facial ipsilateral primary motor cortex (1mm anterior to bregma, 1mm lateral and 0.8mm from brain surface). These electrodes were made of 50  $\mu$ m, Teflon-coated tungsten wire (Advent Research Materials Ltd, Eynsham, UK). The final position of the recording electrodes was determined using as a guide the field potential depth profile evoked by paired (40 ms of interval) pulses presented at the S1 area (Troncoso et al., 2007). A bare silver wire (0.1 mm) was affixed to the skull as a ground. Wires were connected to a four-pin socket and the socket was fixed to the skull with the help of two small screws and dental cement (Gruart et al., 2006).

**Experiment 2.** 10 rats were surgically implanted only with recording electrodes at PrL cortex and stimulating electrodes at MDTh and VTA (see coordinates previously specified). These electrodes were made from 50  $\mu$ m, Teflon-coated, tungsten wire (Advent Research, Eynsham, UK). Each electrode consisted of three individual tungsten wires with their tips spaced 300  $\mu$ m along the extent of the electrode. In this surgical session animals were also implanted with 26-gauge stainless steel guide cannula at PrL cortex. The electrodes implanted at PrL cortex were accurately attached to the cannula guide to ensure a correct effect of the drug in the site of recording. The guide cannula were anchored to the skull by dental cement. Stainless steel stylets were inserted into the guide cannula, and left in place until injections were made.

**Experiment 3.** Following the stereotactic coordinates from Paxinos and Watson atlas (1998), rats were chronically implanted with recording electrodes aimed at the PrL (2.7 mm anterior to bregma, 0.8 mm lateral and 3.6 mm from 11 the brain surface), the nucleus accumbens (1.7 mm anterior to bregma, 1.4 mm lateral and 7.6 mm from the brain surface), the primary motor cortex (1.0 mm anterior to bregma, 2.3 mm lateral and 2.0 mm from the brain surface), the mediodorsal thalamic nucleus (3.0 mm posterior to bregma, 0.5 mm lateral and 5.3 mm from the brain surface), the hippocampal CA1 area (3.8 mm posterior to

bregma, 2.0 mm lateral and 2.5 mm from the brain surface), and the ventral tegmental area (6.0 mm posterior to bregma, 0.5 mm lateral and 7.8 mm from the brain surface). As in **experiment 2**, each electrode consisted of three individual tungsten wires (50 $\mu$ m; Teflon-coated) with their tips spaced 300  $\mu$ m along the extent of the electrode

With the aim of recording the unitary activity present in the PrL cortex of rats, 5 additional animals were implanted in the PrL cortex with the same recording electrode but with the addition of a home-made multielectrode. The multielectrode was composed of six 25  $\mu$ m, Teflon-coated, tungsten wire (Advent Research).

In order to determine whether vibrissal movements were related with LFPs recorded at the PrL cortex, a pair of recording electrodes was implanted in the center of the contralateral whisker pad in the above mentioned animals. Vibrissal electrodes were made from 50  $\mu$ m, Teflon-coated, annealed stainless steel wire (A-M Systems, Carlsborg, WA). A bare silver wire was affixed to the bone as ground.

Finally, since the presence of recording wires could represent a significant impairment for the proper acquisition of the pattern-triggered tasks, an additional group (n = 5) of rats were chronically implanted with five 50  $\mu$ m tungsten recording electrodes aimed at the PrL cortex. These electrodes, plus a ground wire, were connected to a Bakelite integrated circuit (Cibertec, S.A., Madrid, Spain) equipped with an 8-pin Omnetics socket (RS Amidata, Madrid, Spain).

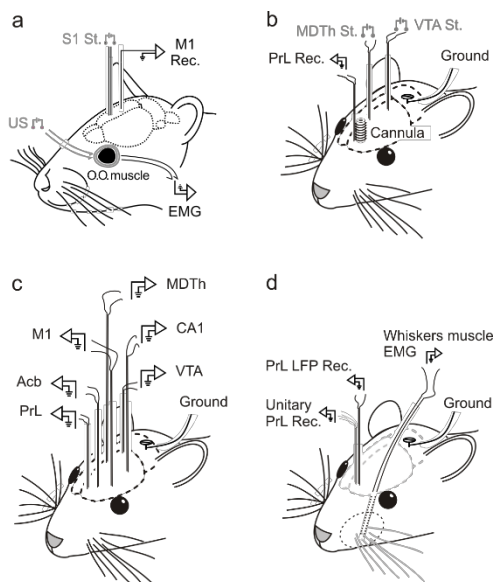


**Figure 3.2. Summary of surgeries for different experiments.** **a. Experiment 1:** Mice were implanted with stimulating electrodes in trigeminal nerve and recording electrodes in O.O. muscle to evaluate the learning progress for classical conditioning. Additionally, stimulating electrodes in S1 and recording electrodes in M1 informed about the synaptic efficacy of the path during associative learning. **b. Experiment 2:** Two stimulating electrodes were placed in MDTh and VTA and one recording electrode attached to a cannula for lidocaine infusion in PrL mPFC to functionally characterize the thalamocortical and mesocortical pathways. Moreover, effect of lidocaine inactivation of PrL cortex during early phase of an instrumental learning was examined **c** and **d**. **Experiment 3:** Two groups of rats were chronically implanted with different sets of recording electrodes. One group (**c**) were implanted in six regions: PrL,

M1, Acb, MDTh, CA1 and VTA to control a BCI with oscillatory activity pattern (LFPs) and to test the source of these pattern. The second group (**d**) was implanted in PrL with electrodes for LFP recording and unitary activity recording to describe the sort of neuronal activity of this pattern and

recording electrodes into the whisker pad to determine the influence of vibrissal movement in the PrL activity.

### 3.4. STIMULATION AND RECORDING PROCEDURES

Both the EMG activity of the orbicularis oculi muscle and fPSPs in mice (**experiment 1**), fPSP in rats (**experiment 2**), as well as EMG activity of the whisker pad, LFPs and unitary activity (**experiment 3**) were recorded with Grass P511 differential amplifiers (Grass-Telefactor, West Warwick, Rhode Island, USA), at a bandwidth of 0.1 Hz–10 kHz. A high-impedance probe ( $2 \times 10^{12} \Omega$ ; 10 pF) was used for fPSP recordings. In **experiment 3** additional wireless recordings were carried out with the help of a 5-channel TBSI head-stage system (Harvard Bioscience Inc., Holliston, MA). Unitary recordings were carried out with high-impedance probes ( $2 \times 10^{12} \Omega$ , 10 pF) and filtered between 450 Hz and 4500 Hz, with the help of an FIR filter.

**Experiments 1 and 2.** Electrical stimulus applied to the S1 (**experiment 1**), MDTh and VTA (**experiment 2**) regions consisted of 100 ms, square, biphasic pulses presented alone, paired or in trains. Stimulus intensities ranged from 0.02 to 0.4mA for the construction of the input/output curves. For paired pulse test, the stimulus intensity was set well below the threshold for evoking a population spike, usually 30–40% of the intensity (mA) necessary for evoking a maximum fPSP response (Gureviciene et al., 2004). Paired pulses were presented at different pulse intervals from 10 to 500 ms (generally 10, 20, 40, 100, 200 and 500 ms for all groups).

For LTP induction, the stimulus intensity was also set at 35% of peak fPSP values. An additional criterion for selecting stimulus intensity for LTP induction was that a second stimulus, presented 40 ms after a conditioning pulse, evoked a synaptic field potential 20% larger than the first fPSP (Bliss and Gardner-Medwin, 1973). After 15 to 30 min of baseline records (1 stimulus per 20 s), each animal was presented with an HFS protocol consisting of five trains (200 Hz, 100 ms) of pulses at a rate of 1 per second. This protocol was presented six times in total, at intervals of 1min. After the HFS protocol, evolution of fPSPs was followed at least for 30 min at the same stimulation rate (1 stimulus per 20 s). Additional recording sessions from 15 to 30 min were carried out the following days (Gruart et al., 2006; Madroñal et al., 2009).

#### 3.4.1. Electrical disruption of the PrL cortex

**Experiment 3.** In order to determine whether the PrL area in rats was related with cognitive processes involved in the operant conditioning paradigm, we checked



the effects of its electrical stimulation on the ongoing behavioral sequence of touching a touch-screen tablet (iPad®) and going to collect the rewarded pellet. The PrL cortex was stimulated at the precise moment of each correct touch on the screen. For the electrical stimulation of the PrL region during operant conditioning, we used a 200 Hz train of pulses (50- $\mu$ s negative-positive) lasting 200 ms. The train was triggered, with a delay  $< 0.5$  ms, by a touch of the square virtual button on the touch-screen. In order to avoid excessive stimulations of the experimental animal, subsequent touches within a 6 seconds window did not trigger any stimulus. Stimulus intensities ranged from 0.5 mA to 1 mA. For each animal, we selected the minimum intensity evoking a short-lasting disruption in the expected behavioral sequence (touch the visual display, go to the feeder, eat the pellet; see Jurado-Parras et al., 2012, for details).

### **3.5. CLASSICAL CONDITIONING: EYEBLINK CONDITIONING**

**Experiment 1.** Experimental sessions were carried out with three mice at a time. Animals were placed in separate small ( $5 \times 5 \times 10$  cm) plastic chambers located inside a larger ( $30 \times 30 \times 20$  cm) Faraday box. Animals were classically conditioned using a trace paradigm. For this, a tone (20 ms, 2.4 kHz, 85 dB) was presented as CS, while the US consisted of a 500  $\mu$ s,  $3 \times$  threshold, square, cathodal pulse applied to the supraorbital nerve 500 ms after the end of the CS. A total of two habituations and 10 conditioning sessions (one session per day) were carried out for each animal. A conditioning session consisted of 60 CS–US presentations, and lasted for  $\approx 30$  min. For a proper analysis of conditioned responses, the CS was presented alone in 10% of the cases. CS–US presentations were separated at random by  $30 \pm 5$  s. For habituation sessions, only the CS was presented, also for 60 times per session, at intervals of  $30 \pm 5$  s. As a criterion, we considered a ‘conditioned response’, the presence, during the CS–US interval, of EMG activity lasting  $> 20$  ms and initiated  $> 50$  ms after CS onset. In addition, the integrated EMG activity recorded during the CS–US interval had to be at least 2.5 times greater than the averaged activity recorded immediately before CS presentation (Gruart et al., 2006; Porrás-García et al., 2005).

During habituation and conditioning sessions, fPSPs were evoked in the motor cortex area by single 100  $\mu$ s, square, biphasic (negative–positive) pulses applied to the S1 region 300 ms after CS presentation. As above-indicated, pulse intensity was set at 30–40% of the amount necessary to evoke a maximum fPSP response (range, 0.05–0.15 mA). An additional criterion for selecting stimulus intensity was that a second stimulus, presented 40 ms later, evoked a larger

(>20%) synaptic field potential than the first (Madroñal et al., 2009; Bliss and Gardner-Medwin, 1973).

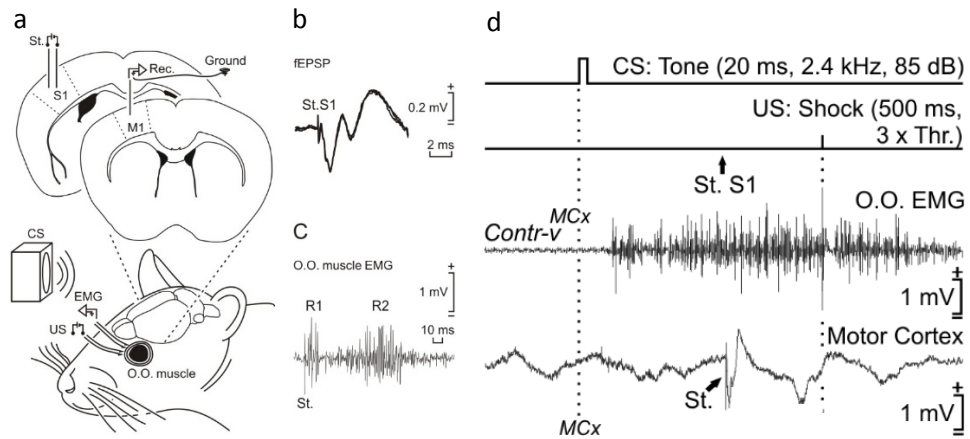


**Figure 3.3. Diagrammatic experimental design for eyeblink conditioning. (Experiment 1).** **a.** Coronal sections illustrating the sites of stimulation in S1 and recording in M1 (top) to know synaptic state of the S1-M1 pathway during the eyeblink conditioning paradigm. Additional recording electrodes are implanted in the orbicularis oculi (O.O.) muscle of the upper eyelid to detect the conditioned response (CR) and stimulating electrodes on the trigeminal nerve to generate the unconditioned stimulus (US; electric shock) (bottom). **b.** fEPSP evoked in the motor cortex by single pulses applied to the S1 region are illustrated. **c.** Corneal reflex responses evoked at the O.O. muscle by electrical stimulation of the trigeminal nerve in a mouse are also illustrated. **d.** A schematic representation of the trace conditioning paradigm, illustrating CS and US stimuli, and the moment at which a single electrical pulse was presented to S1 (St. S1). An example of an EMG record from the O.O. muscle and an extracellular record of M1 activity are shown.

### 3.6. INTRACRANIAL DRUG INFUSION

**Experiment 2.** Before injecting the drug a 15 minutes baseline was recorded in order to compare any effect on the field PSPs evoked in PrL after infusion. After baseline recording, rats were gently restrained by hand and the stylets were removed from the guide cannula. For intra-PrL injections of drugs, a 5 $\mu$ L Hamilton syringe, mounted on a SP100i infusion pump (WPI, Sarasota, FL, USA), was connected with a polyethylene tubing to a 28 gauge stainless steel infusion cannula that extended 1 mm beyond the tip of the guide cannula. The injections were delivered at a rate of 0.25  $\mu$ L/min for 2 minute and the injection cannula was left on the place for one additional minute to facilitate the diffusion of the drug.

Lidocaine was dissolved in 0.9% sterile saline to make a 10% solution (100  $\mu$ g/ $\mu$ L). Concentrations of lidocaine hydrochloride (Sigma-Aldrich, Madrid, Spain) were determined in accordance with previous reports (Kantak et al., 2002;

Ball and Slane, 2012) and following preliminary tests carried out in an implanted pilot group of rats.

### 3.7. INSTRUMENTAL CONDITIONING.

Mice (**experiment 1**) training and testing took place in five Skinner box modules measuring  $12.5 \times 13.5 \times 18.5$  cm (MED Associates, St Albans, Vermont, USA). The operant conditioning boxes were housed within independent sound-attenuating chambers ( $90 \times 55 \times 60$  cm), which were constantly illuminated (19 W lamp) and exposed to a 45 dB white noise (Cibertec SA, Madrid, Spain). Rats (**experiment 2** and **3**) were trained for operant conditioning in a basic Skinner box module measuring  $29.2 \times 24.1 \times 21$  cm (MED Associates, St. Albans, VT, USA). In all experiments, each Skinner box was equipped with a food dispenser from which pellets (Noyes formula P; 45 mg; Sandown Scientific, Hampton, UK) could be delivered by pressing a lever (**experiment 1** and **2**; **Fig. 3.4a** and **3.4b**) or a virtual button (a  $200 \times 200$  pixels, i.e.,  $3.4 \times 3.4$  cm white square) on a touch-screen tablet (**experiment 2** and **3**; **Fig. 3.4c** and **3.4d**). Before training, animals were handled daily for 7 days and food-deprived to 85% of their free-feeding weight. Training took place for 20 min during successive days, in which animals were allowed to press the lever or the touch-screen (depending on experiments) to receive pellets from the feeder using a fixed ratio 1 (FR1) schedule. The start and end of each session was indicated by a tone (2 kHz, 200 ms, 70 dB) provided by a loudspeaker located in the isolating chamber. Animals were maintained on this fixed ratio 1 schedule at least until they reached the selected criterion—to obtain  $\geq 20$  pellets (mice; **experiment 1**) or  $\geq 80$  pellets (rats; **experiment 2**) for two successive sessions.

#### 3.7.1. Light/dark instrumental conditioning protocol

**Experiment 1.** Once mice reached the criterion for the fixed ratio 1 schedule (to obtain  $\geq 20$  pellets for two successive sessions), conditioning was carried out for 10 additional days using a light/dark protocol. In this protocol, only lever presses performed during the light period (in which a bulb into the operant chamber was turned on for 20 s) were reinforced with a pellet. In contrast, lever presses performed during the dark period (bulb turned off for  $20 \pm 10$  s) were not reinforced. Moreover, lever presses carried out during the dark period increased its duration in up to 10 additional seconds.

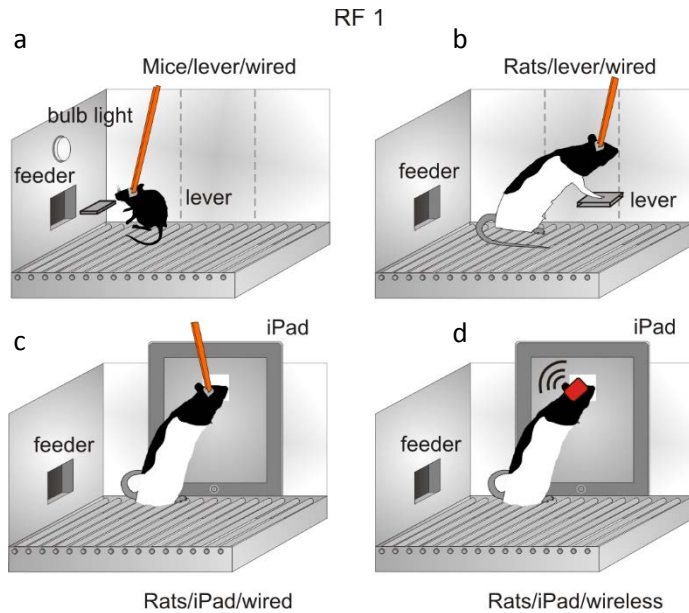


**Figure 3.4. Summary of the four designs for different instrumental conditioning tasks and transfer systems of brain activity used in the three experiments. Experiment 1:** (a) mice learned to press the lever in order to obtain a pellet (fixed ratio 1). Then, they continued with a more complex instrumental learning; “light/dark instrumental conditioning protocol” in which only presses when the light was turned on were reinforced with one pellet and presses during dark period were penalized. **Experiment 2:** (b and c) rats began the instrumental learning in a Skinner box with lever in which they obtained one pellet every time they press the lever (fixed ratio 1). Once they reached the criterion ( $\geq 80$  pellets for two successive sessions) and performed nine sessions (1 per day) the lever was substituted with a touch-screen tablet in which a virtual button appeared on the screen and rats touched to obtain a pellet (fixed ratio 1). **Experiment 3:** (c and d) Rats carried out a fixed ratio 1 schedule in a Skinner box equipped with touch screen and were connected to the recording system with cables (c) or through a wireless system (d). After eleven sessions in this schedule they started a neural conditioning protocol in which the generation of a selected pattern of neural activity in the PrL mPFC of the rat activated the virtual button on the screen that they could touch to get a pellet.

### 3.7.2. Brain activity closed-loop training.

**Experiment 3.** In one of the experiments, rats were trained to activate a virtual button (a  $200 \times 200$  pixels, i.e.,  $3.4 \times 3.4$  cm white square) displayed on a touch screen by LFP activity patterns recorded from PrL cortex. First, they were pre-trained in a fixed ratio 1 schedule until they reached the above specified criterion (to obtain  $\geq 80$  pellets for two successive sessions) (**Fig 3.4c** and **3.4d**). For this, a capacitive multi-touch-screen device (iPad® 2 model from Apple Inc., Cupertino, CA) with a 9.7-inch LED-back-lit glossy widescreen display with IPS technology (Leising et al., 2013) was used.

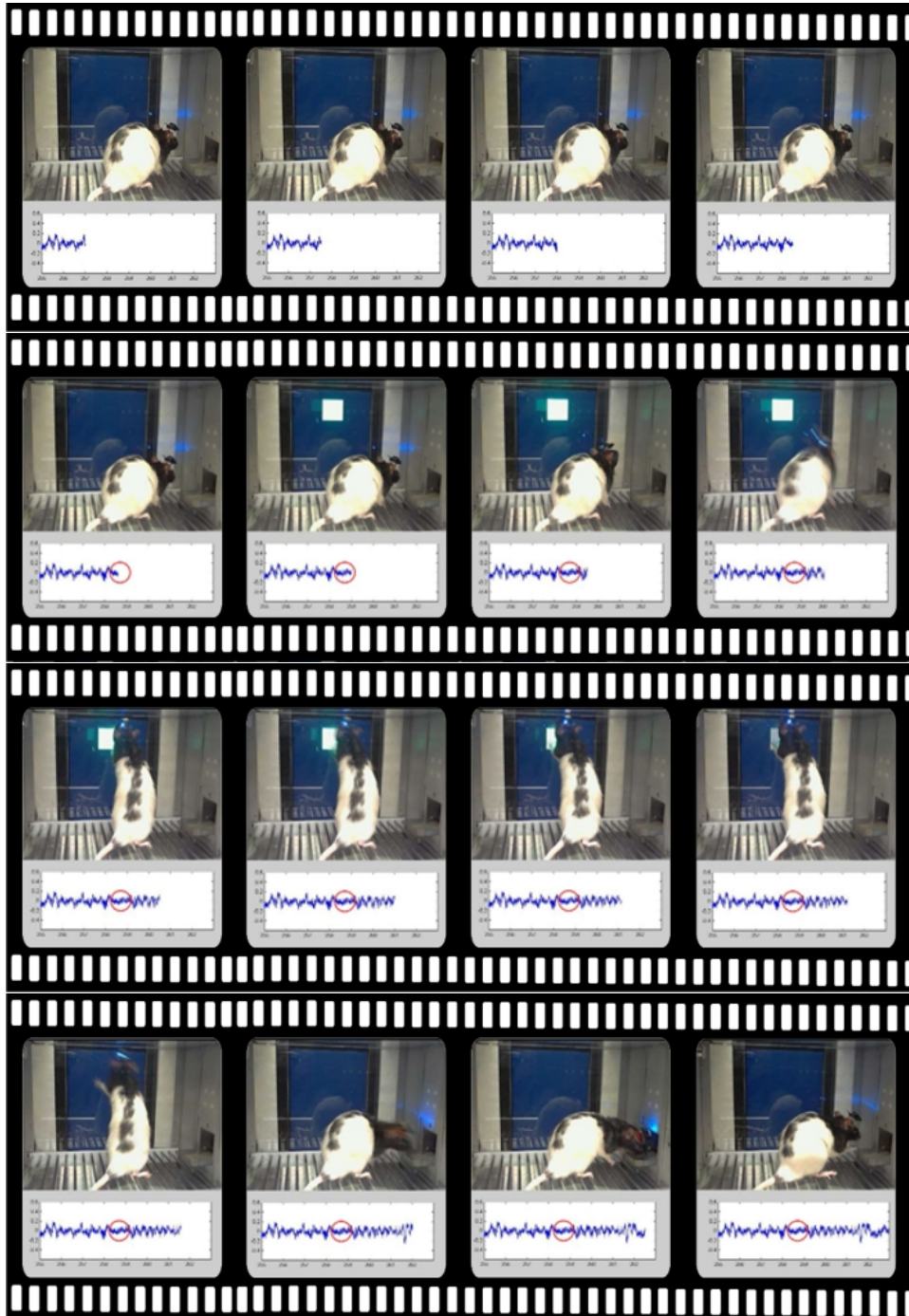


**Figure 3.5. Operant conditioning of oscillatory activity sequence.** Images showing a Lister Hooded rat with a wireless head-stage during the 8<sup>th</sup> session of neural operant conditioning. In the first row of images rat try to generate the selected activity (low power oscillatory activity in  $\theta$ ,  $\beta$  and  $\gamma$ ) that appears in the second row highlighted with a red circle. The transducer detects this pattern of activity and generates a signal that control the activation of the virtual button (the white square on

the screen). Then, the rat touches the button (third row), a pellet is released in the feeder (fourth row) and the animal runs to get it.

The detection of this LFP activity pattern was based on the instantaneous calculation of the power in a wide band of frequency between 3 Hz and 150 Hz that included three oscillatory bands of neural activity: theta ( $\theta$ ), beta ( $\beta$ ) and gamma ( $\gamma$ ). This spectral analysis was carried out with the help of a home-made program implemented with Spike2 software (CED 1401 Plus; Cambridge Electronics Design, Cambridge, England; RRID: SCR\_000903). Power of was calculated using the Fast Fourier Transform (FFT) with a raised cosine window. In addition to the above, a spectral power threshold was selected to detect the moment when the power for the three bands fell below it. When the power threshold was reached the RatButton system was activated. This threshold was calculated from LFPs recorded during preliminary baseline and training sessions and it was maintained during the whole experiment. According to the intrinsic characteristics of the LFP recordings from each experimental rat, the criterion values assigned to the threshold ranged from 0.00125 V<sup>2</sup> to 0.00215 V<sup>2</sup>. Thresholds were calculated as the average of the minimum values of power between 3 Hz and 150 Hz plus  $3 \times SD$ . The detections of the selected  $\theta/\beta$ - $\gamma$  transition pattern generated a new event channel in Spike2 which was translated into a command system to display the visual stimulus (the white square) on the touch screen (**Fig. 3.5** and **3.6**).

For the command system, we developed an ad hoc software (RatButton 2.1.3. for iOS 8.4) for stimulus presentation on the touch screen triggered by the selected LFP activity pattern. The same software also activated the feeder to supply the reward and quantified the number and time of correct screen touches. The RatButton software was developed with X-Code in object-oriented programming language Objective-C. Stimulus color (sRGB IEC61966-2.1: 0, 240, 100 – a green square) and luminance (150 cd/m<sup>2</sup> at 20 cm distance) were adapted to rats' vision with the help of a colorimeter (Minolta Chroma Meter xy-1; Minolta Camera Co., Ltd., Osaka, Japan) and a photometer (Sekonic DualMaster L-558/L; Sekonic Corporation, Nerima-Ku, Tokyo, Japan) (Jacobs et al., 2001).

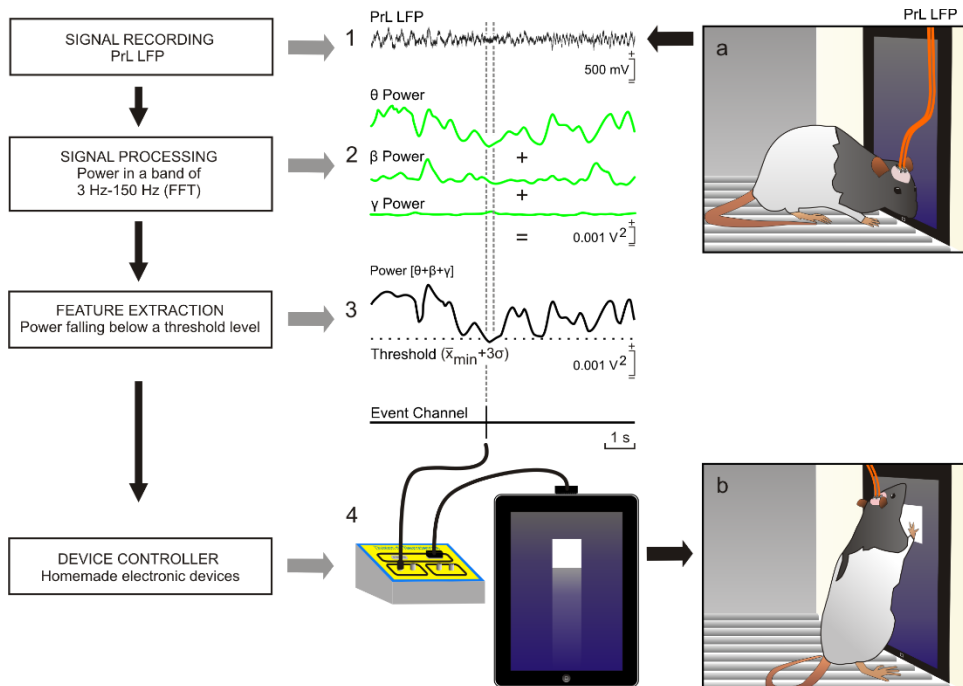


**Figure 3.6. Experimental procedure to detect the selected LFP activity pattern.** LFPs recorded in the PrL cortex (1) were recorded from behaving rats located in a modified Skinner box (a) and were processed on-line using a fast Fourier transform (2) with the help of the Spike2 software implemented on a CED 1401. Spectral power of recorded LFPs was analyzed within a band of 3-150 Hz (3). As illustrated by the representative record (1), the selected pattern (space between dashed lines) was characterized by a decrease in the spectral power of the  $\theta$  band, with no noticeable change in the power of the  $\beta$  and  $\gamma$  bands (2). In order to detect the selected pattern activity a power threshold was calculated (3; horizontal dashed line). This threshold was determined from LFPs recorded during habituation sessions. Its value was defined as the average of the minimum values of the spectral power for the 3-150 Hz band plus 3 times its standard deviation. When the spectral power fell below this threshold, it was detected from the LFP recorded in the PrL cortex by means of the Spike2 software. Then, a home-made command system sent a signal to the RatButton software, triggering the display of a square virtual button on the touch screen (4). Finally, the experimental animal was able to touch the square button in order to obtain its reward (b).

### 3.8. PERFUSION AND HISTOLOGY

At the end of the recording sessions, mice or rats were deeply anesthetized (sodium pentobarbital,  $50 \text{ mg kg}^{-1}$ ) and perfused transcardially with saline and 4% phosphate-buffered paraformaldehyde. Brains were dissected, postfixed overnight at  $4^\circ\text{C}$ , and cryoprotected in 30% sucrose in PBS. Sections were obtained in a microtome (Leica, Wetzlar, Germany) at  $50 \mu\text{m}$ . Depending on the experiment, selected sections including M1, S1, PrL, Acb, MDTh, VTA or CA1 regions were mounted on gelatinized glass slides and stained using the Nissl

technique with 0.1% toluidine blue to determine the location of stimulating and recording electrodes.

### 3.9. ACQUISITION AND DATA ANALYSIS

Field PSPs, EMG, LFP, pattern detections, 5 V rectangular pulses corresponding to lever presses, CS and US presentations, iPad touches and pellet delivery as well as video recordings were stored digitally on a computer through an analog-to-digital converter (CED 1401 Plus; Cambridge Electronics Design). Data were analyzed offline for quantification of conditioned responses, fPSP slopes or amplitudes, animal performance in the Skinner box,  $\theta/\beta$ - $\gamma$  pattern presentations and characteristics, power ratio index of the  $\theta/\beta$ - $\gamma$  pattern, and power spectrum of selected LFP recordings with the Spike2 and Signal software (Cambridge Electronics Design). The slope of evoked field PSPs was computed as the first derivative ( $V s^{-1}$ ) of field PSP recordings (V). For this, five successive field PSPs were averaged, and the mean value of the slope during the rise time period (that is, between the initial and final 10% of the fPSP) was determined.

These computed results were processed for statistical analysis using Sigmaplot 10 (Systat Software Inc., San Jose, CA). Unless otherwise indicated, data are always represented as the mean  $\pm$  SEM. Acquired data were analyzed using one-way or two-way repeated measures ANOVA. The Friedman Repeated Measures Analysis of Variance on Ranks (non-parametric) statistical test was used if normality or equal variance test failed. All of them were followed by Holm-Sidak or Tukey Test post hoc testing depending on the previous statistical test. The Student's t-test was applied when necessary. The corresponding degrees of freedom were reported accompanying the F,  $\chi^2$ , or t statistic values. The analytical procedures of the LFP recordings to obtain the time–frequency representation (spectrogram) and the coherence between pairs of different brain regions (coherograms) were developed with the help of the Chronux toolbox (MATLAB, MathWorks, Natick, MA). In most representations, we selected the following frequency bands:  $\theta$ , 3–12 Hz;  $\beta$ , 12–30 Hz; low  $\gamma$ , 30–50 Hz, and high  $\gamma$ , 50–150 Hz. Comparisons between spectrograms of two different groups of data were processed for statistical analysis using the EEGLAB Statistics toolbox (MATLAB, MathWorks) and Sigmaplot 10 (Systat Software Inc.).





## 4. RESULTS



## 4. RESULTS

### EXPERIMENT 1

#### 4.1. EFFECT OF FUNCTIONAL LOSS OF THE NMDA RECEPTOR IN M1

##### 4.1.1. In vivo LTP measurements

Initial in vivo experiments were aimed to determine the electrophysiological properties of S1–M1 synapses in behaving *Grin1-v $\Delta$ <sup>MCx</sup>* mice as compared with *Contr-v<sup>MCx</sup>* mice. Stimulating and recording electrodes were implanted in the corresponding facial areas of the primary somatosensory (S1) and motor cortices (Paxinos, 2001; Troncoso et al., 2007) (**Fig. 4.1a**). Both *Contr-v<sup>MCx</sup>* and *Grin1-v $\Delta$ <sup>MCx</sup>* mice (n=10 per group) presented similar ( $F_{(1,19,18)}=2.310$ ;  $P=0.145$ ) increases in the slope of field postsynaptic potentials (fPSPs) evoked at the M1 cortex following the presentation of single pulses of increasing intensity to the ipsilateral S1 region (**Fig. 4.1b**). These relationships were best fitted by sigmoid curves ( $r>0.92$ ;  $P\leq 0.001$ ), suggesting normal functioning of this synapse in both groups of mice. In addition, no significant facilitation (or depression) of fPSPs evoked during the paired-pulse test ( $F_{(5,54,48)}=1.577$ ;  $P=0.185$ ) or significant ( $F_{(1,9,58)}=0.000494$ ;  $P=0.982$ ) differences between the groups (n=5 per group) were observed (**Fig. 4.1c**).

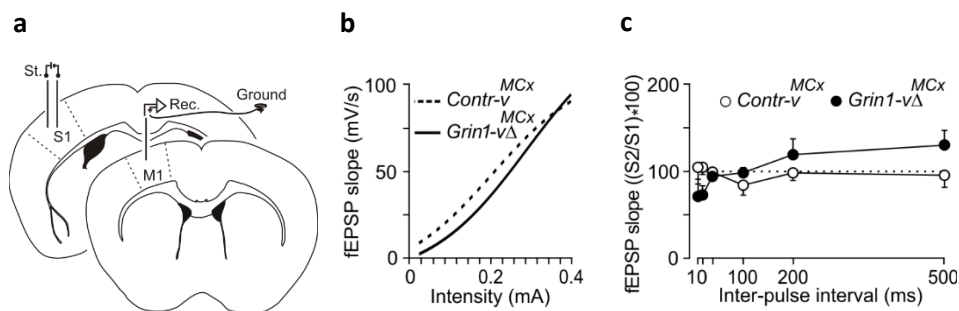


**Figure 4.1. Input/output curves and paired-pulse facilitation for the S1-M1 synapse. A.** Schematic depicting electrode implanted in vivo for stimulating neurons in the S1 and recording in M1. **B.** A single pulse was presented to S1 at increasing intensities (in mA), while recording the evoked fPSP at the motor cortex for *Contr-v<sup>MCx</sup>* (white circle and dashed line) and *Grin1-v $\Delta$ <sup>MCx</sup>* (black circle and continuous line) mice. The best sigmoid adjustment to the collected data is represented ( $r>0.92$ ;  $P\leq 0.001$ ; non-linear regression analysis). There were no significant differences between groups (n=10 per group;  $P=0.145$ ;  $F_{(1,19,18)}=2.310$ ; two-way ANOVA). **C.** Responses to paired-pulse stimulation. The data shown are mean  $\pm$  SEM slopes of the second fPSP expressed as a percentage of the first for six (10, 20, 40, 100, 200 and 500 ms) interstimulus intervals. The two groups (n=5 per group) of mice presented a similar ( $P=0.185$ ;  $F_{(5,54,48)}=1.577$ ; two-way ANOVA) result for paired-pulse test at intervals of 40–100 ms.

These results indicate that the S1–M1 synapse does not present the paired-pulse facilitation typical of hippocampal synapses in behaving mice (Madroñal et al., 2009) and that no pre-synaptic changes (Zucker and Regehr, 2002) were evoked by deletion of the *Grin1* gene.

Interestingly, the LTP study revealed significant differences between *Grin1-vΔ<sup>MCx</sup>* and their littermate controls (n=10 per group). Thus, high-frequency stimulation (HFS) of the S1 region in *Grin1-vΔ<sup>MCx</sup>* mice did not evoke any significant ( $F_{(6,54,63)} = 0.308$ ;  $=0.580$ ) increase in fPSP slopes in the motor cortex (Fig. 4.2). In contrast, we observed in *Contr-v<sup>MCx</sup>* mice a long-lasting LTP, significantly ( $F_{(6,54,63)} = 11.915$ ;  $P < 0.001$ ) larger than values collected from *Grin1-vΔ<sup>MCx</sup>* mice. After the second day of recording the potentiation of the pathway decreased to control littermate values of fPSPs. In this case, results indicate that the NMDAR is necessary to evoke long-lasting postsynaptic changes in the M1 cortex following HFS of S1 neurons.

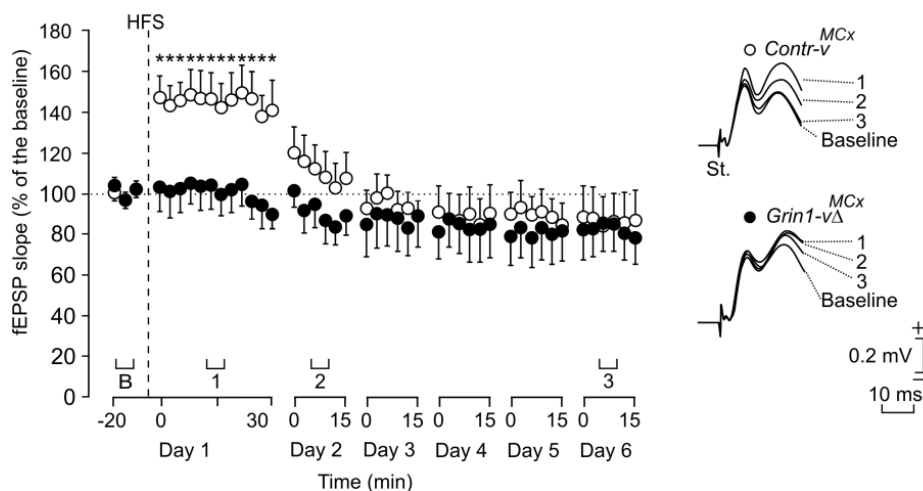


**Figure 4.2. Long-term potentiation induction in S1-M1 synapse and evolution of fPSPs.** At the right margin are illustrated examples of fPSPs collected from selected *Contr-v<sup>MCx</sup>* (white circles) and *Grin1-vΔ<sup>MCx</sup>* (black circles) mice (n = 10 per group) before (B, baseline) and after HFS of S1-M1 synapse. The graph illustrates the time course of LTP evoked in the motor cortex (fPSP mean  $\pm$  SEM) following HFS for *Contr-v<sup>MCx</sup>* and *Grin1-vΔ<sup>MCx</sup>* mice. The HFS was presented after 15 minutes of baseline recordings, at the time indicated by the dashed line. The fPSP is given as a percentage of the baseline (B = 100%) slope. *Grin1-vΔ<sup>MCx</sup>* mice have not LTP. In addition, values collected from the *Contr-v<sup>MCx</sup>* group were significantly ( $*P < 0.01$ ;  $F_{(6,54,63)} = 11.915$ ; two-way ANOVA) larger than those collected from *Grin1-vΔ<sup>MCx</sup>* mice.

#### 4.1.2. Synaptic plasticity and the conditioned response

Next, we implanted electrodes in Contr- $v^{\text{MCx}}$  (n=10) and Grin1- $v\Delta^{\text{MCx}}$  (n=11) mice (see **Fig. 3.3a** in Material and Methods section) to record fPSPs evoked at the S1–M1 synapse during the classical conditioning of eyelid responses, with an auditory signal as the CS and an electrical shock of the trigeminal nerve as the US (Gruart et al., 2006; Troncoso et al., 2007) (**Fig. 4.3a**). After multiple trials of CS–US pairings, an association was formed, enabling a conditioned stimulus alone to elicit a conditioned response (CR), measured by electromyography (EMG) in the orbicularis oculi muscle (**Fig. 4.3b**). First, we confirmed that reflexively evoked eye blinks collected from Grin1- $v\Delta^{\text{MCx}}$  mice were similar from a kinematic point of view to those already described in Contr- $v^{\text{MCx}}$  mice (Gruart et al., 2006). Control mice (Contr- $v^{\text{MCx}}$ ) acquired the classical conditioning test with a progressive increase in the percentage of CRs, reaching asymptotic values by the 7th conditioning session (**Fig. 4.3d**). In contrast, Grin1- $v\Delta^{\text{MCx}}$  mice presented a non-significant ( $F_{(11,99,108)}=1.670$ ;  $P=0.0905$ ) slow increase in the percentage of CRs, reaching values significantly ( $P\leq 0.05$ ) lower than those presented by the control group from the 4th to the 10<sup>th</sup> conditioning sessions (**Fig. 4.3d**). These results indicate that Grin1- $v\Delta^{\text{MCx}}$  mice, lacking the essential NMDA receptor subunit 1 (GluN1), were unable to acquire this type of associative learning task. Interestingly, and in opposition to results collected from Contr- $v^{\text{MCx}}$  mice, Grin1- $v\Delta^{\text{MCx}}$  mice did not present any sign ( $F_{(1,19,18)}=2.410$ ;  $P=0.149$ ) of learning-dependent changes in synaptic strength at the S1–M1 synapse (**Fig. 4.3c and e**). As already reported for hippocampal synapses during classical EBC (Gruart et al., 2006), the S1–M1 synapse presented a significant ( $P<0.05$ ) increase in fPSP slopes across conditioning. However, in Grin1- $v\Delta^{\text{MCx}}$  mice, the increase in fPSP slopes across conditioning sessions was impaired (**Fig. 4.3e**). These results indicate that the proper functioning of NMDARs located in the facial motor cortex is necessary both for the acquisition of classical EBC and to evoke the concomitant learning-dependent synaptic plasticity at cortical circuits.

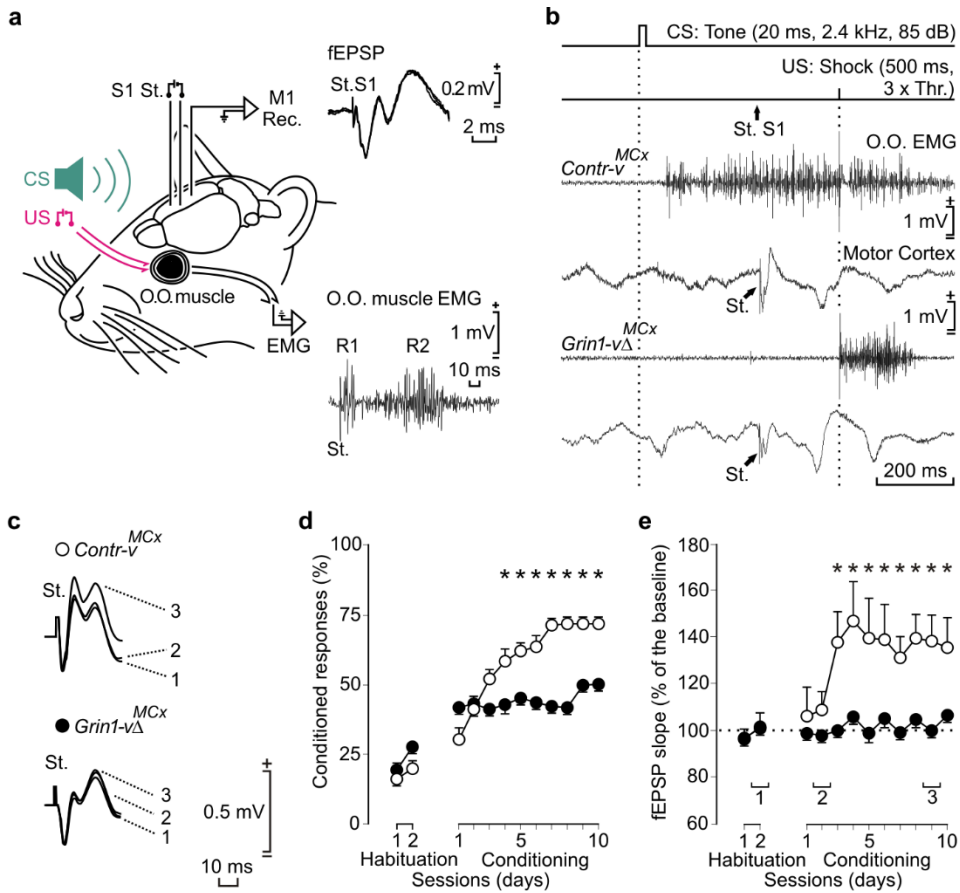


**Figure 4.3. Electrophysiological recordings and classical EBC in behaving animals.** **a.** For classical EBC, animals were implanted with stimulating (St.) electrodes (for US presentation) on the left trigeminal nerve and with electrodes to record (Rec.) the EMG activity of the ipsilateral orbicularis oculi (O.O.) muscle (for recording conditioned responses). The CS consisted of tones delivered from a loudspeaker located 50 cm from the animal's head. At the top are shown stimulating electrodes implanted in the right primary somatosensory cortex (S1) and recording electrodes implanted in the ipsilateral primary motor cortex (M1). fEPSP evoked in the motor cortex by single pulses applied to the S1 region are illustrated. Corneal reflex responses evoked at the O.O. muscle by electrical stimulation of the trigeminal nerve in a  $Grin1-v\Delta^{MCx}$  mouse are also illustrated. Note the presence of the two (R1, R2) components of the corneal reflex. **b.**  $Grin1-v\Delta^{MCx}$  mice were unable of acquiring a conditioned eyeblink response and the accompanying activity-dependent changes in synaptic strength in cortical S1–M1 synapse as  $Contr-v^{MCx}$  mice did. From top to bottom are illustrated the conditioning paradigm, representative O.O. EMG and electrocortical recordings during paired CS–US presentations for  $Contr-v^{MCx}$  and  $Grin1-v\Delta^{MCx}$  mice. The time of S1 stimulation (St. S1) is indicated, as are the times of presentation of CS and US (dotted lines). Data shown were collected during the 9th conditioning session. **c.** fEPSPs collected from  $Contr-v^{MCx}$  (white circles) and  $Grin1-v\Delta^{MCx}$  (black circles) mice during the conditioning sessions (1–3) indicated in **4.3e** section. **d.** Percentage (mean  $\pm$  SEM) of conditioned responses reached by the two experimental groups ( $n \geq 10$  per group). Values presented by  $Contr-v^{MCx}$  mice (white circles) were significantly ( $*P < 0.05$ ,  $F_{(1,20,19)} = 7.800$ , two-way ANOVA) larger than those reached by  $Grin1-v\Delta^{MCx}$  mice (black circles) from the 4th to the 10th sessions. **e.** Evolution of fEPSPs evoked at the S1–M1 synapse across conditioning for  $Contr-v^{MCx}$  (white circles) and  $Grin1-v\Delta^{MCx}$  (black circles) mice. Differences in fEPSP slopes (mean  $\pm$  SEM) between  $Contr-v^{MCx}$  and  $Grin1-v\Delta^{MCx}$  groups were statistically significant from the 3rd to the 10th conditioning sessions ( $*P < 0.05$ ,  $F_{(1,19,18)} = 8.889$ , two-way ANOVA).

#### 4.1.3. Instrumental learning

We also checked whether Grin1- $v\Delta^{MCx}$  mice ( $n=12$ ) could acquire an instrumental learning task in the same way as their littermate controls (Contr- $v^{MCx}$ ;  $n=12$ ). In a first experimental step, animals were trained to acquire a fixed (1:1) ratio schedule—namely, when placed in a Skinner box, they have to learn to obtain a food pellet every time they pressed a lever located nearby the feeder (**Fig. 4.4a**). Control mice (Contr- $v^{MCx}$ ) reached the selected criterion (to obtain 20 pellets in 20 minutes for two successive sessions) slightly (but not significantly; Student's  $t$ -test = -1.746;  $P=0.096$ ) before the Grin1- $v\Delta^{MCx}$  mice (**Fig. 4.4b** and **c**). In a second step, animals were trained to press the lever only when an overlying light bulb was switched on (**Fig. 4.5**). Pressing the lever during the dark period was not rewarded and, in addition, delayed the appearance of the lighted period (see Methods). This new conditioning paradigm presented more difficulties to the experimental animals than the early fixed (1:1) ratio schedule. Indeed, Contr- $v^{MCx}$  mice performed this task significantly ( $F_{(1,23,11)}=17.159$ ;  $P<0.05$ ) better than Grin1- $v\Delta^{MCx}$  mice (**Fig. 4.5**), again indicating that NMDAR function in motor cortex circuits is necessary for the acquisition of this type of associative learning task.

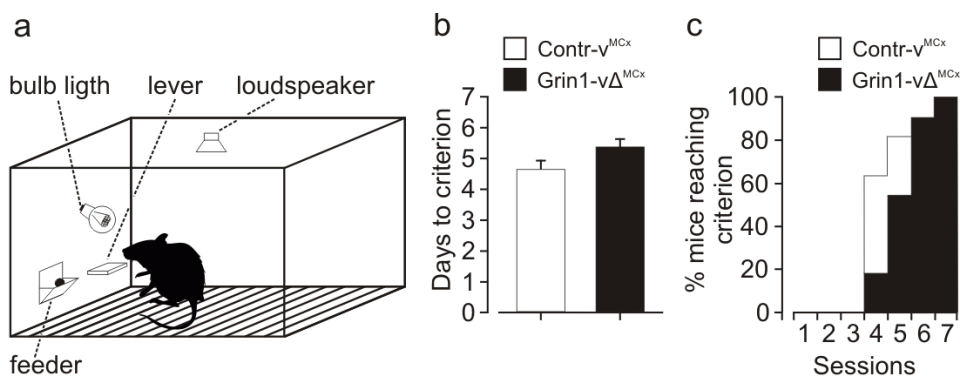


**Figure 4.4. Performance for a fixed ratio 1:1 operant conditioning task.** Experimental set-up. Mice were trained in a Skinner box to press a lever to obtain a food pellet with a fixed-ratio (1:1) schedule. **b.** Number of days necessary to reach criterion (mean  $\pm$  SEM) for Contr- $v^{MCx}$  (white bar) and Grin1- $v\Delta^{MCx}$  (black bar) mice. **c.** Percentage of mice reaching criterion across training. Note in (b) and (c) those Contr- $v^{MCx}$  mice ( $n=10$ ) reached criterion before Grin1- $v\Delta^{MCx}$  ( $n=11$ ) mice.



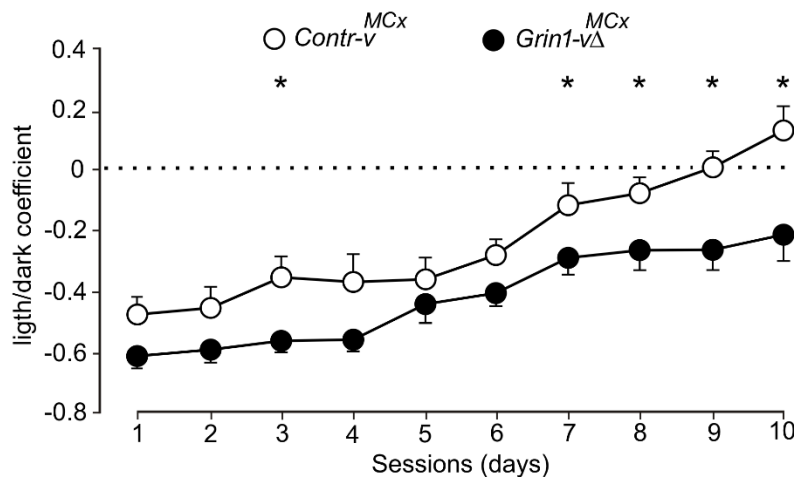


**Figure 4.5. Performance during a complex operant conditioning tasks.** Performance of the light/dark test. After reaching criterion for a fixed (1:1) schedule, animals were presented with a more difficult task in which lever presses were rewarded only when a light bulb was switched on. In this situation, Contr-*v*<sup>MCx</sup> mice presented a significantly ( $*P \leq 0.05$ , two-way ANOVA) better performance than Grin1-*v*Δ<sup>MCx</sup> mice. The light/dark coefficient was calculated as: (number of lever presses during the light period – number of lever presses during the dark period)/total number of lever presses (mean  $\pm$  SEM).

## EXPERIMENT 2

### 4.2. CONTRIBUTION OF PRL CORTEX IN EARLY PHASES OF INSTRUMENTAL LEARNING

#### 4.2.1. Validation of a Skinner box with touch-screen.

In order to understand how the use of a tactile touch-screen as a cue, instead of a lever in the operant Skinner box, affects learning performance in the Skinner box, a comparative study was designed among these different “manipulandi” (or cues; lever vs. touch-screen) as experimental variable. Animals were divided in two groups ( $n = 5$  each) and trained until reaching criterion (obtaining  $> 80$  pellets for two consecutive sessions) in a conventional Skinner box, as well as in a modified box including a multi-touch (iPad®) screen, using in both cases a fixed ratio 1 (FR1) (Fig. 4.6a). Although performance with the touch screen was significantly lower than with the lever [ $F_{(1,9,98)} = 4.896$ ,  $P = 0.028$ , two-way ANOVA] (Fig. 4.6b), the two groups of animals reached the selected criterion at similar number of sessions [ $F_{(1,9,8)} = 0.395$ ,  $P = 0.547$ , one-way ANOVA] (Fig. 4.6c). Both tasks (press the lever and touch the button on the iPad) were employed in a later experimental step in where an operant learning paradigm was performed by other groups of rats.

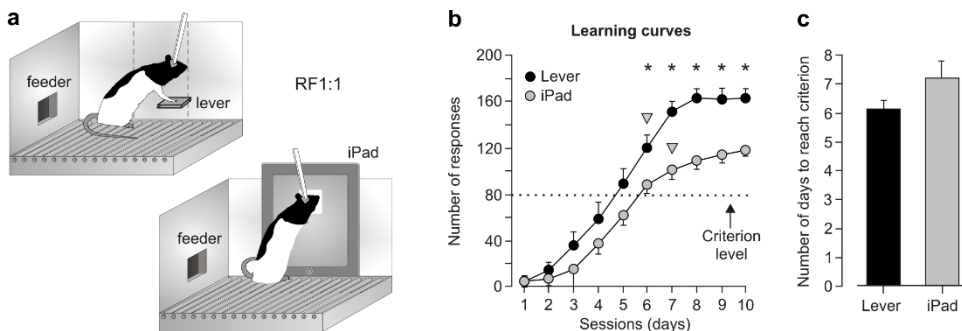


**Figure 4.6. Validation of the touch-screen system compared with a classic lever one using the same instrumental conditioning paradigm.** **a.** Design of the two different Skinner box that were compared. **b.** Learning curves corresponding to the two groups of rats. The selected criterion was to obtain  $> 80$  pellets for two successive sessions (gray triangles). Asterisks indicate significant differences [ $F_{(1,9,98)} = 4.896$ ,  $P = 0.028$ , two-way ANOVA] for the number of responses between the group trained in the conventional Skinner box and the Skinner box modified with touch-screen tablet. **c.** The touch-screen group reached the selected criterion after the lever group, but without significant differences [ $F_{(1,9,8)} = 0.395$ ,  $P = 0.547$ , one-way ANOVA].

#### 4.2.2. Input/output curves and paired pulse stimulation test

In a first experimental step, we obtained the input/output curves for the thalamocortical and mesocortical pathways by means of the presentation of single pulses to the MDTh and the VTA at different increasing intensities, which evoked in the PrL area the corresponding field PSPs (**Fig 4.7a**). Both curves showed similar sigmoidal shapes and similar maximum field PSPs amplitude for the same intensity ( $t_{(23,0.05)} = 0.296$ ,  $P = 0.771$ , Student's  $t$ -test) suggesting normal functioning of both synapses.

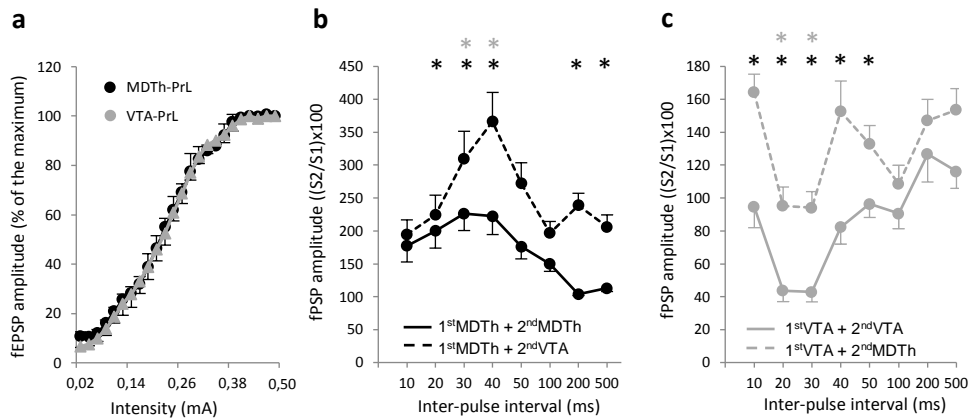


**Figure 4.7. Input/output curves and paired-pulse stimulation test of the MDTh-PrL and VTA-PrL synapses.** **a.** Relationship between the intensity (in mA) of a single stimulus in MDTh (black circles) or VTA (gray circles) and the amplitude of the field PSPs evoked in the PrL. **b.** Responses to paired-pulse stimulation with facilitation. Field PSPs were evoked in PrL with a pair of pulses in MDTh (black circles and continuous line) or a first pulse in MDTh and a second pulse in VTA (black squares and dashed line). **c.** Responses to paired-pulse stimulation with partial depression. Field PSPs were evoked in PrL with a pair of pulses in VTA (gray circles and continuous line) or a first pulse in VTA and a second pulse in MDTh (gray squares and dashed line) for eight (10, 20, 30, 40, 50, 100, 200 and 500 ms) interstimulus intervals. The data shown are mean  $\pm$  SEM amplitude of the second fPSP expressed as a percentage of the first. These data were collected from 5 animals. Grey asterisks indicate significant paired pulse facilitation or depression for groups represented with continuous line. Black asterisks show significant differences between dashed line and continuous line groups.

Paired-pulse stimulation test was performed at 0,20 mA of intensity (40% of the intensity for maximum field PSP amplitude) and eight interstimulus intervals (10, 20, 30, 40, 50, 100, 200 and 500 ms). Two modalities of paired-pulse interstimulus were applied in each one of the pathways. In thalamocortical pathway two consecutive pulses in MDTh (1<sup>st</sup>MDTh + 2<sup>nd</sup>MDTh) for each one of the different interstimulus intervals and a combination of a first pulse in MDTh followed by a second pulse in VTA (1<sup>st</sup>MDTh + 2<sup>nd</sup>VTA). Both curves showed a similar evolution for each pulse interval but the combined mode of pulses (1<sup>st</sup>MDTh + 2<sup>nd</sup>VTA) generated a larger amplitude of field PSPs that were

significantly for intervals from 20 to 40 ms and 200 to 500 ms [ $F_{(7,144,159)} = 2.420$ ,  $P = 0.023$ , two-way ANOVA, multi-comparison Holm-Sidak method  $P \leq 0.036$ ] (black asterisks in **Fig. 4.7b**). Moreover, there was facilitation in both modalities but only significantly [ $F_{(7,144,159)} = 2.420$ ,  $P = 0.023$ , two-way ANOVA, multi-comparison Holm-Sidak method  $P \leq 0.040$ ] for the combination of pulses in different sites (1<sup>st</sup>MDTh + 2<sup>nd</sup>VTA; grey asterisks in **Fig. 4.7b**) in response to the second pulse for time intervals between 30 and 40 ms. The mesocortical pathway showed an opposite evolution. VTA stimulation (continuous grey line in **Fig. 4.7c**) provoked paired pulse depression for short interstimulus intervals (20-30 ms) that was statistically significant [ $F_{(1,144,159)} = 2.074$ ,  $P \leq 0.05$ , two-way ANOVA, multi-comparison Holm-Sidak method  $P \leq 0.05$ ] (grey asterisks in **Fig. 4.7c**) and a slight facilitation for long interstimulus intervals (200-500 ms). Again, combination of pulses in different sites but in opposite order (a first pulse in VTA and a second in MDTh; dashed grey line in **Fig. 4.7c**) generated an evolution of the amplitudes of field PSPs similar to that observed in the stimulation with two consecutive pulses in VTA (1<sup>st</sup>VTA + 2<sup>nd</sup>VTA) but significantly greater for interstimulus interval from 10 to 50 ms [ $F_{(1,144,159)} = 23.749$ ,  $P \leq 0.003$ , two-way ANOVA, multi-comparison Holm-Sidak method  $P \leq 0.05$ ] (black asterisks in **Fig. 4.7c**).

#### *4.2.3. PrL inactivation with lidocaine and HFS on thalamocortical and mesocortical pathways*

Another test of interest to typify the synaptic functioning in the PrL was the study of the HFS effect in some important synaptic afferents to this area: the thalamocortical and the mesocortical convergent paths. For that, HFS protocol in MDTh and VTA and the corresponding fPSPs evolution was recorded in PrL mPFC were carried out in rats in which PrL cortex activity was inhibited with lidocaine (“lidocaine” in **Fig. 4.8**) and in a control group without any sort of pharmacological treatment but injected with a saline vehicle (“sham” in **Fig. 4.8**). Single pulses in MDTh and recording of the evoked fPSP in PrL (thalamocortical synapse) evidenced a significant LTP [ $F_{(1,168,215)} = 19.803$ ,  $P \leq 0.001$ , two-way ANOVA, multi-comparison Holm-Sidak method,  $P \leq 0.043$ ] compared with the group of rats treated with lidocaine (**Fig 4.8a**). Curiously, next day to the HFS, both groups showed a slight potentiation of the MDTh-PrL synapse. Moreover, the same stimulation protocol in MDTh evoked in the control group an early synaptic potentiation in mesocortical (VTA-PrL) synapse that lasted approximately 10 minutes [ $F_{(1,168,215)} = 16.149$ ,  $P \leq 0.001$ , two-way ANOVA, multi-comparison Holm-Sidak method,  $P \leq 0.05$ ] but this HFS had no effect in the group of rats injected with lidocaine (**Fig. 4.8b**).

HFS in VTA sham group induced a short and slight depression in thalamocortical synapse lasting 30 minutes (**Fig 4.8c**). These results and the data previously described above suggest some sort of functional relationship between thalamocortical and mesocortical paths. The group with lidocaine did not show any change after HFS but there was a significant increase in fPSPs during the second day in the thalamocortical synapse [ $F_{(1,168,215)} = 2.682$ ,  $P < 0.001$ , two-way ANOVA, multi-comparison Holm-Sidak method,  $P \leq 0.05$ ].

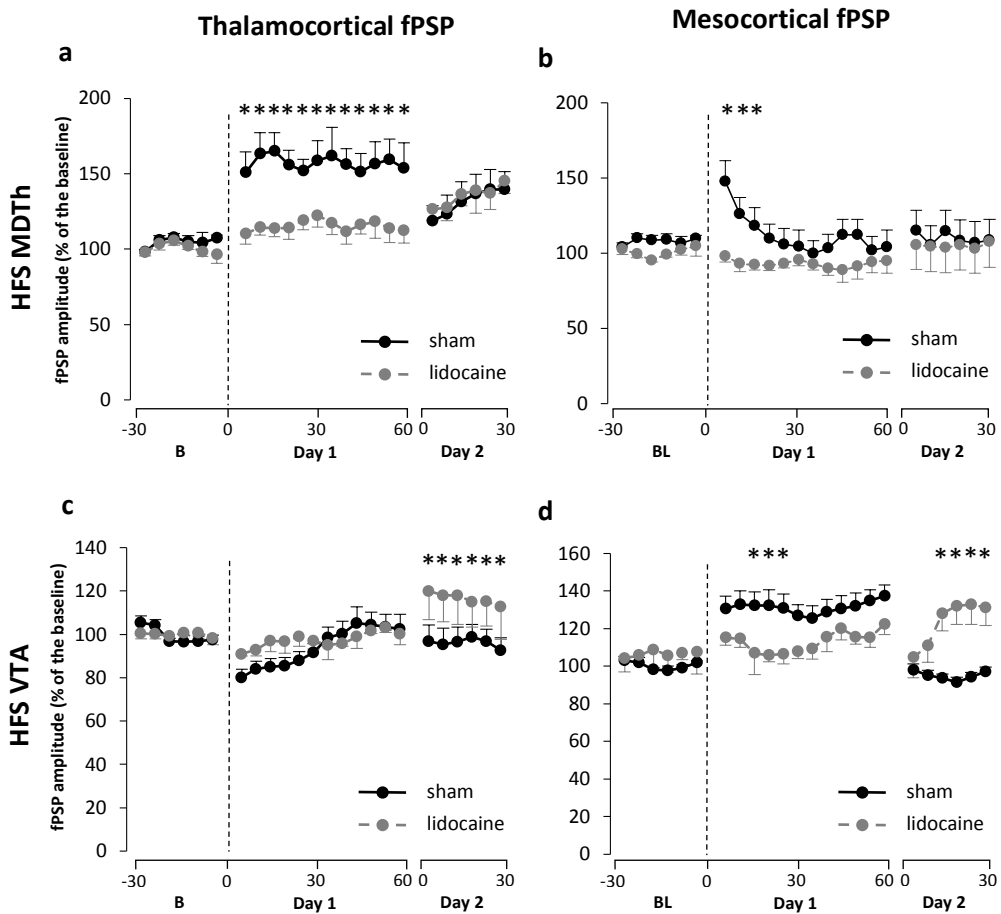


**Figure 4.8. HFS effect in thalamocortical and mesocortical synapses.** The graph illustrates the time course of LTP evoked in the PrL cortex (fPSP mean  $\pm$  SEM) following HFS for sham group (black line and circles) and rats with PrL activity inhibition by lidocaine infusion (grey line and circles). The HFS was presented after 30 minutes of baseline recordings, at the time indicated by the dashed line. The fPSP is given as a percentage of the baseline (B = 100%) slope. Lidocaine group of rats had no LTP after MDTh HFS or after VTA HFS (see **a**, **b**, **c**, and **d** grey line and circles). In addition, values collected from the sham group were significantly ( $P < 0.05$ ; two-way ANOVA) larger than those collected from lidocaine group for thalamocortical synapse after HFS in MDTh (**a**) and mesocortical synapse after HFS in MDTh (**b**) and HFS in VTA (**d**).

Finally, this HFS in VTA evoked a significant long-lasting potentiation greater than the group of rat injected with lidocaine (**Fig 4.8d**). However, the second day after HFS this group showed that potentiation after ten minutes of recording as was observed in thalamocortical synapse [ $F_{(23,120,167)} = 2.682$ ,  $P < 0.001$ , two-way ANOVA, multi-comparison Holm-Sidak method,  $P \leq 0.05$ ].

#### 4.2.4. Lidocaine inactivation of PrL cortex during an instrumental learning

*Lever Task Stage.* Two groups of 5 rats performed an instrumental learning paradigm in a Skinner box in which pressing a lever delivered a pellet (reward) in a fixed ratio 1 (FR1). The aim of this first experimental step was to check these tens animals were able to perform an instrumental learning task with similar capability in order to be divided into two groups (“sham” and “lidocaine”) of equal skills for subsequent test. Both groups carry out this paradigm without differences in task performance [ $F_{(1,45,62)} = 0.798$ ,  $P = 0.376$ , two-way ANOVA]; **Fig. 4.10b Lever Task**). In addition, the evolution of fPSP in the thalamocortical synapse presented a similar progress in both groups of rats [ $F_{(8,54,71)} = 0.355$ ,  $P = 0.939$ , two-way ANOVA] (**Fig. 4.9a Lever Task**). During the recording of the fPSPs in the “lever task” stage (**Fig. 4.9.a “Lever Task”**) a significant increase of the synaptic strength in the fourth day was observed in both groups [ $H = 19.145$  with 8 degrees of freedom,  $P = 0.014$ , Kruskal-Wallis One Way Analysis of Variance on Ranks; Multiple Comparison (Tukey Test); grey asterisk in “Lever Task”], [ $H = 24.937$  with 8 degrees of freedom,  $P = 0.002$ , Kruskal-Wallis One Way Analysis of Variance on Ranks; Multiple Comparison (Tukey Test); black asterisk in “Lever Task” ] that immediately decreased to basal levels the next day. This potentiation of the thalamocortical synapse coincided with the first days of maximum performance of the task (**Fig 4.10b, Lever Task**).

Similar result were obtained for fPSPs evolution of the mesocortical synapse during the performance of the instrumental conditioning with lever in both groups (lidocaine and sham) [ $F_{(8,54,71)} = 0.355$ ,  $P = 0.939$ , two-way ANOVA]. fPSPs showed a slight increase in synaptic strength during the third and fourth session (**Fig. 4.10a, “Lever Task”**) but not significantly in any group of rats [ $F_{(8,32,36)} = 1.262$ ,  $P = 0.303$ , one-way ANOVA], [ $F_{(8,32,36)} = 1.320$ ,  $P = 0.276$ , one-way ANOVA].

*Task Change Stage.* Once rats correctly performed this modality of instrumental conditioning the lever was substituted by a touch-screen tablet in order to begin a new instrumental learning paradigm in which one group of rats was intracranially injected with lidocaine through a cannula implanted in the PrL cortex and a sham group was used as control group injecting a saline vehicle to investigate the roll of

the PrL cortex during the early phase of learning in which is observed the increase of the synaptic strength seen in the previous experimental step. Thalamocortical and mesocortical synapses exhibited a decrease of the fPSP amplitudes after the change of the task into the Skinner box that was replicated in all groups of rats.

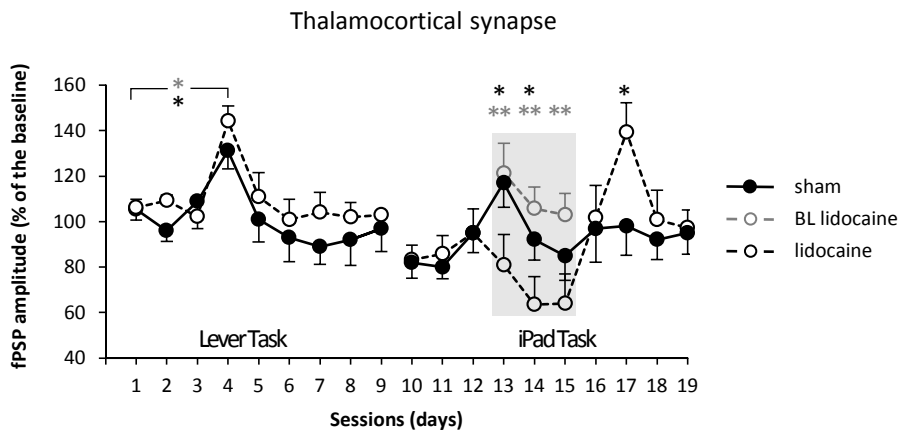


**Figure 4.9. Evolution of fPSPs in the thalamocortical synapse during instrumental learning.** Two different task are shown “Lever Task” and “iPad Task” for two groups of rats “sham” (black circles and continuous line) and “lidocaine” (white circles and black, dashed line). Base-line for lidocaine group (white circles and grey, dashed line) was recorded before lidocaine injection (shaded grey box). Black asterisks indicate statistical significance between “sham” and “lidocaine” groups; grey asterisks compare “BL lidocaine” versus “lidocaine” groups.

*iPad Task Stage.* Every day a base-line was recorded during ten minutes to check the day in which the amplitude of the MDTh fPSPs was increased with the porpoise of inhibiting the PrL cortex. The fourth day of instrumental conditioning lidocaine or saline was infused (depending on the group of rats, “lidocaine” or “sham” respectively), every day (and during 3 consecutive days) before training session, through a cannula implanted in the PrL area of the mPFC. Lidocaine group performed the task significantly worse than the sham group [ $F_{(1,12,17)} = 108.984$ ,  $P < 0.001$ , two-way ANOVA, multi-comparison Holm-Sidak method]. In particular, sham group reached criterion (obtaining  $> 80$  pellets for two consecutive sessions) 3 days before lidocaine group (**Fig. 4.10b**). Moreover it was recorded a significant decrease of the lidocaine group fPSPs by effect of the drug in the thalamocortical synapse compared with the base-line before injecting the drug [ $F_{(1,12,17)} = 27.630$ ,  $P < 0.002$ , two-way ANOVA, multi-comparison Holm-Sidak method; **Fig. 4.9a**, grey asterisks in “iPad Task” ] and the sham group [ $F_{(1,12,17)} = 7.349$ ,  $P < 0.019$ , two-way ANOVA, multi-comparison Holm-Sidak method; **Fig. 4.9a**, black asterisks in “iPad Task”]. Similar effects were detected in mesocortical synapse after infusion of lidocaine which provoked an amplitude decrease of the fPSPs in

lidocaine group compared with the base-line [ $F_{(1,12,17)} = 11.657$ ,  $P < 0.005$ , two-way ANOVA, multi-comparison Holm-Sidak method] and the sham group of rats [ $F_{(1,15,20)} = 5.776$ ,  $P < 0.030$ , two-way ANOVA, multi-comparison Holm-Sidak method].

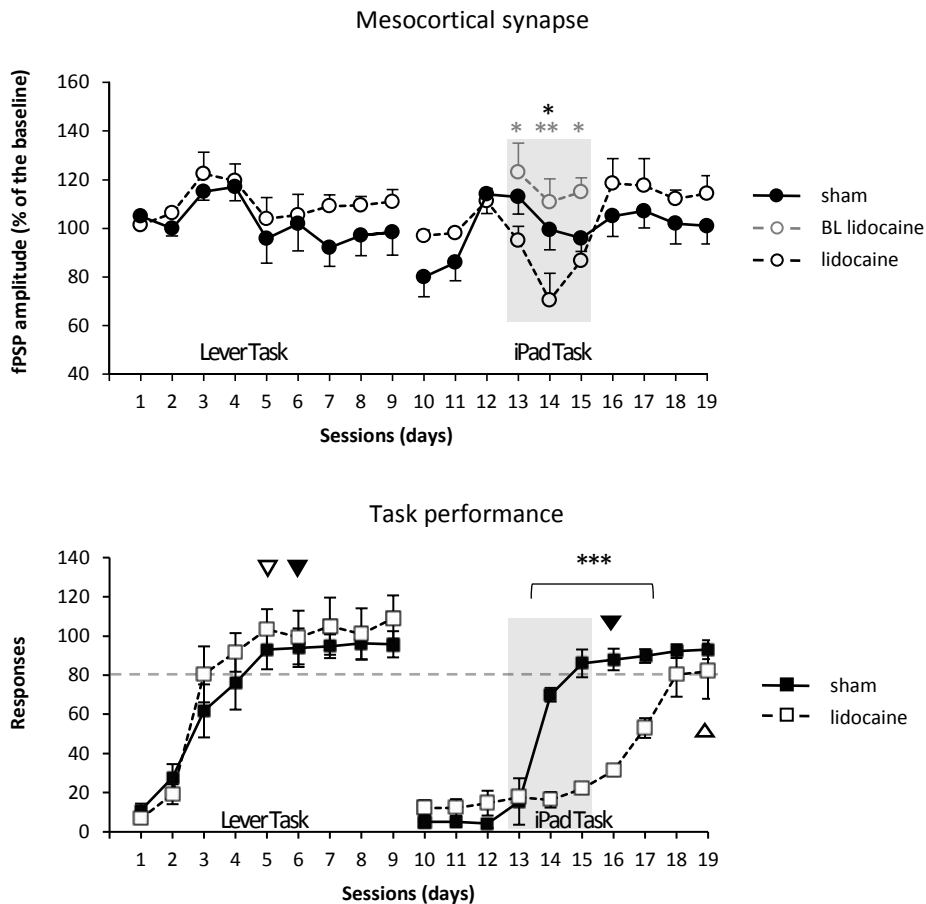


**Figure 4.10. Evolution of fPSPs in the mesocortical synapse and task performance during the instrumental learning.** **a.** Two different task are shown “Lever Task” and “iPad Task” for two groups of rats “sham” (black circles and continuous line) and “lidocaine” (white circles and black, dashed line). Base-line for lidocaine group (white circles and grey, dashed line) was recorded before lidocaine injection (shaded grey box). Black asterisks indicate statistical significance between “sham” and “lidocaine” groups; grey asterisks compare “BL lidocaine” versus “lidocaine” groups. **b.** Task performance of two groups of rats: “sham” (black squares and continuous line) and “lidocaine” (white squares and black, dashed line). Black asterisks indicate statistical significance between both groups. Significant differences are indicated. \*,  $P < 0.05$ ; \*\*,  $P < 0.01$ ; \*\*\*,  $P < 0.001$ .

Again, the increase in the amplitude of the fPSPs during the early phase (3<sup>rd</sup> - 4<sup>th</sup> day) of learning of this new task (iPad) was observed in the sham group of rats in thalamocortical (**Fig 4.9**, iPad Task, 13<sup>th</sup> session) and mesocortical (**Fig**



**4.10a**, iPad Task synapse, 12<sup>th</sup> and 13<sup>th</sup> sessions). The rats injected with lidocaine exhibited this increase in fPSPs during the recording of the base-line (grey, dashed circles and line during iPad Task in **Fig 4.9** and **Fig. 4.10a**) but it decreased after drug injection. One important point to take into account is the significant increase of the amplitude of the fPSPs in thalamocortical synapse during the execution of the iPad task (**Fig. 4.9**, black asterisk in lidocaine group and session 17) that coincided with the progressive improve in the iPad task performance (**Fig 4.10b**, lidocaine group, 17-19<sup>th</sup> sessions).

### EXPERIMENT 3

#### 4.3. NEURAL ACTIVITY CHANGES DURING AN ASSOCIATIVE LEARNING WITH BCIS

##### 4.3.1. Validation of a wireless recording system.

In order to understand how the presence or absence of recording cables between the animal and the recording system can interfere in the development of the learning task in the Skinner Box, a comparative study was designed among these two different types of data transferring (plugged vs wireless) as experimental variable. In this experiment, animals were divided in two groups ( $n = 5$  each) and trained until reaching criterion (obtaining  $> 80$  pellets for two consecutive sessions) in a modified Skinner box including a multi-touch (iPad®) screen, using in both cases a fixed ratio 1 (FR1). Animals were implanted with either recording wires ( $n = 5$ ) or a wireless system ( $n = 5$ ). Both groups of animals reached the selected criterion at similar times [ $F_{(1,9,8)} = 0.037$ ,  $P = 0.853$ , one-way ANOVA].

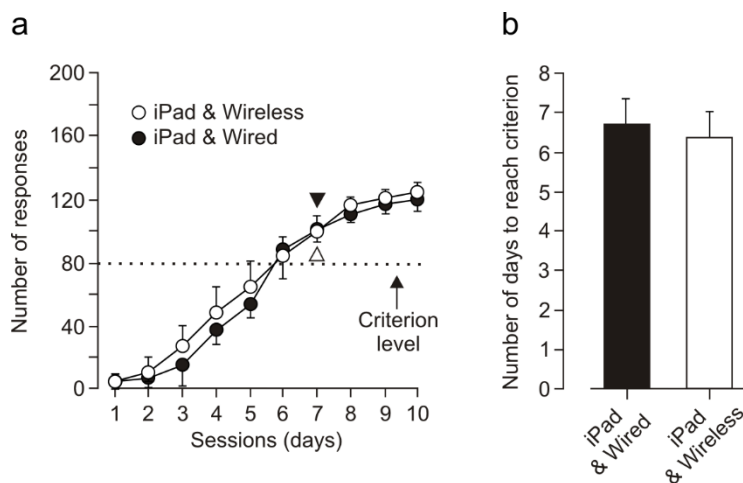


**Figure 4.11. Validation of the wireless system compared with a classic wired system using the same instrumental conditioning paradigm. a.** Learning curves corresponding to the two groups of rats. The selected criterion was to obtain  $> 80$  pellets for two successive sessions (yellow triangles). There was not significant differences [ $F_{(1,9,98)} = 0.013$ ,  $P = 0.911$ , two-way ANOVA] between the group trained with the wireless system and the wired system group. **b.** The two groups reached the selected criterion similarly [ $F_{(1,9,8)} = 0.037$ ,  $P = 0.853$ , one-way ANOVA].

### 4.3.2. Properties of the transition pattern

The analysis of LFPs recorded during those operant conditioning sessions, carried out in the box equipped with the touch screen, showed the presence of short time periods ( $<1$  s) characterized by a marked decrease in spectral power, mostly in the  $\theta$  band (**Fig. 4.13a, b, d and e**)

This peculiar pattern appeared during performance of specific behaviors, such as remaining still (i.e., motionless but without freezing) in the cage, and during rearing or looking into the feeder (**Fig. 4.12a, b and c** respectively).

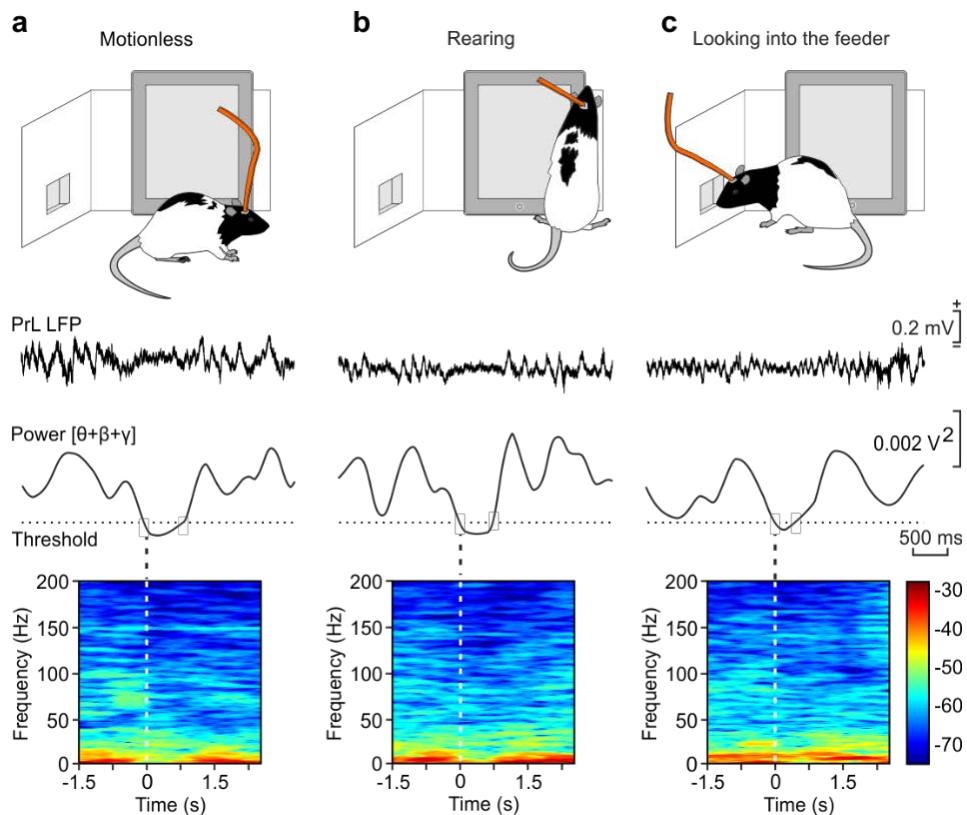
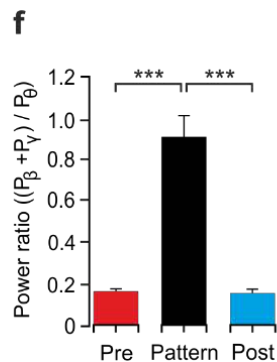
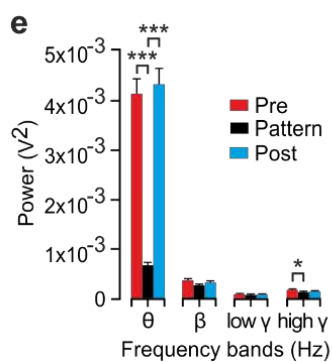
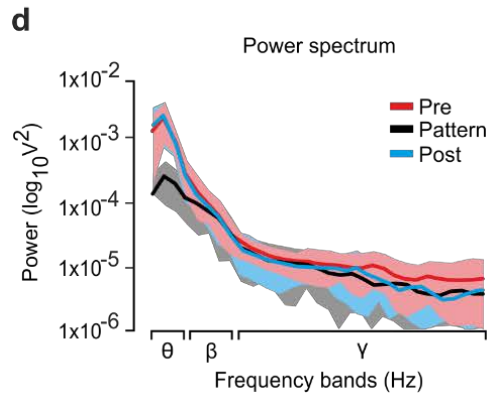
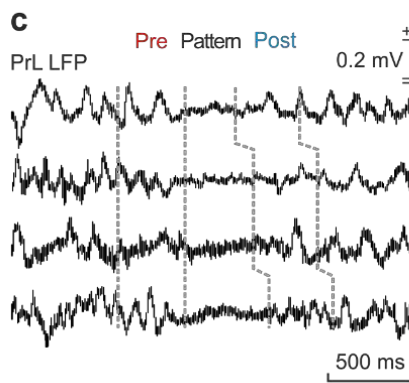
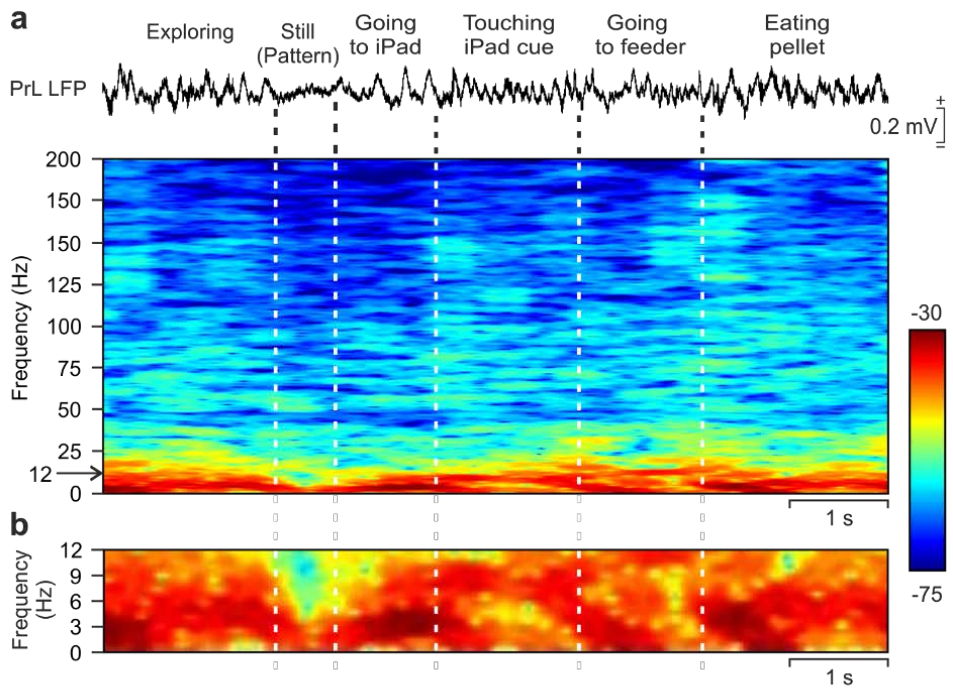


**Figure 4.12. Different behaviors during which the selected oscillatory transition pattern was recorded in the PrL cortex. a, b, c.** Representative examples of LFPs recorded in the PrL cortex during the performance of the illustrated behaviors: (a), motionless; (b), rearing; and (c), looking into the feeder. For (a-c) and from top to bottom are illustrated the selected behavior, the corresponding LFP pattern, the evolution of the added spectral power for the  $\theta + \beta + \gamma$  bands across the recorded LFP, and the time-frequency representation of the LFP illustrated above. Note the decreased power of the  $\theta$  band during the pattern. Analyses illustrated here were carried out with the help of the Chronux application programmed in Matlab.

The power in the  $\theta$  band was decreased significantly ( $\chi^2 = 150.32$ , freedom degrees = 2,  $P \leq 0.001$ , Friedman test) during the presence of this selected activity when it was compared with the periods of time immediately before (Pre) and after (Post) it (**Fig. 4.13d, e**). Smaller but significant differences ( $\chi^2 = 18.98$ , freedom degrees = 2,  $P \leq 0.05$ , Friedman test) were found for the high- $\gamma$  band between Pre and Pattern periods (**Fig. 4.13e**) due to a decrease of the power in this frequency oscillatory band during the generation of the pattern and subsequently.

At this stage, we wondered whether this peculiar oscillatory transition pattern could be used to trigger the presentation of the selected visual display on the touch screen. In this way, the experimental animal would be able to control the iPad® with a specific LFP pattern generated in its PrL cortex. In order to facilitate this task, we quantified two parameters: the spectral power for the  $\theta + \beta + \gamma$  bands (Supplementary Fig. S4) and the power ratio =  $(P_\beta + P_\gamma) / P_\theta$  during the Pre, Pattern, and Post periods (**Fig. 4.13f**), but only the first parameter was used as iPad® trigger (see **Fig. 3.6 in Material and Methods**). Pre and Post periods presented similar power ratio values (0.17 and 0.16, respectively,  $\chi^2 = 136.82$ , freedom degrees = 2,  $P > 0.05$ ; Tukey post hoc test for Friedman test). In contrast, the power ratio for the Pattern period reached a value significantly larger (0.91,  $\chi^2 = 136.82$ ; freedom degrees = 2,  $P \leq 0.001$ , Tukey post hoc test for Friedman test). Quotients between *Pre/Pattern* or *Post/Pattern* periods for each power spectral ( $\theta$ ,  $\beta$  and  $\gamma$ ) band yielded similar values (**Fig. 4.13g**). The quotient for  $\theta$  band was approximately 6 times larger for the *Pre/Pattern* (6.19) and *Post/Pattern* (6.47) periods, but  $\beta$  and  $\gamma$  frequency bands presented minor differences (**Fig. 4.13g**). On the whole, these analyses indicate that the selected pattern was mainly characterized by a notable decrease in the  $\theta$  band during the Pattern period.



**g**

Ratio	■ : ■	■ : ■
$\theta$	6.19	6.47
$\beta$	1.38	1.23
low $\gamma$	0.99	1.00
high $\gamma$	1.39	1.12

**Figure 4.13. Functional characteristics of the selected oscillatory transition pattern during a single operant conditioning sequence.** **a.** Dynamic changes in LFP activity recorded in the PrL cortex during a sequence of behaviors performed during operant conditioning task. From top to bottom are illustrated the behaviors and LFPs recorded in the PrL during this time window. The time-frequency representation of this LFP activity is included below. Note the dominant spectral power (in dB, see the calibration bar) in the  $\theta$  band across the whole behavioral sequence, but its decrease during the moment ( $> 1$  s) when the rat was still (motionless) before approaching the touch screen. **b.** An enlargement of the time-frequency analysis corresponding to the band of 0-12 Hz. **c.** Four examples of the selected oscillatory transition pattern. *Pre* and *Post* delimit (as indicative time periods for subsequent analysis) the LFP activity during the 350 ms preceding and following the decrease in spectral power in the  $\theta$  band. **d.** Averaged ( $n = 40$  samples; mean  $\pm$  SD) power spectrum of each of the three periods (*Pre*, *Pattern*, *Post*) delimited in **c**. Note the large difference in the power for the  $\theta$  band during the pattern. **e.** Analysis of the spectral power of the  $\theta$ ,  $\beta$ , low- $\gamma$  and high- $\gamma$  bands for data illustrated in **d** ( $\chi^2 = 150.32$ , freedom degrees = 2,  $P \leq 0.001$  for the  $\theta$  band and  $\chi^2 = 18.98$ , freedom degrees = 2,  $P \leq 0.05$  for the high- $\gamma$  band, Friedman test). **f.** Power ratio index of  $\beta + \gamma$  bands with respect to the  $\theta$  band [Power ratio =  $(P_\beta + P_\gamma) / P_\theta$ ] for each of the three periods ( $n = 100$  samples collected from 5 animals;  $\chi^2 = 136.82$ , freedom degrees = 2,  $P \leq 0.001$ , Friedman test). **g.** Quotients for the spectral powers of each frequency band corresponding to LFPs recorded before and during the pattern (*Pattern/Pre*, second column) and after and during the pattern (*Pattern/Post*, third column). These ratios were computed from the data illustrated in **e**.

#### 4.3.3. Learning curves for instrumental conditioning tasks.

In a second series of experiments, a group of implanted rats were trained to touch a visual display that appeared automatically on the touch screen (**Fig. 4.14a**). In this situation, they reached criterion between the 5th and the 9th conditioning sessions (*Automatic cue*; **Fig. 4.14c**). Rats were maintained with this operant task for up to 11 sessions and then they were trained to activate the appearance of the same visual display with the generation of the selected oscillatory pattern (**Fig. 4.14b**). In order to trigger the appearance of a visual display on the touch screen a program was implemented to detect the oscillatory transition from *Pre* to *Pattern* periods (**Fig. 4.13c**) with a delay of  $< 0.25$  s. During the initial operant task the rats spontaneously generated the pattern  $24 \pm 4$  times per recording session (**Fig. 4.14**, *Automatic cue* stage, black circles) but in this new situation mediated through a BCI, rats presented a constant increment in the number of oscillatory transition patterns during the first eight sessions, followed by a stabilization ( $80 \pm 9$  patterns and  $\approx 60$  touches) from the 9th to the 18th training sessions (*Pattern-evoked cue*; **Fig. 4.14c**). Although the number of evoked patterns reached criterion, the number of screen touches did not (**Fig. 4.14c**, *Pattern-evoked cue* stage, black and white circles respectively).

As illustrated in **Fig. 4.14c**, there were no significant changes in the number of oscillatory transition patterns for the two baseline (*B*) and 11 training sessions (*Automatic-cue*) in which the visual display was presented automatically ( $P > 0.05$ ). In contrast, during the sessions in which the visual display was triggered by the oscillatory transition pattern (*Pattern-evoked cue*), the number of screen touches progressed in parallel with a significant ( $F_{(30,270,310)} = 9.007$ ,  $P \leq 0.001$ , one-way ANOVA) increase in the number of pattern generations from the 6th to the 13th conditioning sessions.

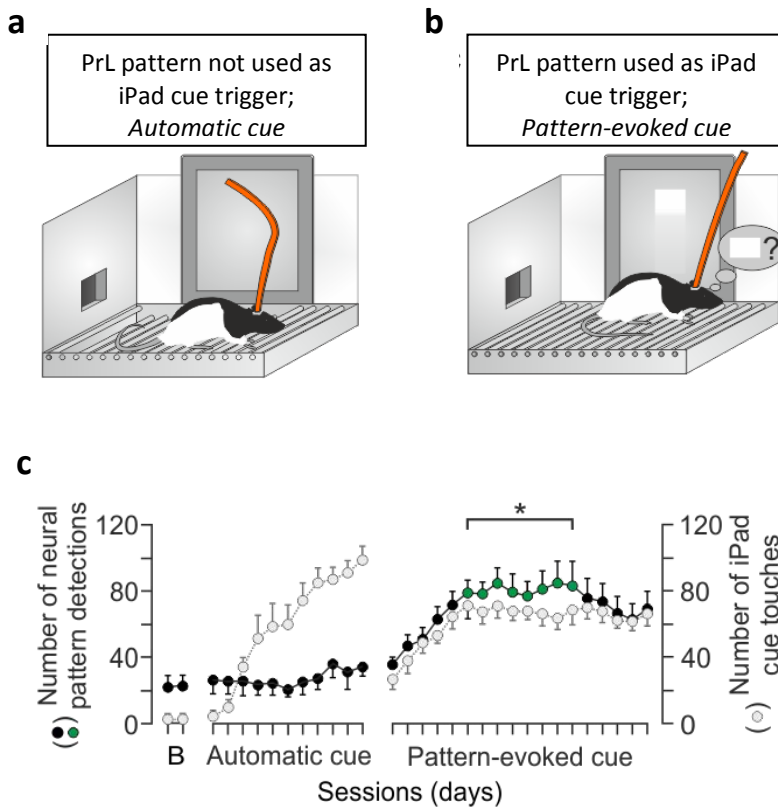


**Figure 4.14. Evolution of the selected oscillatory transition pattern across training with the touch-screen task.** **a.** Diagram of the first experimental stage for instrumental conditioning with iPad and RF1 schedule. During this stage, the cue (a white square) automatically appeared on the touch-screen display at random. **b.** Diagram of the second experimental stage for oscillatory activity conditioning. In this phase, the generation of the PrL pattern activated the cue on the touch-screen. The neural patterns detected during both sessions were recorded **c.** Evolution of the number of screen touches during baseline (*B*) recordings, when the square virtual button display appeared automatically on the touch screen (*Automatic cue*) and when its appearance was triggered by the oscillatory transition pattern recorded in the PrL cortex (*Pattern-evoked cue*). Data collected and averaged from 10 animals. Note that pattern presentation showed no significant ( $P > 0.05$ ) changes during *automatic cue* sessions, but increased significantly (green circles; [ $F_{(1,9,339)} = 30.096$ ,  $P \leq 0.001$ , two way ANOVA]) for *pattern-evoked cue* sessions.

#### 4.3.4. Changes in duration and power ratio index $[\theta/(\beta+\gamma)]$ after the use of the pattern in a BCI

We checked whether the use of the oscillatory transition pattern to trigger the iPad® modified its properties regarding duration and the values reached by the power ratio index  $[\theta/(\beta+\gamma)]$ . As shown in **Fig. 4.15a**, when used to trigger the iPad® (*Pattern-evoked cue*), the duration of the pattern increased steadily from the 1st to the 8th training sessions (from 150 ms to 197 ms,  $\chi^2 = 47.098$ , freedom degrees = 30,  $P \leq 0.05$ , Friedman test), decreasing afterwards to intermediate values (from 186 ms to 160 ms). In contrast, the power ratio reached peak values at the end of the automatic cue sessions, being significantly smaller during pattern evoked cue sessions ( $\chi^2 = 55.423$ , freedom degrees = 30,  $P \leq 0.05$ , Friedman test; **Fig. 4.15b**). The use of the oscillatory transition pattern to trigger the touch screen introduces small but significant changes in its duration and spectral power characteristics.

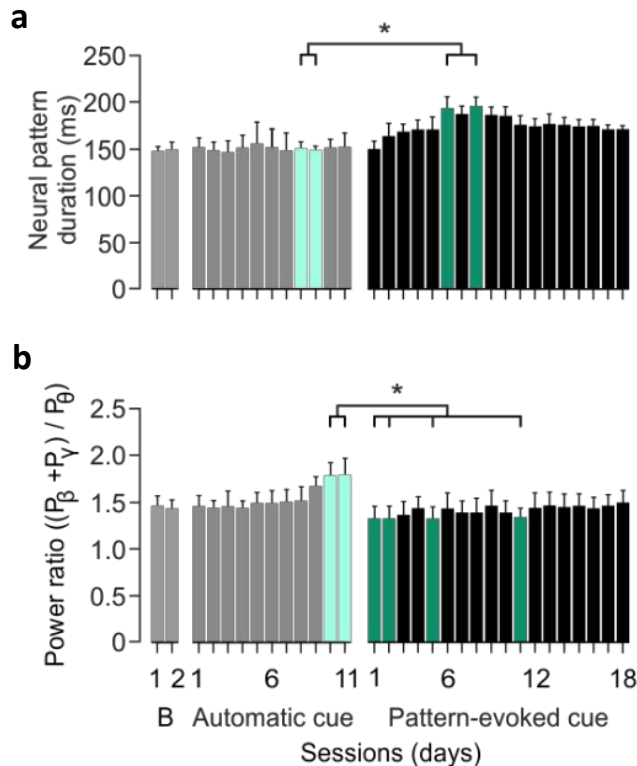


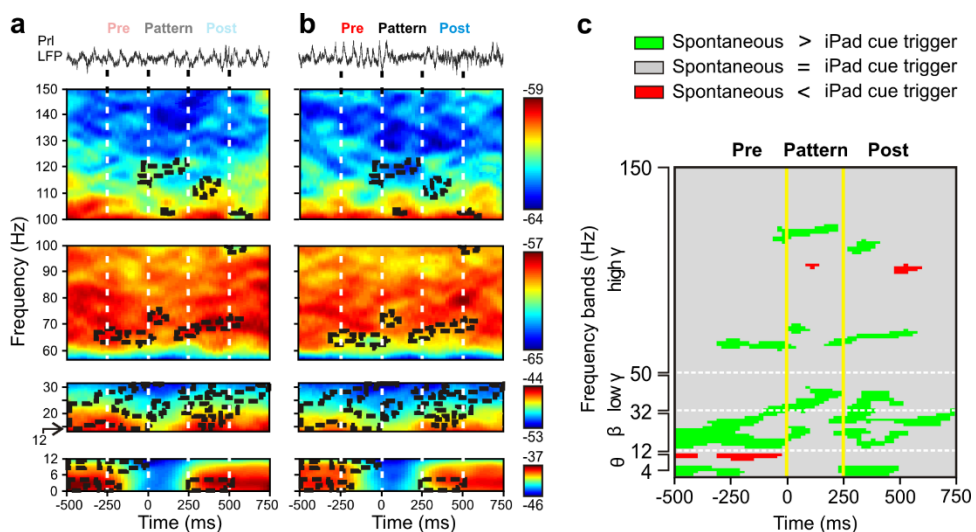
**Figure 4.15. Evolution of pattern duration and power ratio index  $[(P_\beta + P_\gamma) / P_\theta]$  across training sessions.** **a.** Note the slight increase in duration across the first sessions in which the pattern was used to trigger the visual display on the touch screen (*Pattern-evoked cue*). Significant differences are indicated between cyan and green color bars ( $\chi^2 = 47.098$ , freedom degrees = 30,  $P \leq 0.05$ , Friedman test). This increase in pattern duration disappeared after the first 10 sessions of the *pattern evoked cue* stage. **b.** Evolution of the power ratio  $(P_\beta + P_\gamma) / P_\theta$  across training sessions. Power ratio was larger for *automatic* than for *pattern-evoked cue* sessions. Significant differences are indicated between cyan and green color bars ( $\chi^2 = 55.423$ , freedom degrees = 30,  $P \leq 0.05$ , Friedman test).



#### 4.3.5. Changes in spectral power property of the pattern used as a trigger in a BCI

These previous different results of the power ratio index between the instrumental conditioning paradigm (*Automatic cue*) and the oscillatory activity conditioning paradigm (*Pattern-evoked cue* stage) led us to accurately evaluate how the use of the LFP pattern as a trigger modified its spectral characteristics. As mentioned above, rats, already trained to touch the screen to obtain a reward (*Automatic cue* in **Fig.4.14** and **Fig. 4.15**), generated spontaneously the oscillatory transition pattern when looking towards the feeder, motionless in the cage, or rearing (**Fig. 4.12a-c**). When the pattern was used to activate the touch screen (*Pattern-evoked cue*), the rat usually generated it by standing still near the iPad® (first and second row of the sequence of images in **Fig. 3.5**).

**Fig. 4.16a** and **b** shows an averaged (150 times) time–frequency representation (1250 ms time window) triggered by the oscillatory transition



**4.16. Differences in the spectral properties of the selected oscillatory transition pattern when generated spontaneously and when used to trigger touch-screen cues.** **a.** At the top is illustrated a representative example of LFP including the presence of the transition pattern evoked spontaneously. Below are illustrated time–frequency representations averaged from 150 traces ( $n = 5$  rats) including the selected pattern recorded from automatic cue sessions. **b.** The same as for **(a)** but corresponding to LFPs recorded during pattern-evoked cue operant conditioning sessions (150 traces collected from 10 rats). Dot-surrounded areas correspond to observed differences between the two time–frequency displays. **c.** Significant differences ( $P \leq 0.05$ ) between the averaged time–frequency displays illustrated in **a** and **b**. Green-colored areas indicate when the spectral power was larger for patterns evoked spontaneously and red-colored areas those cases in which the spectral power was larger for patterns used to trigger the visual cue. Yellow lines delimit the period of time in which the pattern is generated. White and dashed lines delimit the different oscillatory bands for  $\theta$ ,  $\beta$ , low  $\gamma$  and high  $\gamma$ .

pattern during the two different experimental situations previously defined and illustrated in **Fig. 4.14a** and **b**. A precise study of the high- $\gamma$  band revealed a significant decrease ( $P \leq 0.05$ ) of the power in a narrow range of frequencies (115–122 Hz; **Fig. 4.16c**) that coincided with the detection of the LFP pattern when it was used to activate the touch-screen cue. Similar results were obtained for the low- $\gamma$  band and, particularly, in the range of frequencies between 32 Hz and 41 Hz ( $P \leq 0.05$ ). Interestingly, these frequencies did not change their spectral powers before and after the *Pattern* period. This alternation in the decrease of power during the use of the pattern to activate the cue between the three different time periods (*Pre*, *Pattern* and *Post*) was observed in some frequencies of the  $\theta$ ,  $\beta$ , and low- $\gamma$  bands (**Fig 4.16c**; green color areas).

#### 4.3.6. Coherence between different regions and the PrL cortex

An interesting question was to determine whether the selected oscillatory transition pattern was originated in a neural area other than the PrL cortex or was propagated from it to other cortical and subcortical areas. In **Fig. 4.17a** are illustrated the LFPs recorded in the six selected areas during a complete operant conditioning sequence from going to the iPad® to touch the visual display until eating the provided pellet. As illustrated in **Fig. 4.17b**, there was a very low coherence for the  $\theta$  band ( $0.06 \leq C \leq 0.19$ ) and a slightly higher one for the  $\beta$  ( $0.29 \leq C \leq 0.51$ ) when the PrL cortex was compared with the other five regions. Only the  $\gamma$  band (especially at high frequencies) presented a high coherence ( $C \leq 0.62$ ) between the PrL and M1 cortices.

A detailed analysis of coherence between these six regions revealed peaks of coherence in some frequencies, with values close to 0.6 during the generation of the transition pattern. When LFPs recorded in the PrL cortex were compared with those recorded in the M1 cortex, three peaks of medium-level coherence were found in low- $\gamma$  and high- $\gamma$  frequencies (42-65 Hz, 109-122 Hz, and 139-150 Hz,  $0.60 \leq C \leq 0.67$ ; **Fig. 4.17c**). Coherograms for LFPs calculated for PrL-mediadorsal thalamic nucleus and PrL-ventral tegmental area showed a generalized low coherence in most of the bands, apart from the low- $\gamma$  band (43-63 Hz and 45-51 Hz respectively;  $0.60 \leq C \leq 0.67$ ; **Fig. 4.17c, d**), mostly during the *Pre* and the beginning of the *Pattern* periods. As illustrated in **Fig. 4.17d**, the nucleus accumbens septi and the hippocampal CA1 area presented the lowest coherence in the  $\theta$ ,  $\beta$ , and low- $\gamma$  bands ( $0.06 \leq C \leq 0.37$ ), even though a narrow range of frequencies (between 146 Hz and 150 Hz) reached coherence values from 0.60 to 0.62 for PrL and nucleus accumbens septi LFPs.

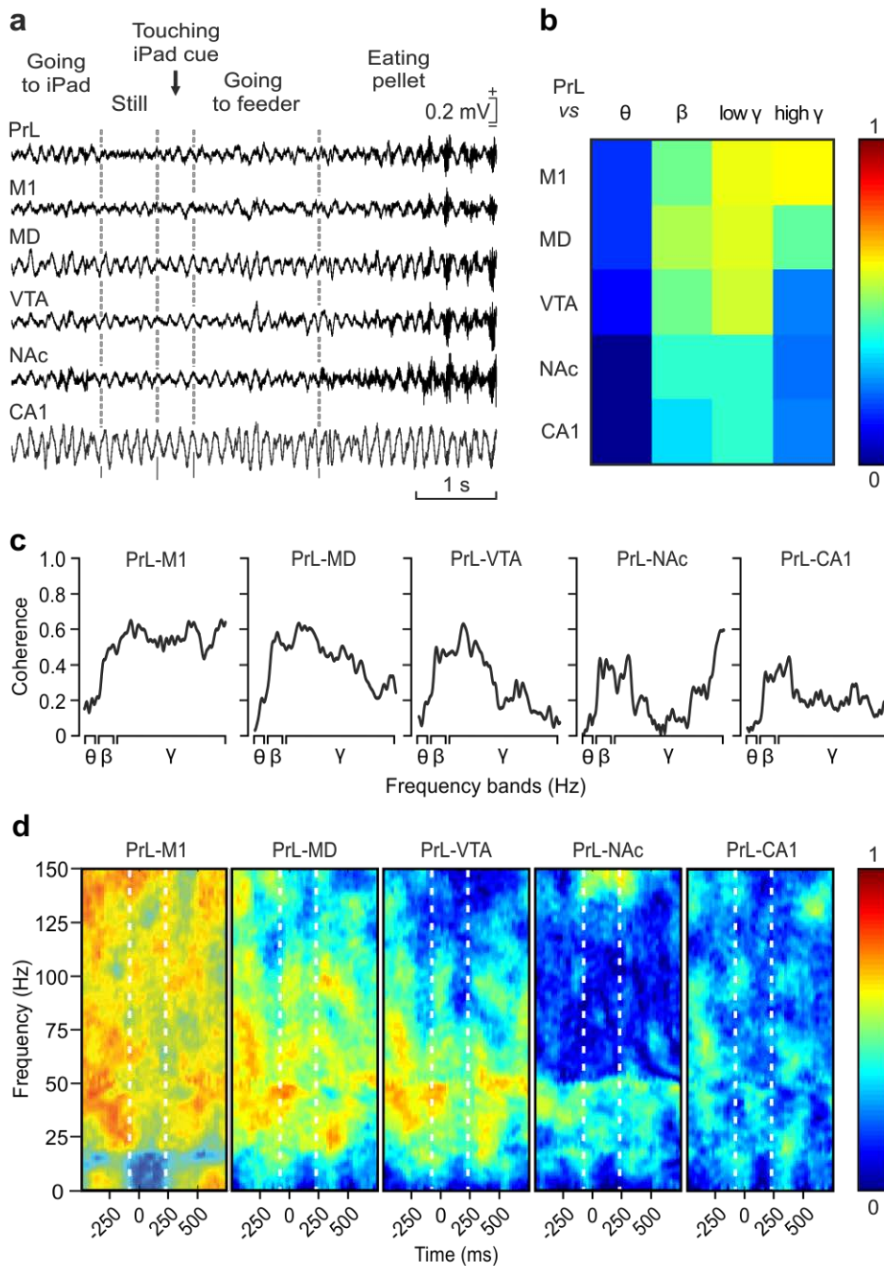


**Figure 4.17. The selected oscillatory transition pattern is restricted to the PrL cortex. a.** LFPs recorded simultaneously in six different cortical and subcortical sites during a sequence of the touch-screen operant conditioning task. **b.** Analysis of coherence between the oscillatory transition patterns recorded in the PrL cortex and the other five recording sites for the  $\theta$ ,  $\beta$ , low- $\gamma$ , and high- $\gamma$  bands. Note that the highest coherence (0.62, see color scale) was between the PrL and the M1 for high- $\gamma$  band. **c.** Coherence profiles for the activity of  $\theta$ ,  $\beta$ , low- $\gamma$ , and high- $\gamma$  bands in PrL and the other five recording sites during the appearance of the oscillatory transition pattern. **d.** Maps of time-frequency coherence between the *Pre*, *Pattern* and *Post* periods for LFPs recorded in the PrL cortex and the other five recording sites. Illustrated maps correspond to the average of 100 samples collected from 5 different animals. Note the high coherence between recordings collected from PrL and M1 recording sites, mostly for the *Pre* and *Post* periods.

#### 4.3.7. Unitary activity in the PrL cortex in presence of the oscillatory transition pattern

A particular attention was paid to the firing activities of PrL cortex neurons recorded in simultaneity with the spontaneous appearance of the selected oscillatory transition pattern (*Automatic cue*; **Fig. 4.18a**) or during its use to trigger the visual display in the iPad® (*Pattern-evoked cue*; **Fig. 4.18b**). Most (80%) of the recorded units (36 out of 45) were considered as putative PrL pyramidal

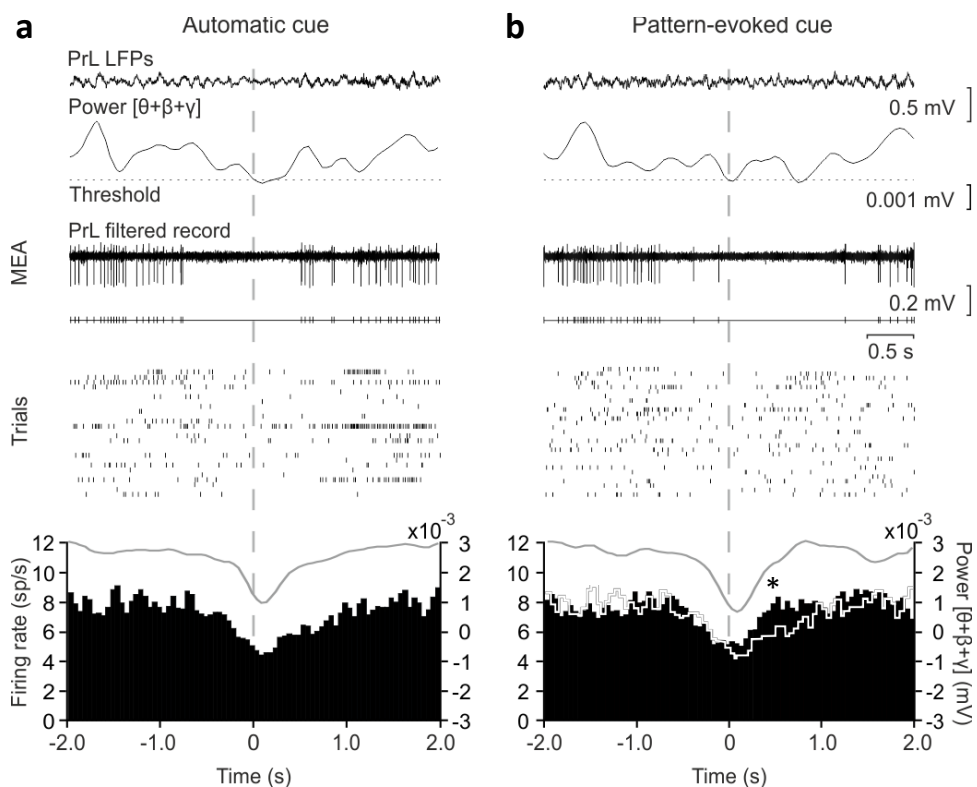


**Figure 4.18. Unitary activity in the PrL cortex when the selected transition pattern was generated spontaneously and when used to trigger touch-screen cues. a.** Unitary activity recorded in the PrL cortex in coincidence with the spontaneous appearance of the pattern during the automatic presentation of the visual cue (square virtual button) on the touch screen (*Automatic cue*). From top to bottom are illustrated a representative example of LFP including the presence of the pattern, the evolution of the added spectral power for the  $\theta + \beta + \gamma$  bands across the recorded LFP, the firing activity of a PrL neuron, the raster plot of  $\geq 25$  successive trials of the same recording session, and the averaged firing rate (spikes/s) of pyramidal neurons from PrL recorded during the same number of spontaneous oscillatory transition patterns (the gray line indicated the averaged  $\theta + \beta + \gamma$  power, in  $V^2$ ). **b.** Same neurons than in **a** recorded during pattern-evoked cue sessions (*Pattern-evoked cue*). The white line profile corresponds to the mean firing rate collected during the *Automatic cue* period. The statistical analysis of collected data indicated that there was a depression in the firing rate of the recorded neurons ( $n = 36$ ) during the transition pattern ( $F_{(78,320,399)} = 6.994$ ,  $P < 0.05$ , one-way ANOVA) and that this depression was recovered significantly (\*,  $t_{(19,0,05)} = -6.552$ ,  $P < 0.001$ , Paired Student's  $t$ -test) before, by the same neuronal group, during *Pattern-evoked cue* trials.

neurons, based on the duration of the recorded spikes ( $> 0.5$  ms) and on their spontaneous mean firing rates (2-15 spikes/s). These PrL neurons presented sustained tonic firings interrupted sometimes by short burst of activity. Because of their firing properties they appeared to be similar to the regular-spiking, slow adapting pyramidal cells recorded by Dégenères et al. (2002) in anesthetized rats and by Leal-Campanario et al. (2013) in alert behaving rabbits. In accordance with the collected results, averaged PrL pyramidal neurons presented a significant ( $F_{(78,320,399)} = 6.994$ ,  $P < 0.05$ , one-way ANOVA) decrease in their mean firing rate in coincidence with the spontaneous appearance of the  $\theta/\beta$ - $\gamma$  transition pattern (**Fig. 4.18a**) or during its use as *Pattern-evoked cue* (**Fig. 4.18b**). Nevertheless, the same set of neurons recovered significantly ( $t_{(19,0.05)} = -6.552$ ,  $P < 0.001$ , Paired Student's *t*-test) faster their firing rates following oscillatory transition patterns used as a cue than during their spontaneous presentations.

#### 4.3.8. Vibrissal muscles activity and pattern correlation

In order to determine whether vibrissal movements were related with LFPs recorded at the PrL cortex, a pair of recording electrodes was implanted in the center of the contralateral whisker pad (**Fig. 4.19a**)

The selected oscillatory transition pattern was related with a small ( $\approx 50\%$ ) decrease in vibrissal activity (**Fig 4.19b**) but there was no correlation between both variables, spectral power decrease of the LFP PrL and presence or absence of whiskers movement ( $r = 0.073$ , freedom degrees = 348,  $P = 0.336$ , Pearson's *r*). In fact, a wide variability of whisker muscle activity was recorded during the generation of the oscillatory transition pattern (**Fig. 4.19a, b and c**). The data suggests that this specific activity of the PrL cortex was not related with somatosensory information or exploratory behaviors, contrarily to what has been described for the S1 and M1 cortical areas (Zagha et al., 2013).

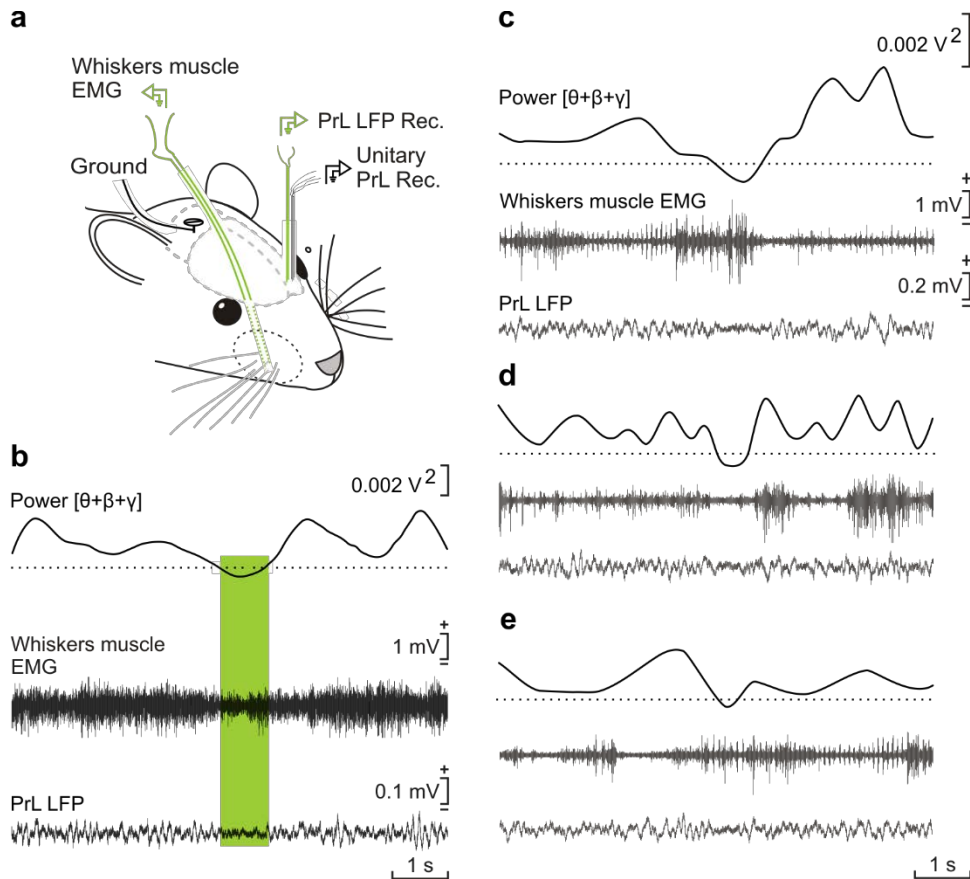


**Figure 4.19. The selected oscillatory transition pattern was not related with whisker motor responses.** **a.** Experimental design. The EMG activity of whisker muscles and the LFP generated in the PrL cortex were recorded simultaneously in alert behaving rats during operant conditioning sessions in which the iPad® was triggered by the oscillatory transition pattern. **b.** Averaged ( $n = 175$  traces collected from 3 animals) EMG recordings collected from whisker muscles and LFPs collected from the PrL cortex. Although the averaged EMG activity of whisker muscles presented a minimum value during the presence of the selected pattern, no linear relationship was observed between the two variables ( $r = 0.073$ , freedom degrees = 348,  $P = 0.336$ , Pearson's  $r$ ). **c, d, e.** Three representative examples of LFPs recorded in the presence of the selected pattern in the PrL cortex accompanied by different levels of activity in whisker muscles. These results suggest that both neural and muscle activities were not correlated.

#### 4.3.9. The electrical stimulation of the PrL cortex prevented the proper performance of the operant conditioning task

It is well known that the PrL cortex from which the oscillatory transition pattern was recorded is involved in cognitive, volitional, and valuation processes (Fuster, 2009; Kable and Glimcher, 2009; Graybeal et al., 2011). Specifically, its electrical stimulation seems to prevent the proper performance of an operant conditioning task (Jurado-Parras et al., 2012). In this regard, we checked whether the recorded area was also involved in these volitional processes. For this, we stimulated (a train

of 200 Hz for 200 ms; **Fig. 4.20b**) in the PrL cortex in animals trained to touch the visual display to obtain a pellet as a reward.

Control rats performed the task consistently, visiting the feeder and getting the pellet after each screen touch, with a performance index close to 1 ( $0.97 \pm 0.01$ ; **Fig. 4.20c**). In contrast, electrical stimulation of the PrL cortex (**Fig. 4.20a**) disturbed this sequential behavior, because, although cortically stimulated rats touched the screen as many times as controls ( $t_{(8,0.05)} = 1.043$ ,  $P = 0.328$ , Student's *t*-test), they either did not visit the feeder ( $t_{(8,0.05)} = 5.008$ ,  $P = 0.001$ , Student's *t*-test), or tried to visit it but returned to the touch screen without eating the reward ( $t_{(8,0.05)} = 5.334$ ,  $P \leq 0.001$ , Student's *t*-test). In addition, the time elapsed before visiting the feeder was significantly increased [ $U_{(8,0.05)} < 0.001$ ,  $P = 0.008$ , Mann-Whitney Rank Sum Test] (**Fig. 4.20d**; "Time to feeder"). PrL-stimulated rats did not visit the feeder and get the pellets delivered as effectively as controls did (**Fig. 4.20d**; "Feeder visits"), which produced a significantly [ $t_{(8,0.05)} = 2.586$ ,  $P = 0.032$ , Student's *t*-test] lower performance index ( $0.58 \pm 0.15$ ) than in the control group (**Fig. 4.20c**; red color bar). These results suggest that the electrical stimulation of PrL recording sites disturb the proper performance of specific behavioral sequences related to the operant task.

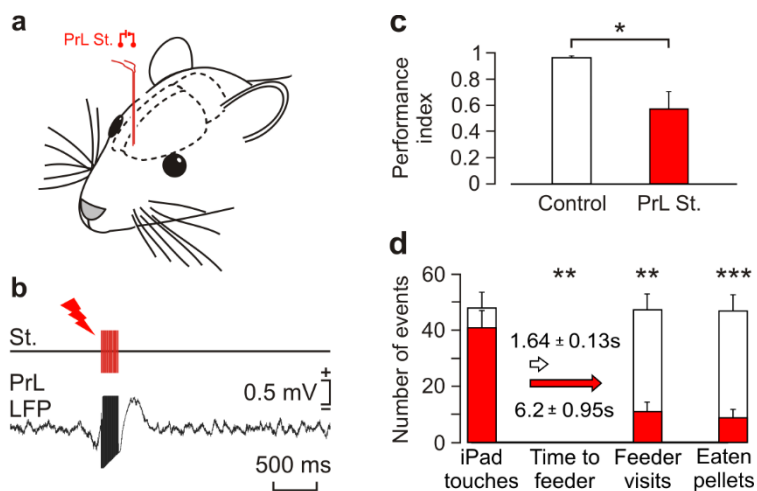


**Figure 4.20. Effect of electrical stimulation of the PrL cortex with a train of pulses. a.** Experimental design for animal stimulation in the PrL cortex. **b.** The experimental animal was stimulated for 200 ms (50  $\mu$ s pulses at 200 Hz) at the moment it touched the screen. A total of 5 rats/group was used. **c.** Differences in the Performance index (index =  $N_{\text{feeder}} + N_{\text{eat}} / N_{\text{feeder}} + N_{\text{touches}}$ , where N = number of events). Control rats reached an index of  $0.97 \pm 0.01$  (white bar), while stimulated rats reached significantly lower values ( $0.58 \pm 0.15$ ,  $t_{(8,0.05)} = 2.586$ ,  $P \leq 0.05$ , Student's *t*-test). **d.** Other quantitative differences in operant conditioning performance between the control and the stimulated groups. Although the number of screen touches was similar for the two groups ( $t_{(8,0.05)} = 1.043$ ;  $P = 0.328$ ; Student's *t*-test), the stimulated group spent a significantly longer time to reach the feeder ( $P = 0.001$ ; Mann-Whitney Rank Sum Test), paid fewer visits to the feeder ( $t_{(8,0.05)} = 5.008$ ,  $P < 0.001$ , Student's *t*-test), and ate fewer pellets ( $t_{(8,0.05)} = 5.334$ ,  $P < 0.001$ , Student's *t*-test).

## 5. DISCUSSION





## 5. DISCUSSION

### 5.1. Experiment 1: EFFECT OF FUNCTIONAL LOSS OF THE NMDA RECEPTOR IN M1

In the current study, we have developed a combinatorial genetic approach utilizing rAAVs equipped with tet-controlled genetic switches and *loxP*-engineered knock-in mice for Dox-induced, cell-type-specific *Grin1* gene knockout, selectively in the M1 cortex of mice. We provide here very strong evidence that functional loss of the NMDA receptor abolished *in vivo* LTP in the cortex. We also found that synaptic strengthening of synapses between somatosensory and motor cortices was impaired during associative learning. Importantly, in the same mice, there was strong impairment of conditioned-evoked behavioral responses and learning was significantly reduced in the Skinner-box test.

Interestingly, we observed that the *Grin1*- $\Delta^{MCx}$  mice showed some residual learning, both in the classical EBC task and the instrumental conditioning. We anticipate two possible explanations for this interesting observation. First, with ~80% of neurons targeted by rAAVs (Lutcke et al., 2010; Wallace et al., 2008) and with redundancy in neuronal coding for the same behavioral task in the motor cortex (Huber et al., 2012; Rokni et al., 2007), possibly to improve behavioral performance (Takiyama and Okada, 2012), it is possible that the remaining untargeted neurons in the M1 cortex (without the *Grin1* gene deletion) might have contributed in executing some residual learning function. Second, it is also possible that in *Grin1*- $\Delta^{MCx}$  mice, the cerebellar function, in part, might have participated in trace EBC (Woodruff-Pak and Disterhoft, 2008).

Although a simple EBC is a prototypical example of a non-declarative memory, trace and delay EBC are fundamentally different kinds of learning (Clark et al., 2001). An introduction of a ‘trace’ (Cheng et al., 2008) component in the EBC endows it with some common features shared with the declarative memory. With dynamic feedforward and top-down interactions between different cortical and subcortical brain regions, involving both localized (McCormick and Thompson, 1984) and widely distributed (Fuster, 2009) neuronal networks, distinct cortical cell ensembles representing different experiences might be linked by learning to form unique memories. Our results provide convincing evidence that the memory of acquired trace eyeblink-

conditioned responses is localized in the M1 cortex. Therefore, dissecting the mechanisms of trace EBC in the M1 cortex is bound to provide deeper insight into the molecular and cellular mechanisms of declarative memory (Clark, 2011).

Curiously, in earlier studies, genetically modified mice with deletion of the *Grin1* gene in CA1 showed deficit in acquisition of both spatial (Tsien et al., 1996) and temporal (Huerta et al, 2000) memories. However, it was later found that, over time (several months), the *Grin1* gene deletion in these mice had also spread to all cortical layers (Fukaya et al., 2003), leaving open the possibility that a cortical component might be having a crucial role in forming associations between spatial cues (Tsien et al., 1996) and between temporally separated events (Huerta et al, 2000). With an improved genetic mouse model, a recent study provides the best evidence thus far that the NMDAR in the dorsal CA1 subfield and dentate gyrus is not required for the acquisition of spatial memories, despite impaired hippocampal LTP in these mice. Instead, hippocampal NMDARs are needed to resolve conflict between competing spatial cues (Bannerman et al., 2012). Notably, deletion of the *Grin1* gene specifically in CA3 also did not interfere with trace EBC. However, CA3-NMDARs tend to have a crucial role in the memory of adaptive CR timing (Kishimoto et al., 2006). It thus seems quite plausible that while the hippocampus is needed for organizing spatial computations, it is in the cerebral cortex, where spatial memories (Tsien et al., 1996) and temporal associations (Huerta et al, 2000) are acquired and, perhaps, even stored (Fuster, 2009; Miyamoto et al., 2013), possibly involving both localized and widely distributed cortical cell assemblies (Osada et al., 2008). Interestingly, it was found that during classical EBC, the CA3–CA1 synapses and the S1–M1 synapses were similarly strengthened (Gruart et al., 2006; Troncoso et al., 2007). As hippocampus lesion is known to impair eyeblink trace conditioning (Moyer et al., 1990; Kishimoto et al, 2006), it is quite important to investigate the role of CA1-NMDAR function in this particular associative learning paradigm.

Our virus-based, chemically controlled genetic approach allows for inducible control of gene expression (Zhu et al., 2007; Sprengel and Hasan, 2007) and inducible gene knockout in mouse brain. With these powerful tools, it is now possible to precisely manipulate the function of individual neuronal cell types, cortical layers and brain regions in different mammalian species. In

our current study, the AAVs of hybrid serotype 1 and 2 targeted cortical neurons (Lutcke et al., 2010; Wallace et al., 2008) of layer 2/3 and layer 5, thereby deleting in these cells the *Grin1* gene and impairing NMDAR function. In future studies, our virus-based inducible genetic approach should further help to investigate, in cortical layer- and cell-type-specific manner, whether motor cortex NMDAR function is required for consolidation and retrieval of the conditioned eyeblink response.

## **5.2. Experiment 2: CONTRIBUTION OF PrL CORTEX IN EARLY PHASES OF INSTRUMENTAL LEARNING**

### *5.2.1. Electrophysiological characteristics of the thalamocortical and mesocortical synapses*

The preliminary study of both synapses in rats with singles pulses of increasing intensities suggested normal functioning since they showed a sigmoidal shape for input/output curves similar to those observed in mice for S1-M1 cortical synapse (experiment 1), as well as for CA3-CA1 synapse of hippocampus (Madrónal et al., 2009). More interesting were the results obtained for pair pulse stimulation test collected from animals stimulated with a pair of pulses in the same synapse (thalamocortical or mesocortical) compared with stimulation of thalamocortical and mesocortical pathways consecutively. The second situation (a first pulse in VTA and a second in MDTh or vice versa) provoked a higher postsynaptic response for the second pulse in both synapses. This increase in the fPSP may be partially explained by the presence of direct and indirect projections from the VTA to the MDTh (via Nucleus Accumbens and Ventral Pallidum) that may interact increasing the amplitude of the second pulse. This outstanding effect that is provoked by converging activity of MDTh and VTA may interact in a cooperative manner with another brain areas as hippocampus (Floresco and Grace, 2003) to regulate executive functions governed by the PFC. In addition, the modulatory effect of the mesocortical pathway on the glutamatergic receptors of the thalamocortical synapse by means of the local circuitry of the PrL area may participate in this increased synaptic response. Electrophysiological evidences support the main inhibitory effect of the VTA neurons over prefrontal cortex (in coincidence with the pair pulse depression effect on VTA synapse) as well as blocking the excitatory responses evoked from the MDTh (as was observed in the pair pulse in combination with VTA and MDTh) (Ferron et al., 1984). However, the synaptic complexity of neurotransmitters, presence of inhibitory (70-80%) and excitatory (20-30%) synapses between the VTA and the PrL neurons as well as a substantial population of inhibitory neurons in the VTA sending axons to PrL

local interneurons with a disinhibitory effect (Carr and Sesack, 2000; see Yokofujita et al., 2008 for review) makes it complex to understand the global functioning of the neuronal populations of prelimbic cortex under the influence of both regions (VTA and MDTh). In any case, these results suggests some sort of time-interval dependent synaptic relation between both pathways that it is concluded from results of the pair pulse test in two different sites at same time producing different effect than the stimulation of a single pathway. This differences may be generated by local circuitry in the PrL cortex as well as direct and indirect connectivity between VTA and MDTh regions (Oades and Halliday, 1987; Smith et al., 2013).

The stimulation of the MDTh with a train of pulses evoked a long lasting potentiation in the thalamocortical synapse as well as an initial augmentation of the mesocortical synapse. According to that, MDTh may participate in long lasting learning processes and to a greater extent than mesocortical synapse which showed potentiation during only some minutes. Moreover mesocortical recording showed high inter-individual variability with some cases in which no potentiation was detected. Taking into account that both, MDTh and VTA neurons send axon terminals onto common pyramidal cells in layer V of the PrL cortex (Kuroda et al., 1996), the reciprocal connectivity between the PrL cortex and the VTA (Sesack and Pickel, 1992) and general properties of specificity and associativity of LTP, some sort of functional connectionist relationship between MDTh and VTA may exist in order to evoked this slight potentiation in the mesocortical pathway after HFS in MDTh. Thus, if there was some wick activity in mesocortical synapse during high frequency stimulation of the thalamocortical pathway, associativity property of the LTP could explain this slight and short lasting potentiation of the mesocortical path. Associativity is expected in any network of neurons that links one set of information with another (Purved et al., 2001).

The application of the same stimulation protocol in the VTA evoked a slight potentiation in mesocortical synapse while a small depression in thalamocortical pathway was induced, probably through mechanisms of heterosynaptic LTD (Staubli and Ji, 1996; Chistiakova et al., 2014) on MDTh after HFS of the VTA. It may suppose some dopamine-dependent effect on the thalamocortical synaptic transmission as it was observed in hippocampal-prefrontal cortex pathway (Gurden et al., 1999; Goto and Grace, 2008).

### 5.2.2. *Involvement of PrL cortex in early stages of associative learning*

Some important points were observed during the instrumental learning of two different tasks. First, it was observed a potentiation of the thalamocortical and mesocortical synapses that coincided with the initial improvement in the task performance. This is a stage characterized by an initial phase of rapid improvement in performance that is generally followed by a phase of more gradual improvements as the skills are consolidated and performance asymptotes (Karni et al., 1998) initial stage of learning in which the animal goes from a trial-error phase to another in which the association between the stimulus (food) and the response (press the lever / touch-screen) begins to be generated. The global increase in the synaptic transmission of small populations of neurons seems to be closely related with early learning phases since lidocaine infusion impairs the PrL synaptic transmission and task performance during the sessions in which control animals solved the mechanism to obtain the pellet. Several studies have revealed considerable changes in activity of neuronal ensemble in cortical regions within the first session of some learning paradigms that became less evident during subsequent sessions (Costa et al., 2004; Leal-Campanario et al., 2013). In fact, in our study, once the animals reached the selected learning criterion both synapses reverted to basal levels of fPSPs. From these data it may be deduce that thalamocortical and mesocortical nuclei seems to play a specific role in the acquisition of new relevant information rather than to the retention of previously acquired information that allows to the PrL cortex to encode and integrate this information during these early stages (Romero-Granados et al., 2010) . Both pathways showed similar synaptic transmission conditions along the sessions suggesting a common functional participation in learning acquisition.

Another important data that supports the relevance of the PrL cortex during the first learning stages were the high basal levels of fPSPs before lidocaine injection during the days in which the lidocaine group theoretically would start to perform the task and the subsequent peak of amplitude of the fPSPs after lidocaine treatment sessions that accompanied the improvement in task performance. All of these results support the hypothesis that an increase in learning ability is preceded or, at the least, accompanied by an increase in synaptic strength at selected neural sites.

The change from one learned task to a new another one produced a decrease in the amplitude of the fPSPs. According to this, both synapses seem to be sensitive to some essential changes in the environment such as the modification of the "manipulandum" (the lever was replaced by a touch screen) in the Skinner box.

### 5.3. Experiment 3: NEURAL ACTIVITY CHANGES DURING AN ASSOCIATIVE LEARNING WITH BCIs

Present results indicate that the use of definite LFP patterns generated in the PrL cortex can be safely used as an alternative for functional studies associated with BCIs and other neural processes related to neuro-feedback procedures.

#### 5.3.1. *The PrL cortex related to goal-directed behaviors*

As already described, and further confirmed here, the PrL cortex is involved in volitional and valuation processes (Vertes, 2004; Hoover and Vertes, 2007; Kable and Glimcher, 2009; Graybeal et al., 2011; Fuster, 2015;) including classical and operant conditioning tasks (Leal-Campanario et al., 2007; Jurado-Parras et al., 2012). In particular, the effects of the electrical stimulation of the PrL cortex during the operant sequence used here suggest the involvement of this area in ongoing cognitive processes related to the association between touching the screen and getting the corresponding reward—a finding also reported in mice during a similar operant conditioning task (Jurado-Parras et al., 2012).

In addition, the electrical stimulation of the recording area evoked disturbing effects on the animal's performance during the operant task not related to any visible deficit in its motor activities (Humani et al., 2010). In accordance, these results indicate that the stimulation of the PrL cortex disturbed specific cognitive processes underlying the expected behavioral sequences (Jackson et al., 2001; Jurado-Parras et al., 2012).

#### 5.3.2. *Neural correlates between behavior and the oscillatory activity pattern*

The behaviors (i.e., motionless, rearing, and looking into the feeder; **Fig. 4.12**) during which the selected oscillatory transition pattern was observed, as well as its intrinsic spectral characteristics (a significant decrease in power of the theta band associated with smaller changes in the  $\beta$  and  $\gamma$  bands), could be related to the proposal that LFPs presenting low amplitudes and high- $\gamma$  frequencies are involved in attentive processes (Moruzzi and Magoun, 1949; Fries et al., 2001; Poulet and Petersen, 2008; Zaghera et al., 2013) and with specific hypervigilance rhythms associated with immobility and focused attention (Bouyer et al., 1981; Wang, 2008; Koralek et al., 2012). Interestingly, an LFP pattern similar to the one described here has been reported to be present in neocortical S1 and M1 areas during whisking conditions (Zaghera et al., 2013). Nevertheless, apart from this similitude, the present oscillatory transition pattern was better related with a

significant decrease in the activity of whisker motor responses. In fact, coherence in LFPs recorded simultaneously in PrL and M1 cortices decreases during the apparition of the oscillatory transition pattern. In accordance, this pattern seems not to be related with specific  $\beta$  activities present in the M1 cortex during selected motor responses (Zagha et al., 2013; Khanna and Carmena, 2015).

It can be questioned whether the oscillatory transition pattern was just a byproduct of the preferred behavior (sitting still or motionless) used by the experimental rats to activate the iPad®. In this regard, the same LFP pattern was present during the performance of other behaviors (as rearing or looking into the feeder) and, at the same time, was not always present when the animal remained motionless in the cage—immobility per se is not enough to generate this LFP pattern (Gervasoni et al., 2004). Although in early conditioning sessions, animals generated the LFP pattern in different locations within the Skinner box, the animal selected this behavior (sitting still nearby the iPad®) across training because its adaptive value. In addition, given their rather poor visual acuity (Prusky et al., 2002) being nearly the iPad® will facilitate an early detection of the visual cue. Thus, it can safely be expected that a paralyzed animal should still be able of generate this (and related) LFP patterns without the need of associate it to a given behavior, involving movements or, at the least, postural adjustments.

### *5.3.3 Operant conditioning of oscillatory activity in the PrL cortex*

The learning curve generated by the pattern-evoked cue presented a sigmoidal shape similar to (although with a slower evolution than) that generated by experimental animals during the automatic presentation of the cue on the touch screen (**Fig. 4.14**) or during rewarded lever pressing in the Skinner box (Karni et al., 1998; Buitrago et al., 2004; Jurado-Parras et al., 2012). These results suggest that the use of an LFP pattern generated in the PrL cortex to activate an operant conditioning task does not represent an unviable burden for the experimental animal.

Pattern-evoked cue sessions generated some minor changes in the selected oscillatory transition pattern, including a progressive increase in pattern duration, a decrease in the power ratio  $(P_{\beta} + P_{\gamma}) / P_{\theta}$ , as faster recovery in the firing rate of PrL neurons, and a significant decrease in the spectral power of  $\beta$  and  $\gamma$  bands. In fact, these changes in spectral power increased the probability of activating the touch screen, since a decrease in  $\theta + \beta + \gamma$  powers facilitated reaching the selected threshold. Interestingly, these changes were not observed during the training



period in which the cue was presented automatically, a fact suggesting that changes in the selected oscillatory transition pattern were not due to learning processes due to the association between the cue (square virtual button) and the reward, but by the association between the oscillatory transition pattern and the activation of the cue on the touch screen. These results are in coincidence with available reports on neuronal operant conditioning in which the reward is obtained with changes in the discharge rate of conditioned neurons (Opris et al., 2011; Arduin et al., 2013). It should be noted that the reported changes in the selected oscillatory transition pattern observed during pattern-evoked cue sessions did not modify the main spectral characteristic of the pattern—namely, a significant decrease in  $\theta$  band.

Interestingly enough, the selected oscillatory transition pattern appeared in simultaneity with a significant decrease in the mean firing rate of PrL cells putatively considered as pyramidal neurons because of their firing properties (Dégenères et al., 2002; Povysheva et al., 2006; Leal-Campanario et al., 2013). In this regard, it has been recently proposed that rostromedial prefrontal cortex plays an active role in preventing the release of newly acquired motor responses until advanced stages of the acquisition process and, in general, in the control of the ongoing behavior depending on environmental and social constraints (Leal-Campanario et al., 2007, 2013). The inhibition of PrL cortex neurons during the oscillatory transition pattern suggest that this pattern corresponds to a time window for the release of specific behaviors involving cognitive processes (see **Fig. 4.20**).

#### *5.3.4. Distribution of the oscillatory activity pattern in the brain*

It is important to point out here the low coherence values between LFPs recorded in the PrL cortex, including the selected oscillatory transition pattern, and LFPs recorded simultaneously in the nucleus accumbens, the motor cortex, the mediodorsal thalamic nucleus, and hippocampal CA1 and ventral tegmental areas. Apparently, the selected oscillatory transition pattern was not generated in and/or propagated to the five mentioned areas, but is an activity restricted to the PrL cortex. In fact, we obtained higher ( $0.60 < R > 0.69$ ) levels of coherence between LFPs recorded in PrL vs. those recorded in the motor cortex, the nucleus accumbens, and the mediodorsal thalamic nucleus in the high- $\gamma$  band during the generation of the pattern. In this regard, an increase has been reported in functional interactions in the high- $\gamma$  band between the PrL cortex and the mediodorsal thalamic nucleus during the acquisition of an instrumental conditioning task (Yu et al., 2012), as well as between the nucleus accumbens and the PrL during a

similar learning task (Chang et al., 2000). The observation of increased coherence values for narrow frequency bands between different cortical and subcortical areas suggests the involvement of different learning and memory processes taking place in these different neural structures in simultaneity with the use of the selected oscillatory transition pattern as a brain-iPad interface.



## 6. CONCLUSIONS



## 6. CONCLUSIONS

- The inactivation of NMDAR in M1 cortex is necessary for learning-dependent synaptic plasticity and acquisition of associative memory for both classical and instrumental conditioning paradigms.
- M1 y PrL presents a relation between associative learning and synaptic strength increase of their population of neurons.
- Synaptic transmission in mesocortical or thalamocortical pathways show a close relationship at the functional level by exerting one on the other effects on synaptic transmission and on mechanisms related to long-term memory in cellular populations that could explain the way PrL cortex participates in learning processes.
- The proper functioning of the PrL cortex circuits are crucial for proper early phases of associative learning. In this sense, PrL seems to intervene in the acquisition of new information relevant to associative learning rather than in the retention of previously acquired information.
- It is possible to carry out the operant conditioning of oscillations of LFPs in regions where information of cognitive nature (PrL) is processed through long-term BCI control.
- The use of oscillatory patterns in the PrL cortex may be safely used because their oscillatory activity stability in their spectral properties.



## 7. REFERENCES





## 7. REFERENCES

### A

Arduin PJ, Fregnac Y, Shulz DE, Ego-Stengel V (2013) “Master” neurons induced by operant conditioning in rat motor cortex during a brain-machine interface task. *J Neurosci* 33:8308–8320. doi: 10.1523/jneurosci.2744-12.2013

Aronoff R, Matyas F, Mateo C, Ciron C, Schneider B, Petersen CC. (2010). Long-range connectivity of mouse primary somatosensory barrel cortex. *Eur. J. Neurosci.* 31: 2221–2233. doi: 10.1111/j.1460-9568.2010.07264.x.

### B

Baeg EH, Kim YB, Huh K, Mook-Jung I, Kim HT and Jung MW (2003). Dynamics of population code for working memory in the prefrontal cortex. *Neuron*. 40:177-88. doi: 10.1016/S0896-6273(03)00597-X

Ball KT & Slane M. (2012). Differential involvement of prelimbic and infralimbic medial prefrontal cortex in discrete cue-induced reinstatement of 3,4-methylene-dioxy-methamphetamine (MDMA; ecstasy) seeking in rats. *Psychopharmacology*. 224:377–385. doi: 10.1007/s00213-012-2762-5

Bannerman DM, Bus T, Taylor A, Sanderson DJ, Schwarz I, Jensen V, Hvalby Ø, Rawlins JN, Seeburg PH, Sprengel R. (2012). Dissecting spatial knowledge from spatial choice by hippocampal NMDA receptor deletion. *Nat. Neurosci.* 15: 1153–1159. doi: 10.1038/nn.3166.

Birbaumer N, Weber C, Neuper C, Buch E, Haapen K, Cohen L (2006). Physiological regulation of thinking: brain-computer interface (BCI) research. *Prog Brain Res.* 159:369-91. doi: 10.1016/S0079-6123(06)59024-7

Bliss TV & Gardner-Medwin AR. (1973). Long-lasting potentiation of synaptic transmission in the dentate area of the anaesthetized rabbit following stimulation of the perforant path. *J. Physiol.* 232: 357–374. doi: 10.1113/jphysiol.1973.sp010273

Bosch M, Castro J, Saneyoshi T, Matsuno H, Sur M, Hayashi Y. (2014) Structural and molecular remodeling of dendritic spine substructures during long-term potentiation. *Neuron* 82, 444–459. doi:10.1016/j.neuron.2014.03.021

Bouton CE, Shaikhouni A, Annetta NV, Bockbrader MA, Friedenber DA, Nielson DM, Sharma G, Sederberg PB, Glenn BC, Mysiw WJ, Morgan AG, Degaonkar M, Rezai AR (2016) Restoring cortical control of functional movement in a human with quadriplegia. *Nature* 533:247-250. doi: 10.1038/nature17435

Bouyer JJ, Montaron MF, Rougeul A (1981) Fast fronto-parietal rhythms during combined focused attentive behaviour and immobility in cat: cortical and thalamic localizations. *Electroencephalogr Clin Neurophysiol* 51:244–252. doi: 10.1016/0013-4694(81)90138-

Buitrago MM, Ringer T, Schulz JB, Dichgans J, Luft AR (2004) Characterization of motor skill and instrumental learning time scales in a skilled reaching task in rat. *Behav Brain Res* 155:249–256. doi: 10.1016/j.bbr.2004.04.025

Buonomano DV & Merzenich MM. (1998). Cortical plasticity: from synapses to maps. *Annu. Rev. Neurosci.* 21: 149–186. doi: 10.1146/annurev.neuro.21.1.149

Burger C, Nguyen FN, Deng J & Mandel RJ. (2004). Systemic mannitol-induced hyperosmolality amplifies rAAV2-mediated striatal transduction to a greater extent than local co-infusion. *Mol. Ther.* 11: 327–331. doi:10.1016/j.ymthe.2004.08.031

Buzsaki, G. (2010). Neural syntax: cell assemblies, synapsembles, and readers. *Neuron* 68: 362–385. doi: 10.1016/j.neuron.2010.09.023.

## C

Callaway EM. (2004). Feedforward, feedback and inhibitory connections in primate visual cortex. *Neural. Netw.* 17: 625–632. doi: 10.1016/j.neunet.2004.04.004

Cambridge SB, Geissler D, Calegari F, Anastassiadis K, Hasan MT, Stewart AF, Huttner WB, Hagen V & Bonhoeffer T. (2009). Doxycycline-dependent photoactivated gene expression in eukaryotic systems. *Nat. Methods.* 6: 527–531. doi: 10.1038/nmeth.1340

Caro-Martín CR, Leal-Campanario R, Sánchez-Campusano R, Delgado-García JM, Gruart A. (2015). A Variable Oscillator Underlies the Measurement of Time Intervals in the Rostral Medial Prefrontal Cortex during Classical Eyeblink Conditioning in Rabbits. *J Neurosci.* 35:14809-21. doi: 10.1523/JNEUROSCI.2285-15.2015.

Carr DB, Sesack SR (2000). GABA-containing neurons in the rat ventral tegmental area project to the prefrontal cortex. *Synapse.* 38:114-23. doi: 10.1002/1098-2396(200011)38:2<114::AID-SYN2>3.0.CO;2-R

Cerf M, Thiruvengadam N, Mormonn F, Kraskov A, Quiroga RQ, Koch C, Fried I. (2010). Online voluntary control of human temporal lobe neurons. *Nature.* 467:1104–1108. doi:10.1038/nature09510

Chapin JK, Moxon KA, Markowitz RS, Nicolelis MA. (1999) Real-time control of a robot arm using simultaneously recorded neurons in the motor cortex. *Nat Neurosci.* 2:664-70. doi: 10.1038/10223

Chang JY, Janak PH, Woodward DJ (2000) Neuronal and behavioral correlations in the medial prefrontal cortex and nucleus accumbens during cocaine self-administration by rats. *Neuroscience* 99:433–443. doi: 10.1016/s0306-4522(00)00218-9

Chen C, Blitz DM, Regehr WG (2002). Contributions of receptor desensitization and saturation to plasticity at the retinogeniculate synapse. *Neuron* 33: 779–788. doi: 10.1016/S0896-6273(02)00611-6

Cheng DT, Disterhoft JF, Power JM, Ellis DA & Desmond JE. (2008). Neural substrates underlying human delay and trace eyeblink conditioning. *Proc. Natl Acad. Sci. USA.* 105: 8108–8113. doi: 10.1073/pnas.0800374105

Chistiakova M, Bannon NM, Bazhenov M, Volgushev M (2014) Heterosynaptic plasticity: multiple mechanisms and multiple roles. *Neuroscientist.* 20:483-98. doi: 10.1177/1073858414529829

Clark RE, Manns JR & Squire LR. (2001). Trace and delay eyeblink conditioning: contrasting phenomena of declarative and nondeclarative memory. *Psychol. Sci.* 12: 304–308. doi: 10.1111/1467-9280.00356

Clark RE. (2011). Eyeblink conditioning and systems consolidation: an ironic yet powerful pairing. *Neurobiol. Learn. Mem.* 95: 118–124. doi: 10.1016/j.nlm.2010.12.003

Costa RM, Cohen D, Nicolelis MA (2004) Differential Corticostriatal Plasticity during Fast and Slow Motor Skill Learning in Mice. *Curr Biol.* 14:1124-34. doi: 10.1016/j.cub.2004.06.053

## **D**

Purves D, Augustine GJ, Fitzpatrick D, Katz LC, LaMantia AS, McNamara JO & Williams SM (2001) *Neuroscience*, 2nd Ed. Sinauer Associates. ISBN-10: 0-87893-742-0

Dégenétais E, Thierry AM, Glowinski J, Gioanni Y (2002) Electrophysiological properties of pyramidal neurons in the rat prefrontal cortex: an in vivo intracellular recording study. *Cereb Cortex* 12:1–16. doi: 10.1093/cercor/12.1.1

Delatour B & Gisquet-Verrier P. (2000). Functional role of rat prelimbic-infralimbic cortices in spatial memory: evidence for their involvement in attention and behavioural flexibility. *Behav Brain Res.* 109:113-28. doi: 10.1016/S0166-4328(99)00168-0

Di Pietro NC, Black YD, Green-Jordan K, Eichenbaum HB and Kantak KM. (2004) Complementary tasks to measure working memory in distinct prefrontal cortex subregions in rats. *Behavioral Neuroscience*, 118:1042-51. doi: 10.1037/0735-7044.118.5.1042

## **E**

Engelhard B, Ozeri N, Israel Z, Bergman H, Vaadia E. (2013). Inducing gamma oscillations and precise spike synchrony by operant conditioning via brain-machine interface. *Neuron.* 77:361–375. doi:10.1016/j.neuron.2012.11.015

Euston DR, Gruber AJ & McNaughton BL (2012). The Role of Medial Prefrontal Cortex in Memory and Decision Making. *Neuron.* 76: 1057-1070. doi: 10.1016/j.neuron.2012.12.002

## **F**

Ferezou I, Haiss F, Gentet LJ, Aronoff R, Weber B and Petersen CC. (2007). Spatiotemporal dynamics of cortical sensorimotor integration in behaving mice. *Neuron.* 56: 907–923. doi: 10.1016/j.neuron.2007.10.007

- Ferron A, Thierry AM, Le Douarin C, Glowinski J (1984) Inhibitory influence of the mesocortical dopaminergic system on spontaneous activity or excitatory response induced from the thalamic mediodorsal nucleus in the rat medialprefrontal cortex. *Brain Res.* 302:257-65. doi: 10.1016/0006-8993(84)90238-5
- Ferster CB & Skinner BF. (1957). *Schedules of Reinforcement*; Prentice-Hall, Inc. ISBN: 978-0-9899839-5-2
- Fetz EE. (1969). Operant conditioning of cortical unit activity. *Science* 163:955–958. doi: 10.1126/science.163.3870.955
- Fetz EE, Finocchio DV. (1971). Operant conditioning of specific patterns of neural and muscular activity. *Science* 174:431–435. doi: 10.1126/science.174.4007.431
- Fetz EE, Finocchio DV. (1972). Operant conditioning of isolated activity in specific muscles and precentral cells. *Brain Res* 40:19–23. doi: 10.1016/0006-8993(72)90100-x
- Flint RD, Wright ZA, Scheid MR, Slutzky MW. (2013) Long term, stable brain machine interface performance using local field potentials and multiunit spikes. *J Neural Eng* 10:056005. doi: 10.1088/1741-2560/10/5/056005 20
- Floresco SB & Grace AA (2003) Gating of hippocampal-evoked activity in prefrontal cortical neurons by inputs from the mediodorsal thalamus and ventral tegmental area. *Journal of Neuroscience.* 23:30-43. [www.jneurosci.org/content/23/9/3930.full.pdf](http://www.jneurosci.org/content/23/9/3930.full.pdf)
- Floresco SB, Block AE, Tse MT. (2008). Inactivation of the medial prefrontal cortex of the rat impairs strategy set-shifting, but not reversal learning, using a novel, automated procedure. *Behav Brain Res.* 190:85-96. doi: 10.1016/j.bbr.2008.02.008.
- Freeman WJ, Holmes MD, Burke BC, Vanhatalo S. (2003). Spatial spectra of scalp EEG and EMG from awake humans. *Clin Neurophysiol* 114:1053–68. doi: 10.1016/S1388-2457(03)00045-2
- Fries P, Reynolds JH, Rorie AE, Desimone R. (2001). Modulation of oscillatory neuronal synchronization by selective visual attention. *Science* 29:1560–1563. doi: 10.1126/science.1055465
- Foster KA, Kreitzer AC, Regehr WG. (2002). Interaction of postsynaptic receptor saturation with presynaptic mechanisms produces a reliable synapse. *Neuron* 36: 1115–1126. doi: 10.1016/S0896-6273(02)01106-6
- Fukaya M, Kato A, Lovett C, Tonegawa S & Watanabe M. (2003). Retention of NMDA receptor NR2 subunits in the lumen of endoplasmic reticulum in targeted NR1 knockout mice. *Proc. Natl Acad. Sci. USA.* 100: 4855–4860. doi: 10.1073/pnas.0830996100
- Funahashi S. (2006). Prefrontal cortex and working memory processes. *Neuroscience.* 139:251-61. doi: 10.1016/j.neuroscience.2005.07.003

Fuster JM. (2015). *The prefrontal cortex*. 4<sup>th</sup> Ed. London, England: Academic Press. ISBN: 978-0-12-373644-4

Fuster JM. (2009). Cortex and memory: emergence of a new paradigm. *J. Cogn. Neurosci.* 21: 2047–2072. doi: 10.1162/jocn.2009.21280

## **G**

Ganguly K, Domitrov DF, Wallis JD, Carmena JM. (2011). Reversible large-scale modification of cortical networks during neuroprosthetic control. *Nat. Neurosci.* 14:662–667. doi:10.1038/nn.2797

Gervasoni D, Lin SC, Ribeiro S, Soares ES, Pantoja J and Nicolelis MAL. (2004). Global forebrain dynamics predict rat behavioral states and their transitions. *J Neurosci* 24:11137–11147. doi: 10.1523/jneurosci.3524-04.2004

Goto Y & Grace AA. (2007). Dopamine modulation of hippocampal-prefrontal cortical interaction drives memory-guided behavior. *Cerebral Cortex.* 18:1407-1414. doi: 10.1093/cercor/bhm172

Gourley SL & Taylor JR. (2016). Going and stopping: dichotomies in behavioral control by the prefrontal cortex. *Nature Neurosciences.* 19, 656-664. doi:10.1038/nn.4275

Graybeal C, Feyder M, Schulman E, Saksida LM, Bussey TJ, Brigman JL, Holmes A. (2011). Paradoxical reversal learning enhancement by stress or prefrontal cortical damage: rescue with BDNF. *Nat Neurosci* 14:1507-1509. doi: 10.1038/nn.2954

Groenewegen HJ & Uylings HB. (2000). The prefrontal cortex and the integration of sensory, limbic and autonomic information. *Prog Brain Res.* 126:3-28. doi:10.1016/S0079-6123(00)26003-2

Gruart A, Muñoz MD and Delgado-García JM. (2006). Involvement of the CA3- CA1 synapse in the acquisition of associative learning in behaving mice. *J. Neurosci.* 26: 1077–1087. doi: 10.1523/JNEUROSCI.2834-05.2006

Gurden H, Tassin JP, Jay TM (1999) Integrity of the mesocortical dopaminergic system is necessary for complete expression of in vivo hippocampal-prefrontal cortex long-term potentiation. *Neuroscience.* 94:1019-27. doi: 10.1016/S0306-4522(99)00395-4

Gureviciene I, Ikonen S, Gurevicius K, Sarkaki A, van Groen T, Pussinen R, Ylinen A & Tanila H. (2004). Normal induction but accelerated decay of LTP in APP + PS1 transgenic mice. *Neurobiol. Dis.* 15: 188–195. doi: 10.1016/j.nbd.2003.11.011

## **H**

Hamani C, Diwan M, Isabella S, Lozano AM, Nobrega JN. (2010). Effects of different stimulation parameters on the antidepressant-like response of medial prefrontal cortex 21 deep brain stimulation in rats. *J Psychiatr Res* 44:683-687. doi: 10.1016/j.jpsychires.2009.12.010

- Hannesson DK, Howland JG and Phillips AG. (2004a). Interaction between perirhinal and medial prefrontal cortex is required for temporal order but not recognition memory for objects in rats. *Journal of Neuroscience*. 24:4596-604. doi: 10.1523/JNEUROSCI.5517-03.2004
- Hannesson DK, Vacca G, Howland JG and Phillips AG. (2004b). Medial prefrontal cortex is involved in spatial temporal order memory but not spatial recognition memory in tests relying on spontaneous exploration in rats. *Behav Brain Res*. 153(1):273-85. doi: 10.1016/j.bbr.2003.12.004
- Hasan MT, Hernández-González S, Dogbevia G, Treviño M, Bertocchi I, Gruart A, Delgado-García JM. (2013). Role of motor cortex NMDA receptors in learning- dependent synaptic plasticity of behaving mice. *Nat Commun* 4:2258. doi: 10.1038/ncomms3258
- Hebb DO. (1949). *The Organization of Behavior: A Neuropsychological Theory*. Wiley and Sons. ISBN-13: 978-0805843002
- Hess G & Donoghue JP. (1994). Long-term potentiation of horizontal connections provides a mechanism to reorganize cortical motor maps. *J. Neurophysiol*. 71: 2543–2547. [jn.physiology.org/content/71/6/2543.long](http://jn.physiology.org/content/71/6/2543.long)
- Hess G, Jacobs KM & Donoghue JP. (1994). N-methyl-D-aspartate receptor mediated component of field potentials evoked in horizontal pathways of rat motor cortex. *Neuroscience* 61: 225–235. doi: 10.1016/0306-4522(94)90226-7
- Hiremath SV, Chen W, Wang W, Foldes S, Yang Y, Tyler-Kabara EC, Collinger JL, Boninger ML. (2015). Brain computer interface learning for systems based on electrocorticography and intracortical microelectrode arrays. *Front Integr Neurosci* 9:40. doi: 10.3389/fnint.2015.00040
- Hong KS, Naseer N, Kim YH. (2015). Classification of prefrontal and motor cortex signals for three-class fNIRS–BCI. *Neurosci Lett* 587:87–92. doi: 10.1016/j.neulet.2014.12.029
- Hoover WB, Vertes RP. (2007). Anatomical analysis of afferent projections to the medial prefrontal cortex in the rat. *Brain Struct Funct* 212:149–179. doi: 10.1007/s00429-007-0150-4
- Horst NK & Laubach M. (2009). The role of rat dorsomedial prefrontal cortex in spatial working memory. *Neuroscience*. 164:444-56. doi: 10.1016/j.neuroscience.2009.08.004
- Hubel DH & Wiesel TN. (1959). Republication of *The Journal of Physiology* (1959) 148, 574-91: Receptive fields of single neurons in the cat's striate cortex. *J. Physiol*. 148: 574–591. doi: 10.1113/jphysiol.2009.174151.
- Huber D, Gutnisky DA, Peron S, O'Connor DH, Wiegert JS, Tian L, Oertner TG, Looger LL and Svoboda K. (2012). Multiple dynamic representations in the motor cortex during sensorimotor learning. *Nature*. 484: 473–478. doi: 10.1038/nature11039
- Huerta PT, Sun LD, Wilson MA & Tonegawa S. (2000). Formation of temporal memory requires NMDA receptors within CA1 pyramidal neurons. *Neuron*. 25: 473–480. doi: 10.1016/S0896-6273(00)80909-5

**I**

Iwasato T, Datwani A, Wolf AM, Nishiyama H, Taguchi Y, Tonegawa S, Knöpfel T, Erzurumlu RS & Itohara S. (2000). Cortex-restricted disruption of NMDAR1 impairs neuronal patterns in the barrel cortex. *Nature*. 406: 726–731. doi: 10.1038/35021059

**J**

Jackson ME, Frost AS, Moghaddam B. (2001). Stimulation of prefrontal cortex at physiologically relevant frequencies inhibits dopamine release in the nucleus accumbens. *J Neurochem* 78:920-923. doi: 10.1046/j.1471-4159.2001.00499.x

Jacobs GH, Fenwick JA, Williams GA. (2001). Cone-based vision of rats for ultraviolet and visible lights. *J Exp Biol* 204:2439–2446.

Jurado-Parras MT, Gruart A, Delgado-García JM. (2012). Observational learning in mice can be prevented by medial prefrontal cortex stimulation and enhanced by nucleus accumbens stimulation. *Learn Mem* 19:99–106. doi: 10.1101/lm.024760.111

**K**

Kable JW, Glimcher PW (2009) The neurobiology of decision: Consensus and controversy. *Neuron* 63:733–745. doi: 10.1016/j.neuron.2009.09.003

Kandel ER, Schwartz JH, Jessell TM, Siegelbaum SA, Hudspeth AJ. (2013). *Principles of neural science*; 5th ed. McGraw-Hill Companies. ISBN: 978-0-07-139011-8

Kantak KM, Black Y, Valencia E, Green-Jordan K, Eichenbaum HB. (2002). Dissociable effects of lidocaine inactivation of the rostral and caudal basolateral amygdala on the maintenance and reinstatement of cocaine seeking behavior in rats. *J Neurosci*. 22:1126-36.

Karni A, Meyer G, Rey-Hipolito C, Jezard P, Adams MM, Turner R, Ungerleider LG (1998) The acquisition of skilled motor performance: fast and slow experience-driven changes in primary motor cortex. *Proc Natl Acad Sci USA* 95:861–868. doi: 10.1073/pnas.95.3.861

Katz B and Miledi R (1968). The role of calcium in neuromuscular facilitation. *J Physiol*. 195:481-92. doi: 10.1113/jphysiol.1968.sp008469

Kesner RP & Churchwell JC. (2011). An analysis of rat prefrontal cortex in mediating executive function. *Neurobiology of Learning and Memory*. 96: 417–431. doi: 10.1016/j.nlm.2011.07.002

Kesner RP & Ragozzino ME. (2003). The role of the prefrontal cortex in object-place learning: a test of the attribute specificity model. *Behav Brain Res*. 146:159-65. doi: 10.1016/j.bbr.2003.09.024

Khanna P, Carmena JM. (2015). Neural oscillations: beta band activity across motor networks. *Curr Opin Neurobiol* 32:60-67. doi: 10.1016/j.conb.2014.11.010



Kishimoto Y, Kawahara S, Kirino Y, Kadotani H, Nakamura Y, Ikeda M & Yoshioka T. (1997). Conditioned eyeblink response is impaired in mutant mice lacking NMDA receptor subunit NR2A. *Neuroreport*. 8: 3717–3721. doi: 10.1097/00001756-199712010-00012

Kishimoto Y, Kawahara S, Mori H, Mishina M & Kirino Y. (2001). Long-trace interval eyeblink conditioning is impaired in mutant mice lacking the NMDA receptor subunit epsilon 1. *Eur. J. Neurosci*. 13: 1221–1227. doi: 10.1046/j.0953-816x.2001.01486.x

Kishimoto Y, Nakazawa K, Tonegawa S, Kirino Y & Kano M. (2006). Hippocampal CA3 NMDA receptors are crucial for adaptive timing of trace eyeblink conditioned response. *J. Neurosci*. 26: 1562–1570. doi: 10.1523/JNEUROSCI.4142-05.2006

Kleim JA, Barbay S, Cooper NR, Hogg TM, Reidel CN, Remple MS & Nudo RJ. (2002). Motor learning-dependent synaptogenesis is localized to functionally reorganized motor cortex. *Neurobiol. Learn. Mem.* 77: 63–77. doi: 10.1006/nlme.2000.4004

Kleim JA, Lussnig E, Schwarz ER, Comery TA & Greenough WT. (1996). Synaptogenesis and Fos expression in the motor cortex of the adult rat after motor skill learning. *J. Neurosci*. 16: 4529–4535. [www.jneurosci.org/content/16/14/4529.long](http://www.jneurosci.org/content/16/14/4529.long)

Kleim JA, Hogg TM, VandenBerg PM, Cooper NR, Bruneau R & Remple M. (2004). Cortical synaptogenesis and motor map reorganization occur during late, but not early, phase of motor skill learning. *J. Neurosci*. 24: 628–633. doi: 10.1523/JNEUROSCI.3440-03.2004

Kobayashi S, Schultz W, Sakagami M. (2010). Operant conditioning of primate prefrontal neurons. *J. Neurophysiol*. 103:1843–1855. doi:10.1152/jn.00173.2009

Komiyama T, Sato TR, O'Connor DH, Zhang YX, Huber D, Hooks BM, Gabitto M & Svoboda K. (2010) Learning-related fine-scale specificity imaged in motor cortex circuits of behaving mice. *Nature* 464: 1182–1186. doi: 10.1038/nature08897

Koralek AC, Jin X, Long JD 2nd, Costa RM, Carmena JM (2012) Corticostriatal plasticity is necessary for learning intentional neuroprosthetic skills. *Nature* 483:331-335. doi: 626 10.1038/nature10845

Kuroda M, Murakami K, Igarashi H, Okada A (1996) The convergence of axon terminals from the mediodorsal thalamic nucleus and ventral tegmental area on pyramidal cells in layer V of the rat prelimbic cortex. *Eur J Neurosci*. 8:1340-9. doi: 10.1111/j.1460-9568.1996.tb01596.x

## L

Larkum, M. E., Nevian, T., Sandler, M., Polsky, A. & Schiller, J. (2009). Synaptic integration in tuft dendrites of layer 5 pyramidal neurons: a new unifying principle. *Science*. 325: 756–760. doi: 10.1126/science.1171958

Leal-Campanario R, Fairén A, Delgado-García JM, Gruart A (2007) Electrical stimulation of the rostral medial prefrontal cortex in rabbits inhibits the expression of conditioned eyelid responses

but not their acquisition. *Proc Natl Acad Sci USA* 104:11459-11464. doi: 10.1073/pnas.0704548104

Leal-Campanario R, Delgado-García JM, Gruart A (2013) The rostral medial prefrontal cortex regulates the expression of conditioned eyelid responses in behaving rabbits. *J Neurosci* 33:4378-4386. doi: 10.1523/jneurosci.5560-12.2013

Lebedev MA, Nicolelis MA (2006) Brain-machine interfaces: past, present and future. *Trends Neurosci* 29:536-546. doi: 10.1016/j.tins.2006.07.004 22

Lee I, Solivan F (2008). The roles of the medial prefrontal cortex and hippocampus in a spatial paired-association task. *Learning and Memory*. 15:357-67. doi: 10.1101/lm.902708.

Leising KI, Wolf JE, Ruprecht C (2013) Visual discrimination learning with an iPad- equipped apparatus. *Behav Processes* 93:140-147. doi: 10.1016/j.beproc.2012.11.013

Lisman J, Yasuda R, Raghavachari S. (2012) Mechanisms of CaMKII action in long-term potentiation. *Nat. Rev. Neurosci.* 13, 169–182. doi:10.1038/nrn3192

Lutcke H, Murayama M, Hahn T, Margolis DJ, Astori S, Zum Alten Borgloh SM, Göbel W, Yang Y, Tang W, Kügler S, Sprengel R, Nagai T, Miyawaki A, Larkum ME, Helmchen F & Hasan MT. (2010). Optical recording of neuronal activity with a genetically encoded calcium indicator in anesthetized and freely moving mice. *Front. Neural. Circuits.* 4: 9. doi: 10.3389/fncir.2010.00009

## M

Madroñal N, Gruart A & Delgado-Garcia JM. (2009). Differing presynaptic contributions to LTP and associative learning in behaving mice. *Front. Behav. Neurosci.* 3:7. doi:10.3389/neuro.08.007.2009

Malenka RC, Bear MF (2004). LTP and LTD: an embarrassment of riches. *Neuron*. 44:5-21. doi:10.1016/j.neuron.2004.09.012

Margolis DJ, Lütcke H, Schulz K, Haiss F, Weber B, Kügler S, Hasan MT and Helmchen F. (2012). Reorganization of cortical population activity imaged throughout long-term sensory deprivation. *Nat. Neurosci.* 15: 1539–1546. doi: 10.1038/nn.3240

Massey PV, Bashir ZI (2007). Long-term depression: multiple forms and implications for brain function. *Trends Neurosci* 30:176-84. doi: 10.1016/j.tins.2007.02.005

Mastakov MY, Baer K, Xu R, Fitzsimons H & During MJ. (2000). Combined injection of rAAV with mannitol enhances gene expression in the rat brain. *Mol. Ther.* 3: 225–232. doi:10.1006/mthe.2001.0246

McCormick DA & Thompson RF. (1984). Cerebellum: essential involvement in the classically conditioned eyelid response. *Science* 223: 296–299. doi: 10.1126/science.6701513

Mehring C, Rickert J, Vaadia E, Cardoso de Oliveira S, Aertsen A, Rotter S (2003) Inference of hand movements from local field potentials in monkey motor cortex. *Nat Neurosci* 6:1253–1254. doi: 10.1038/nn1158

Meyer D, Bonhoeffer T, Scheuss V. (2014) Balance and stability of synaptic structures during synaptic plasticity. *Neuron* 82, 430–443. (doi:10.1016/j.neuron.2014.02.031)

Miyamoto K, Osada T, Adachi Y, Matsui T, Kimura HM & Miyashita Y. (2013). Functional differentiation of memory retrieval network in macaque posterior parietal cortex. *Neuron*. 77: 787–799. doi: 10.1016/j.neuron.2012.12.019

Moruzzi G, Magoun HW (1949) Brain stem reticular formation and activation of the EEG. *Electroencephalogr Clin Neurophysiol* 1:455–473. doi: 10.1176/jnp.7.2.251

Mountcastle VB. (1957). Modality and topographic properties of single neurons of cat's somatic sensory cortex. *J. Neurophysiol.* 20: 408–434. [jn.physiology.org/content/20/4/408.long](http://jn.physiology.org/content/20/4/408.long)

Moyer JR Jr, Thompson LT & Disterhoft JF. (1996). Trace eyeblink conditioning increases CA1 excitability in a transient and learning-specific manner. *J. Neurosci.* 16: 5536–5546. [www.jneurosci.org/content/16/17/5536.long](http://www.jneurosci.org/content/16/17/5536.long)

Moyer JR, Deyo RA & Disterhoft JF. (2015). Hippocampectomy disrupts trace eye-blink conditioning in rabbits. *Behav. Neurosci.* 104: 243–252. doi: 10.1037/bne0000079

## N

Niewoehner B, Single FN, Hvalby Ø, Jensen V, Meyer zum Alten Borgloh S, Seeburg PH, Rawlins JN, Sprengel R & Bannerman DM. (2007). Impaired spatial working memory but spared spatial reference memory following functional loss of NMDA receptors in the dentate gyrus. *Eur. J. Neurosci.* 25: 837–846. doi: 10.1111/j.1460-9568.2007.05312.x

## O

Oades RD, Halliday GM (1987) Ventral tegmental (A10) system: neurobiology. 1. Anatomy and connectivity. *Brain Res.* 434:117-65. doi: 10.1016/0165-0173(87)90011-7

O'Doherty JE, Lebedev MA, Ifft PJ, Zhuang KZ, Shokur S, Bleuler H, Nicolelis MA (2011) Active tactile exploration using a brain-machine-brain interface. *Nature* 479:228-231. doi: 10.1038/nature10489

Opris I, Lebedev M, Nelson R (2011) Motor planning under unpredictable reward: modulations of movement vigor and primate striatum activity. *Front Neurosci* 5:61. doi: 10.3389/fnins.2011.00061

Osada T, Adachi Y, Kimura HM & Miyashita Y. (2008). Towards understanding of the cortical network underlying associative memory. *Philos. Trans. R Soc. Lond. B Biol. Sci.* 363: 2187–2199. doi: 10.1098/rstb.2008.2271

**P**

Paxinos G, Watson C (1998) *The Rat Brain in Stereotaxic Coordinates*. San Diego, CA: Academic Press.

Paxinos G, Franklin KBJ (2001). *The Mouse Brain in Stereotaxic Coordinates*. London: Academic Press.

Pesaran B, Pezaris JS, Sahani M, Mitra PP, Andersen RA (2002) Temporal structure in neuronal activity during working memory in macaque parietal cortex. *Nat Neurosci* 5:805–811. doi: 10.1038/nn890

Porras-Garcia E, Cendelin J, Dominguez-del-Toro E, Vozeh F & Delgado-Garcia JM. (2005). Purkinje cell loss affects differentially the execution, acquisition and prepulse inhibition of skeletal and facial motor responses in Lurcher mice. *Eur. J. Neurosci.* 21: 979–988. doi: 10.1111/j.1460-9568.2005.03940.x

Poulet JF, Petersen CC (2008) Internal brain state regulates membrane potential synchrony in barrel cortex of behaving mice. *Nature* 454:881–885. doi: 10.1038/nature07150

Povysheva NV, Gonzalez-Burgos G, Zaitsev AV, Kröner S, Barrionuevo G, Lewis DA, Krimer LS (2006) Properties of excitatory synaptic responses in fast-spiking interneurons and pyramidal cells from monkey and rat prefrontal cortex. *Cereb Cortex* 16:541–552. doi: 10.1093/cercor/bhj002

Prusky GT, Harker KT, Douglas RM, Wishaw IQ (2002) Variation in visual acuity within pigmented, and between pigmented and albino rat strains. *Behav Brain Res* 136:339–348. doi: 10.1016/S0166-4328(02)00126-2

**R**

Ragozzino ME, Kim J, Hassert D, Minniti N, Kiang C (2003). The contribution of the rat prelimbic-infralimbic areas to different forms of task switching. *Behav Neurosci.* 117:1054–65. doi: 10.1037/0735-7044.117.5.1054

Regehr WG (2012). Short-term presynaptic plasticity. *Cold Spring Harb Perspect Biol.* 4:a005702. doi: 10.1101/cshperspect.a005702.

Rioult-Pedotti MS, Friedman D, Donoghue JP (2000) Learning-induced LTP in neocortex. *Science.* 290: 533–536. doi: 10.1126/science.290.5491.533

Rioult-Pedotti MS, Friedman D, Hess G & Donoghue, JP. (1998). Strengthening of horizontal cortical connections following skill learning. *Nat. Neurosci.* 1: 230–234 (1998). doi: 10.1038/678

Rockstroh B, Elbert T, Canavan A, Lutzenberger W, Birbaumer N. (1989) *Slow cortical potentials and behavior*, 2nd ed. Baltimore, MD: Urban and Schwarzenberg, **ISBN-13:** 978-3541702923

Rokni U, Richardson AG, Bizzi E & Seung HS. (2007). Motor learning with unstable neural representations. *Neuron*. 54: 653–666. doi: 10.1016/j.neuron.2007.04.030

Romero-Granados R, Fontán-Lozano A, Delgado-García JM, Carrión AM (2010) From learning to forgetting: behavioral, circuitry, and molecular properties define the different functional states of the recognition memory trace. *Hippocampus*. 20:584-95. doi: 10.1002/hipo.20669.

Rouse AG, Williams JJ, Wheeler JJ, Moran DW (2013) Cortical adaptation to a chronic micro-electrocorticographic brain computer interface. *J Neurosci* 33:1326–1330. doi: 10.1523/jneurosci.0271-12.2013 23

## **S**

Sakurai Y, Takahashi S (2013). Conditioned enhancement of firing rates and synchrony of hippocampal neurons and firing rates of motor cortical neurons in rats. *Eur J Neurosci*. 37:623-39. doi: 10.1111/ejn.12070.

Sanes JN & Donoghue JP. (2000). Plasticity and primary motor cortex. *Annu. Rev. Neurosci*. 23: 393–415. doi: 10.1146/annurev.neuro.23.1.393

Schafer RJ, Moore T (2011) Selective attention from voluntary control of neurons in prefrontal cortex. *Science* 332:1568-1571. doi: 10.1126/science.1199892

Schneggenburger R, Sakaba T, Neher E (2002). Vesicle pools and short-term synaptic depression: Lessons from a large synapse. *Trends Neurosci* 25: 206–212. doi: 10.1016/S0166-2236(02)02139-2

Schudlo LC, Power SD, Chau T (2013) Dynamic topographical pattern classification of multichannel prefrontal NIRS signals. *J Neural Eng* 10:046018. doi: 10.1088/1741-2560/10/4/046018

Sesack SR, Pickel VM (1992) Prefrontal cortical efferents in the rat synapse on unlabeled neuronal targets of catecholamine terminals in the nucleus accumbens septi and on dopamine neurons in the ventral tegmental area. *J Comp Neurol*. 1992 Jun 8;320(2):145-60. doi: 10.1002/cne.903200202

Shain W, Spataro L, Dilgen J, Haverstick K, Retterer S, Isaacson M, Saltzman M, Turner JN (2003) Controlling cellular reactive responses around neural prosthetic devices using peripheral and local intervention strategies. *IEEE Trans Neural Syst Rehabil* 11:186–188. doi: 10.1109/tnrse.2003.814800

Smith RJ, Lobo MK, Spencer S, Kalivas PW (2013) Cocaine-induced adaptations in D1 and D2 accumbens projection neurons (a dichotomy not necessarily synonymous with direct and indirect pathways). *Curr Opin Neurobiol* 23:546 –552. doi: 10.1016/j.conb.2013.01.026

So K, Dangi S, Orsborn AL, Gastpar MC, Carmena JM (2014) Subject-specific modulation of local field potential spectral power during brain–machine interface control in primates. *J Neural Eng* 11:026002. doi: 10.1088/1741-2560/11/2/026002

Sprengel R & Hasan MT. (2007). Tetracycline-controlled genetic switches. *Handb. Exp. Pharmacol.* 178: 49–72. doi: 10.1007/978-3-540-35109-2\_3

Squire LR, Zola-Morgan S. (1991). The medial temporal lobe memory system. *Science*. 253:1380-6. doi: 10.1126/science.1896849

St Onge JR, Floresco SB (2010). Prefrontal cortical contribution to risk-based decision making. *Cerebral Cortex*. 20:1816-28. doi: 10.1093/cercor/bhp250

Staubli UV, Ji Z-X. (1996) The induction of homo- vs. heterosynaptic LTD in area CA1 of hippocampal slices from adult rats. *Brain Res.* 714:169–176. doi:10.1016/0006-8993(95)01523-X

Sutton MA and Schuman EM (2006). Dendritic protein synthesis, synaptic plasticity, and memory. *Cell*. 49:58-127. doi: 10.1016/j.cell.2006.09.014

## T

Takatsuki K, Kawahara S, Takehara K, Kishimoto Y & Kirino Y (2001). Effects of the noncompetitive NMDA receptor antagonist MK-801 on classical eyeblink conditioning in mice. *Neuropharmacology* 41: 618–628. doi: 10.1016/S0028-3908(01)00113-7

Takiyama K & Okada M. (2012) Maximization of learning speed in the motor cortex due to neuronal redundancy. *PLoS Comput. Biol.* 8: e1002348. doi: 10.1371/journal.pcbi.1002348

Thomson RF (1988). The neural basis of basic associative learning of discrete behavioural responses. *Trends in Neuroscience*. 11:152-55. doi: 10.1016/0166-2236(88)90141-5

Troncoso J, Munera A & Delgado-Garcia JM (2007). Learning-dependent potentiation in the vibrissal motor cortex is closely related to the acquisition of conditioned whisker responses in behaving mice. *Learn. Mem.* 14: 84–93. doi: 10.1101/lm.341807

Tsien JZ, Huerta PT & Tonegawa S (1996). The essential role of hippocampal CA1 NMDA receptor-dependent synaptic plasticity in spatial memory. *Cell*. 87: 1327–1338. doi: 10.1016/S0092-8674(00)81827-9

## U

Uylings HB, Groenewegen HJ, Kolb B (2003). Do rats have a prefrontal cortex? *Behav Brain Res.* 146(1-2):3-17. doi: 10.1016/j.bbr.2003.09.028

## V

Van Boxtel GJM, Böcker KBE (1997). *Brain and behavior past, present, and future*. Tilburg: Tilburg University Press, 1997. pp. 25–39. ISBN 13: 9789036199179

Vertes RP (2004) Differential Projections of the infralimbic and prelimbic cortex in the rat. *Synapse* 51:32–58. doi: 10.1002/syn.10279

## W

Wallace DJ, Meyer zum Alten Borgloh S, Astori S, Yang Y, Bausen M, Kügler S, Palmer AE, Tsien RY, Sprengel R, Kerr JN, Denk W, Hasan MT. (2008). Single-spike detection in vitro and in vivo with a genetic Ca<sup>2+</sup> sensor. *Nat. Methods*. 5: 797–804. doi:10.1038/nmeth.1242

Wander JD, Blakely T, Miller KJ, Weaver KE, Johnson LA, Olson JD, Fetz EE, Rao RP, Ojemann JG (2013) Distributed cortical adaptation during learning of a brain-computer interface task. *Proc Natl Acad Sci USA* 110:10818–10823. doi: 10.1073/pnas.1221127110

Wang XJ (2008) Neurophysiological and computational principles of cortical rhythms in cognition. *Physiol Rev* 90:1195–1268. doi: 10.1152/physrev.00035.2008.

Weible AP, McEchron MD & Disterhoft JF. (2000). Cortical involvement in acquisition and extinction of trace eyeblink conditioning. *Behav. Neurosci.* 114: 1058–1067. doi: 10.1037/0735-7044.114.6.1058

Wise SP (2008). Forward frontal fields: phylogeny and fundamental function. *Trends Neurosci.* 31: 599–608. doi: 10.1016/j.tins.2008.08.008

Woodruff-Pak DS & Disterhoft JF. (2008). Where is the trace in trace conditioning? *Trends Neurosci.* 31: 105–112. doi: 10.1016/j.tins.2007.11.006

## X

Xu NL, Harnett MT, Williams SR, Huber D, O'Connor DH, Svoboda K and Magee JC. (2012). Nonlinear dendritic integration of sensory and motor input during an active sensing task. *Nature*. 492: 247–251. doi: 10.1038/nature11601

Xu T, Yu X, Perlik AJ, Tobin WF, Zweig JA, Tennant K, Jones T & Zuo Y. et al. (2009). Rapid formation and selective stabilization of synapses for enduring motor memories. *Nature* 462: 915–919. doi: 10.1038/nature08389

## Y

Yang ST, Shi Y, Wang Q, Peng JY and Li BM (2014) Neuronal representation of working memory in the medial prefrontal cortex of rats. *Mol Brain*. 7:61. doi: 10.1186/s13041-014-0061-2

Yokofujita J, Oda S, Igarashi H, Sato F, Kuroda M (2008). Synaptic characteristics between cortical cells in the rat prefrontal cortex and axon terminals from the ventral tegmental area that utilize different neurotransmitters. *Int J Neurosci.* 118:1443-59. doi: 10.1080/00207450701870253.

Yu C, Fan D, Lopez A, Yin HH (2012) Dynamic changes in single unit activity and  $\gamma$  oscillations in a thalamocortical circuit during rapid instrumental learning. *PLoS One*. 7(11):e50578. doi: 10.1371/journal.pone.0050578

## **Z**

Zacksenhouse M, Lebedev MA, Carmena JM, O'Doherty JE, Henriquez C, Nicolelis MAL. (2007). Cortical modulations increase in early sessions with brain-machine interface. *PLoSOne* 2:e629. doi:10.1371/journal.pone.0000619

Zagha E, Casale A, Sachdev RNS, McGinley MJ, McCormick DA (2013) Motor cortex feedback influences sensory processing by modulating network state. *Neuron* 79:567– 578. doi: 10.1016/j.neuron.2013.06.008

Zhu P, Aller MI, Baron U, Cambridge S, Bausen M, Herb J, Sawinski J, Cetin A, Osten P, Nelson ML, Kügler S, Seeburg PH, Sprengel R & Hasan MT. (2007). Silencing and un-silencing of tetracycline-controlled genes in neurons. *PLoS One* 2: e533. doi: 10.1371/journal.pone.0000533

Zucker RS & Regehr WG. (2002). Short-term synaptic plasticity. *Annu. Rev. Physiol.* 64: 355–405. doi: 10.1146/annurev.physiol.64.092501.114547





## 8. ANNEXES



ARTICLE

Received 3 Dec 2012 | Accepted 5 Jul 2013 | Published 27 Aug 2013

DOI: 10.1038/ncomms3258

OPEN

# Role of motor cortex NMDA receptors in learning-dependent synaptic plasticity of behaving mice

Mazahir T. Hasan<sup>1,2</sup>, Samuel Hernández-González<sup>3</sup>, Godwin Dogbevia<sup>1</sup>, Mario Treviño<sup>1</sup>, Ilaria Bertocchi<sup>1</sup>, Agnès Gruart<sup>3</sup> & José M. Delgado-García<sup>3</sup>

The primary motor cortex has an important role in the precise execution of learned motor responses. During motor learning, synaptic efficacy between sensory and primary motor cortical neurons is enhanced, possibly involving long-term potentiation and N-methyl-D-aspartate (NMDA)-specific glutamate receptor function. To investigate whether NMDA receptor in the primary motor cortex can act as a coincidence detector for activity-dependent changes in synaptic strength and associative learning, here we generate mice with deletion of the *Grin1* gene, encoding the essential NMDA receptor subunit 1 (GluN1), specifically in the primary motor cortex. The loss of NMDA receptor function impairs primary motor cortex long-term potentiation *in vivo*. Importantly, it impairs the synaptic efficacy between the primary somatosensory and primary motor cortices and significantly reduces classically conditioned eyeblink responses. Furthermore, compared with wild-type littermates, mice lacking primary motor cortex show slower learning in Skinner-box tasks. Thus, primary motor cortex NMDA receptors are necessary for activity-dependent synaptic strengthening and associative learning.

<sup>1</sup>Max Planck Institute for Medical Research, 69120 Heidelberg, Germany. <sup>2</sup>Charité—Universitätsmedizin, NeuroCure Cluster of Excellence, 12101 Berlin, Germany. <sup>3</sup>Division of Neuroscience, University Pablo de Olavide, 41013 Seville, Spain. Correspondence and requests for materials should be addressed to M.T.H. (email: mazahir.hasan@charite.de) or to J.M.D.-G. (email: jmdelgar@upo.es).

The primary motor cortex (M1) is pivotal for sensorimotor integration and precise control of voluntary movements<sup>1</sup>. Sensory signals in the cortex are represented as activity maps, with active neurons organized as functional clusters or modules<sup>2,3</sup>, which are continuously re-shaped by experience and learning<sup>4–7</sup>. However, there are also dynamic interactions between widely distributed functional modules in different cortical and subcortical regions. These interactions, by way of ‘putative’ overlapping functional neuronal assemblies<sup>8</sup>, are thought to form the necessary neural substrates for multimodal processing, and learning and memory consolidation<sup>9</sup>. At a connectivity level, cortical excitatory neurons, with their elaborate basal and apical dendrites, receive synaptic input from distantly located excitatory neurons, and local excitatory as well as inhibitory neurons<sup>10</sup>. Reciprocal corticocortical connections<sup>11</sup> and functional interactions between M1 and the primary somatosensory cortex (S1)<sup>7,12</sup>, possibly involving mechanisms of synaptic integration in different dendritic compartments<sup>13,14</sup>, with recruitment of N-methyl-D-aspartate (NMDA) receptor (NMDAR) channels<sup>13</sup>, are thus hypothesized to have an important role, for example, in organizing an animal’s motor activity plan to changes in the sensory experiences.

In classical associative learning, neurons corresponding to variant sensory cues are linked together to form ‘memory’ representations. It has been hypothesized that cue–response associations occur in the M1 cortex, which enables an animal to make a correct sensory-guided behavioural response. Eyeblink conditioning (EBC) is a form of classical conditioning that is well suited to dissect the cellular and molecular mechanisms of learning and memory consolidation. In EBC, the conditioned stimulus (CS), such as a tone, is paired with the unconditioned stimulus (US), such as a mild shock, to the eyelid. In untrained animals, the US alone elicits an eyeblink as the unconditioned response (UR). However, after repetitive CS–US pairings, the CS alone is sufficient to elicit an eyeblink, or the conditioned response (CR). In the delayed EBC, the CS is presented before the US and the two stimuli end together. In the trace EBC, however, there is a stimulus-free period (trace interval) between the CS and the US. While both of these conditioning paradigms require the cerebellum<sup>15</sup>, the trace EBC also requires the participation of the hippocampus<sup>16,17</sup> and the cortex<sup>18,19</sup>.

During motor learning, sensory signals are transmitted to the M1 cortex, inducing morphological and functional plasticity on multiple timescales<sup>20,21</sup>. Dynamic changes in neuronal activity<sup>7,22</sup> and activation of immediate-early genes<sup>23</sup> in the M1 cortex call into action cellular and molecular processes to strengthen pre-existing sensorimotor synaptic connections and to form new synapses<sup>24,25</sup>. The M1 cortex has the capacity for long-term potentiation (LTP)<sup>26</sup>, a candidate cellular model for learning and memory consolidation, and, importantly, LTP can be induced in this region by learning<sup>27</sup>. Recognizing the crucial role of NMDAR function in learning-induced cortical LTP<sup>28</sup>, map plasticity<sup>29</sup> and trace conditioning<sup>30–32</sup>, we hypothesized that the motor cortex NMDAR might act as a coincident detector for activity-dependent plasticity and associative learning.

To test this hypothesis, we generated mice lacking GluN1 and hence NMDAR specifically in the M1 cortex (*Grin1-vΔ<sup>MCx</sup>*). Here we show for the first time that the NMDAR function in the M1 cortex is important for learning-dependent synaptic plasticity and acquisition of associative memory for both classical and instrumental conditioning paradigms.

## Results

**Cre-mediated *Grin1* gene deletion.** To generate M1 cortex-specific *Grin1* gene knockout mice, we developed a combinatorial

genetic approach using viruses for conditional Cre recombinase (*Cre*) gene expression (Fig. 1a) in genetically engineered mice (*Grin1<sup>tm1.13P</sup>* or *Grin1<sup>2lox</sup>*)<sup>33</sup>, in which exons of the *Grin1* gene were flanked with *loxP* sites (Fig. 1b). We developed two recombinant adeno-associated viruses (rAAVs), which are equipped with the doxycycline (Dox)-controlled genetic switches<sup>34,35</sup>. The first virus (*rAAV-hSYN-rTA*) allows expression of reverse tetracycline transactivator (*rTA*) gene under control of the human synapsin promoter (*hSYN*, *Pro* in the Fig. 1a). The second virus (*rAAV-P<sub>tetbi</sub>-Cre/tdTOM*) is equipped with a bidirectional tet promoter (*P<sub>tetbi</sub>*) to simultaneously express two different genes encoding for the Cre recombinase protein and a red fluorescent protein variant, the tdTomato (tdTOM), for visualizing virus-targeted neurons (Fig. 1a). The *Cre* and the *tdTOM* genes are expressed when rTA binds to *P<sub>tetbi</sub>* in the presence of Dox. To increase the spread of virus in the M1 cortex by hyperosmolarity, D-mannitol/virus mixture was injected in the brain<sup>36</sup> and D-mannitol was also delivered into mice systemically by intraperitoneal injection<sup>37</sup> (Fig. 1c, Supplementary Fig. S1). Viruses were injected in the M1 cortex of age-matched wild-type littermates and *Grin1<sup>2lox</sup>* mice<sup>33</sup> (Fig. 1b). Three weeks after virus injection, Dox-treated mice showed robust tdTOM and Cre expression in the M1 cortex (Fig. 1c, Supplementary Fig. S2). Virus (v)-delivered Cre expression in neurons enabled, by Cre-loxP-mediated gene recombination, the generation of highly specific *Grin1* gene knockout mice, *Grin1-vΔ<sup>MCx</sup>*, in which the *Grin1* gene is selectively deleted (Δ) in the M1 cortex (MCx) (Fig. 1b,d). The virus-injected, age-matched wild-type littermates served as controls (*Cont-v<sup>MCx</sup>*).

By *in situ* RNA hybridization (see Supplementary Methods), we determined that the *Grin1* mRNA was absent specifically in the M1 cortex of *Grin1-vΔ<sup>MCx</sup>* mice (Dox-induced *Grin1* gene deletion) (Fig. 1d). Virus-injected control mice, *Grin1-v<sup>MCx</sup>*, (without *Grin1* gene deletion) showed normal *Grin1* mRNA expression (Fig. 1d). As expected, the expression of the *Grin1* gene encoding the AMPA ( $\alpha$ -amino-3-hydroxy-5-methyl-4-isoxazolepropionic acid) receptor (AMPA) subunit 1 (GluA1) was unaffected in both groups of mice (Fig. 1d), and Nissl-staining revealed no observable loss of neurons due to virus injections (Supplementary Fig. S3).

**NMDA receptor activity in acute brain slices.** As a proof-of-principle, we had arbitrarily targeted the somatosensory cortex (SSCx) for *Grin1* gene deletion. We recorded NMDAR miniature excitatory postsynaptic currents (NMDAR-mEPSCs, see Methods) in acute brain slices prepared from Dox-treated control (*Cont-v<sup>SSCx</sup>*, 12 cells, 4 mice) and Dox-induced *Grin1* gene-deleted brain slices (*Grin1-vΔ<sup>SSCx</sup>*, 15 cells, 4 mice) (Fig. 1e, Supplementary Fig. S4). We found that slices derived from *Cont-v<sup>SSCx</sup>* mice show large NMDAR-mEPSCs, which were blocked by the NMDAR-antagonist APV. However, charge transfer and NMDAR-mEPSCs were quite similar with and without APV in slices derived from the *Grin1-vΔ<sup>SSCx</sup>* mice (Fig. 1e, Supplementary Fig. S4). These results clearly demonstrate that NMDAR function is impaired in the *Grin1-vΔ<sup>SSCx</sup>* mice (Fig. 1e, Supplementary Fig. S4). As expected, *Grin1-vΔ<sup>SSCx</sup>* mice also showed strong reduction in the NMDA/AMPA current ratios (Fig. 1f, Supplementary Fig. S5).

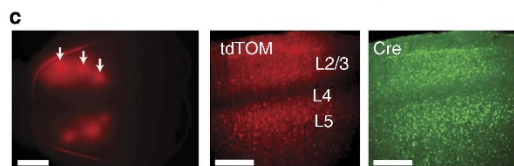
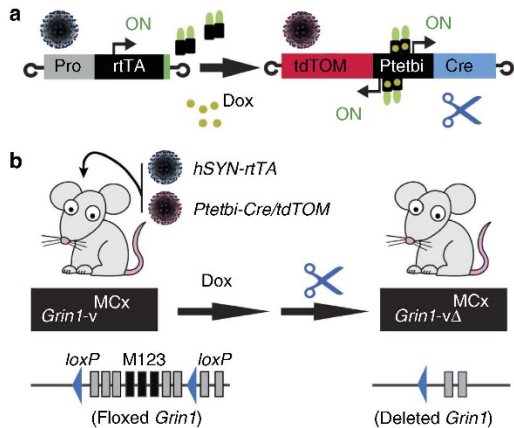
***In vivo* LTP measurements.** Initial *in vivo* experiments were aimed to determine the electrophysiological properties of S1–M1 synapses in behaving *Grin1-vΔ<sup>MCx</sup>* mice as compared with *Cont-v<sup>MCx</sup>* mice. Stimulating and recording electrodes were implanted in the corresponding facial areas of the primary somatosensory (S1) and motor cortices<sup>18</sup> (Fig. 2a). Both *Cont-v<sup>MCx</sup>* and *Grin1-*

$v\Delta^{MCx}$  mice ( $n=10$  per group) presented similar ( $F_{(1,19,18)}=2.310$ ;  $P=0.145$ ) increases in the slope of field excitatory postsynaptic potentials (fEPSPs) evoked at the M1 cortex following the presentation of single pulses of increasing intensity to the ipsilateral S1 region (Fig. 2b). These relationships were best fitted by sigmoid curves ( $r\geq 0.92$ ;  $P<0.001$ ), suggesting

normal functioning of this synapse in both groups of mouse. In addition, no significant facilitation (or depression) of fEPSPs evoked during the paired-pulse test ( $F_{(5,54,48)}=1.577$ ;  $P=0.185$ ) or significant ( $F_{(1,9,58)}=0.000494$ ;  $P=0.982$ ) differences between the groups ( $n=5$  per group) were observed (Fig. 2c). These results indicate that the S1–M1 synapse does not present the paired-pulse facilitation typical of hippocampal synapses in behaving mice<sup>38</sup> and that no pre-synaptic changes<sup>39</sup> were evoked by deletion of the *Grin1* gene.

Interestingly, the LTP study revealed significant differences between *Grin1-v\Delta^{MCx}* and their littermate controls ( $n=10$  per group). Thus, high-frequency stimulation (HFS) of the S1 region in *Grin1-v\Delta^{MCx}* mice did not evoke any significant ( $F_{(6,54,63)}=0.308$ ;  $P=0.580$ ) increase in fEPSP slopes in the motor cortex (Fig. 2d). In contrast, we observed in *Cont-v^{MCx}* mice a long-lasting LTP, significantly ( $F_{(6,54,63)}=11.915$ ;  $P<0.001$ ) larger than values collected from *Grin1-v\Delta^{MCx}* mice. In this case, results indicate that the NMDAR is necessary to evoke long-lasting postsynaptic changes in the M1 cortex following HFS of S1 neurons.

**Synaptic plasticity and the conditioned response.** Next, we implanted electrodes in *Cont-v^{MCx}* ( $n=10$ ) and *Grin1-v\Delta^{MCx}* ( $n=11$ ) mice (Supplementary Fig. S6) to record fEPSPs evoked at the S1–M1 synapse during the classical conditioning of eyelid responses, with an auditory signal as the CS and an electrical shock of the trigeminal nerve as the US<sup>16,18</sup> (Fig. 3a). After multiple trials of CS–US pairings, an association was formed, enabling a CS alone to elicit a CR, measured by electromyography (EMG) (Fig. 3b).



	<i>Grin1-v</i> <sup>MCx</sup>	<i>Grin1-v\Delta</i> <sup>MCx</sup>	<i>Grin1-v\Delta</i> <sup>MCx</sup>
<i>Grin1</i> mRNA			
<i>Gria1</i> mRNA			
Dox	–	+ (1 week)	+ (2 weeks)

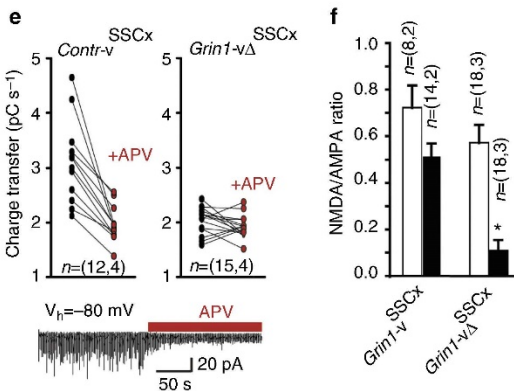


**Figure 1 | Motor cortex-specific *Grin1* gene knockout.** (a) Virus-mediated gene transfer for doxycycline (Dox) induced rtTA-dependent expression of tdTomato (tdTOM) and the Cre recombinase. (b) Cre expression in the brain of *Grin1*<sup>tm1RSP</sup> mice (*Grin1*<sup>2lox</sup>) activated the excision of *loxP*-flanked exons in the *Grin1* gene, thereby generating mice with neuron-specific *Grin1* gene deletion selectively in the M1 cortex (*Grin1-v\Delta*<sup>MCx</sup>). *LoxP* sites, blue triangles; exons, grey rectangles; exons encoding membrane-inserted segments M1–M3, black rectangles. (c) Expression of tdTOM detected on both hemispheres with a three-point virus injection in the M1 cortex (scale bar; 3 mm, left). Cellular resolution tdTOM expression (scale bar; 250  $\mu$ m, middle) and Cre (right) expression was specifically detected in cortical L2/3 and L5 (middle and right). (d) *In situ* mRNA hybridization analyses revealed the absence of *Grin1* mRNA expression in the M1 cortex of *Grin1-v\Delta*<sup>MCx</sup> mice (with Dox for 1 week and 2 weeks), but not in *Grin1-v*<sup>MCx</sup> mice (without Dox). Expression of *Gria1* mRNA in the M1 cortex was detectable in both *Grin1-v*<sup>MCx</sup> and *Grin1-v\Delta*<sup>MCx</sup> mice (Scale bar, 1 mm). (e) NMDAR-mEPSCs recorded at  $V_h = -80$  mV (sample trace at the bottom). NMDAR activity was detected by changes in charge transfer after 15 min of APV perfusion, measured over a time window of 125 s. 50  $\mu$ M APV decreases charge transfer in cells of *Cont-v*<sup>SSCx</sup> mice, but not *Grin1-v\Delta*<sup>SSCx</sup> mice. A multiple comparison one-way ANOVA test was performed on four groups: *Grin1-v\Delta*<sup>SSCx</sup>; *Grin1-v\Delta*<sup>SSCx</sup> + APV; *Cont-v*<sup>SSCx</sup>; and *Cont-v*<sup>SSCx</sup> + APV mice ( $F_{3,49} = 24.11$ ,  $P < 0.001$ ). (f) NMDA/AMPA ratios were averaged from sets of layer 2/3 pyramidal neurons recorded in either the left hemisphere (without virus injection, white bars) or right hemisphere (with virus injection, black bars). Ratios were similar between hemispheres from PBS-injected mice (see Supplementary Fig. S5) and from *Cont-v*<sup>SSCx</sup> mice. However, in *Grin1-v\Delta*<sup>SSCx</sup> mice, there was a substantial decrease in the NMDA/AMPA ratio only in the virus-infected hemisphere (PBS or viruses were injected only on the right hemisphere) (Data from PBS injected animals is illustrated in Supplementary Fig. S5;  $F_{5,68} = 33.85$ ,  $*P < 0.05$ , multiple comparison one-way ANOVA). Error is presented as mean  $\pm$  s.e.m.  $n =$  (cells, mice).

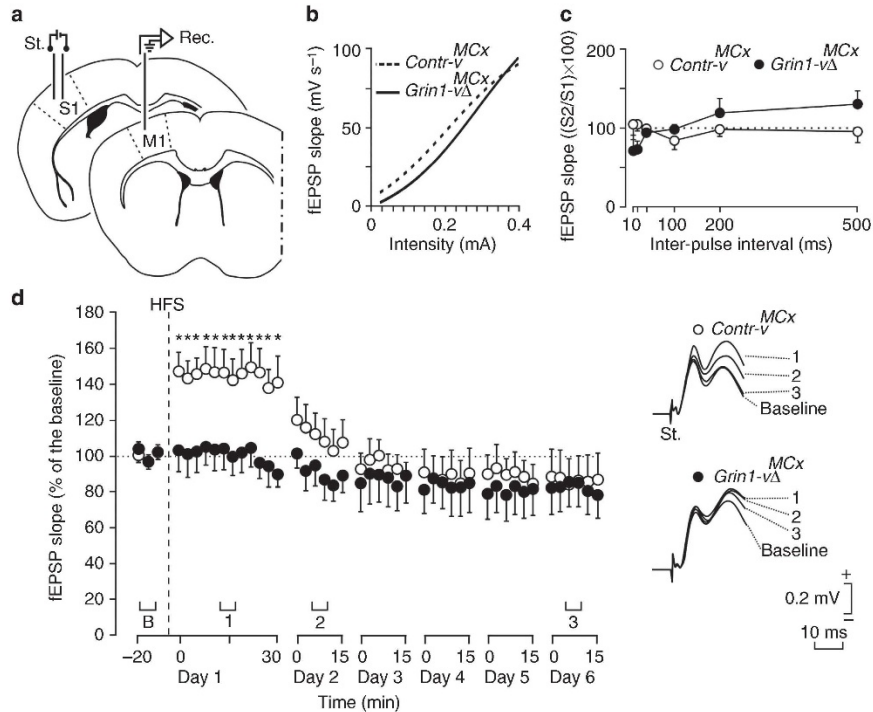


**Figure 2 | Paired-pulse facilitation and long-term potentiation induction.** (a) Schematic depicting electrode implanted *in vivo* for stimulating neurons in the S1 and recording in M1. (b) Input/output curves for the S1-primary motor cortex synapse. A single pulse was presented to S1 at increasing intensities (in mA), while recording the evoked fEPSP at the motor cortex for *Contr-v*<sup>MCx</sup> (white circle and dashed line) and *Grin1-vΔ*<sup>MCx</sup> (black circle and continuous line) mice. The best sigmoid adjustment to the collected data is represented ( $r > 0.92$ ;  $P \leq 0.001$ ; non-linear regression analysis). There were no significant differences between groups ( $n = 10$  per group;  $P = 0.145$ ;  $F_{(1,19,18)} = 2.310$ ; two-way ANOVA). (c) Responses to paired-pulse stimulation. The data shown are mean  $\pm$  s.e.m. slopes of the second fEPSP expressed as a percentage of the first for six (10, 20, 40, 100, 200 and 500) interstimulus intervals. The two groups ( $n = 5$  per group) of mice presented a similar ( $P = 0.185$ ;  $F_{(5,54,48)} = 1.577$ ; two-way ANOVA) paired-pulse facilitation at intervals of 20–100 ms. (d) At the top are illustrated examples of fEPSPs collected from selected *Contr-v*<sup>MCx</sup> (white circles) and *Grin1-vΔ*<sup>MCx</sup> (black circles) mice ( $n = 10$  per group) before (B, baseline) and after HFS of Schaffer collaterals. The bottom graphs illustrate the time course of LTP evoked in the motor cortex (fEPSP mean  $\pm$  s.e.m.) following HFS for *Contr-v*<sup>MCx</sup> and *Grin1-vΔ*<sup>MCx</sup> mice. The HFS was presented after 15 min of baseline recordings, at the time indicated by the dashed line. The fEPSP is given as a percentage of the baseline (100%) slope. *Grin1-vΔ*<sup>MCx</sup> mice have no LTP. In addition, values collected from the *Contr-v*<sup>MCx</sup> group were significantly ( $*P < 0.01$ ;  $F_{(6,54,63)} = 11.915$ ; two-way ANOVA) larger than those collected from *Grin1-vΔ*<sup>MCx</sup> mice.

First, we confirmed that reflexively evoked eye blinks collected from *Grin1-vΔ*<sup>MCx</sup> mice were similar from a kinematic point of view to those already described in *Cont-v*<sup>MCx</sup> mice<sup>16</sup> (Fig. 3b). Control mice (*Cont-v*<sup>MCx</sup>) acquired the classical conditioning test with a progressive increase in the percentage of CRs, reaching asymptotic values by the 7th conditioning session (Fig. 3d). In contrast, *Grin1-vΔ*<sup>MCx</sup> mice presented a non-significant ( $F_{(11,99,108)} = 1.670$ ;  $P = 0.0905$ ) slow increase in the percentage of CRs, reaching values significantly ( $P \leq 0.05$ ) lower than those presented by the control group from the 4th to the 10th conditioning sessions (Fig. 3d). These results indicate that *Grin1-vΔ*<sup>MCx</sup> mice were unable to acquire this type of associative learning task. Interestingly, and in opposition to results collected from *Cont-v*<sup>MCx</sup> mice, *Grin1-vΔ*<sup>MCx</sup> mice did not present any sign ( $F_{(1,19,18)} = 2.410$ ;  $P = 0.149$ ) of learning-dependent changes in synaptic strength at the S1–M1 synapse (Fig. 3c and e). As already reported for hippocampal synapses during classical EBC<sup>16</sup>, the S1–M1 synapse presented a significant ( $P < 0.05$ ) increase in fEPSP slopes across conditioning. However, in *Grin1-vΔ*<sup>MCx</sup> mice, the increase in fEPSP slopes across conditioning sessions was impaired (Fig. 3e). These results indicate that the

proper functioning of NMDARs located in the facial motor cortex is necessary both for the acquisition of classical EBC and to evoke the concomitant learning-dependent synaptic plasticity at cortical circuits.

**Instrumental learning.** We also checked whether *Grin1-vΔ*<sup>MCx</sup> mice ( $n = 12$ ) could acquire an instrumental learning task in the same way as their littermate controls (*Cont-v*<sup>MCx</sup>;  $n = 12$ ). In a first experimental step, animals were trained to acquire a fixed (1:1) ratio schedule—namely, when placed in a Skinner box, they have to learn to obtain a food pellet every time they pressed a lever located nearby the feeder (Fig. 4a). Control mice (*Cont-v*<sup>MCx</sup>) reached the selected criterion (to obtain 20 pellets in 20 min for two successive sessions) slightly (but not significantly; Student's  $t$ -test =  $-1.746$ ;  $P = 0.096$ ) before the *Grin1-vΔ*<sup>MCx</sup> mice (Fig. 4b,c). In a second step, animals were trained to press the lever only when an overlying light bulb was switched on (Fig. 4a). Pressing the lever during the dark period was not rewarded and, in addition, delayed the appearance of the lighted period (see Methods). This new conditioning paradigm presented

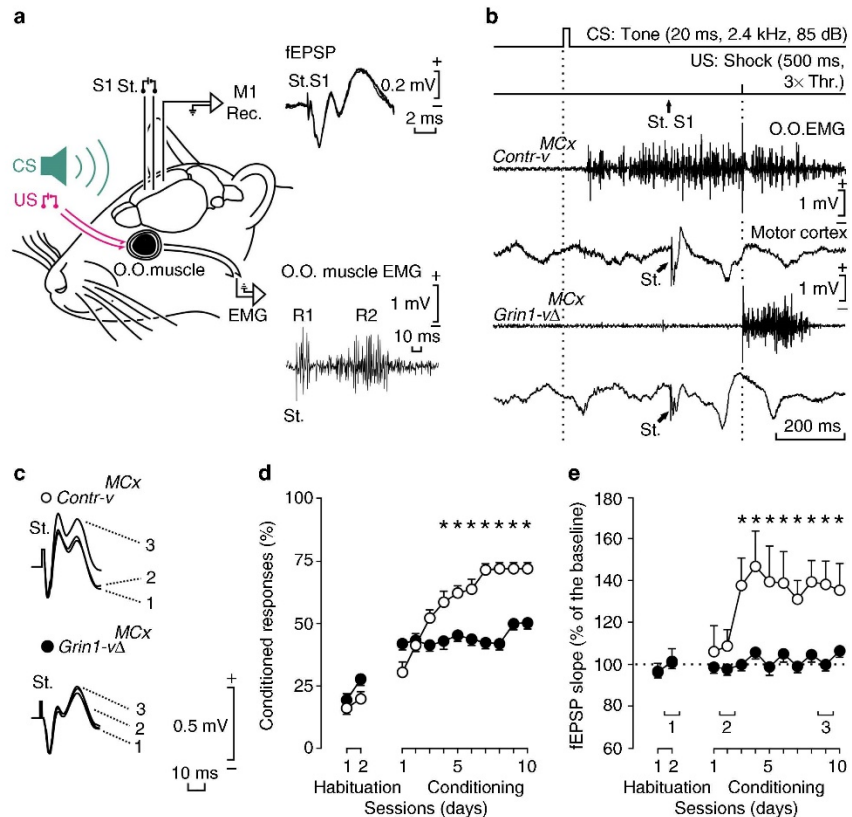


**Figure 3 | Electrophysiological recordings and classical EBC in behaving animals.** (a) For classical EBC, animals were implanted with stimulating (St.) electrodes (for US presentation) on the left trigeminal nerve and with electrodes to record (Rec.) the EMG activity of the ipsilateral orbicularis oculi (O.O.) muscle (for recording conditioned responses). The CS consisted of tones delivered from a loudspeaker located 50 cm from the animal's head. At the top are shown stimulating electrodes implanted in the right primary somatosensory cortex (S1) and recording electrodes implanted in the ipsilateral primary motor cortex (M1). fEPSP evoked in the motor cortex by single pulses applied to the S1 region are illustrated. Corneal reflex responses evoked at the O.O. muscle by electrical stimulation of the trigeminal nerve in a *Grin1-vΔ<sup>MCx</sup>* mouse are also illustrated. Note the presence of the two (R1, R2) components of the corneal reflex. (b) *Grin1-vΔ<sup>MCx</sup>* mice were unable of acquiring a conditioned eyeblink response and the accompanying activity-dependent changes in synaptic strength in cortical (S1-M1) synapses as *Contr-v<sup>MCx</sup>* mice did. From top to bottom are illustrated the conditioning paradigm, representative O.O. EMG and electrocortical recordings during paired CS-US presentations for *Contr-v<sup>MCx</sup>* and *Grin1-vΔ<sup>MCx</sup>* mice. The time of S1 stimulation (St. S1) is indicated, as are the times of presentation of CS and US (dotted lines). (c) fEPSPs collected from *Contr-v<sup>MCx</sup>* (white circles) and *Grin1-vΔ<sup>MCx</sup>* (black circles) mice during the conditioning sessions (1–3) indicated in (e). (d) Percentage (mean  $\pm$  s.e.m.) of conditioned responses reached by the two experimental groups ( $n \geq 10$  per group). Values presented by *Contr-v<sup>MCx</sup>* mice (white circles) were significantly ( $*P < 0.05$ ,  $F_{(1,20,19)} = 7.800$ , two-way ANOVA) larger than those reached by *Grin1-vΔ<sup>MCx</sup>* mice (black circles) from the 4th to the 10th sessions. (e) Evolution of fEPSPs evoked at the S1-primary motor cortex synapse across conditioning for wild-type (white circles) and *Grin1-vΔ<sup>MCx</sup>* (black circles) mice. Differences in fEPSP slopes (mean  $\pm$  s.e.m.) between *Contr-v<sup>MCx</sup>* and *Grin1-vΔ<sup>MCx</sup>* groups were statistically significant from the 3rd to the 10th conditioning sessions ( $*P < 0.05$ ,  $F_{(1,19,18)} = 8.889$ , two-way ANOVA).

more difficulties to the experimental animals than the early fixed (1:1) ratio schedule. Indeed, *Contr-v<sup>MCx</sup>* mice performed this task significantly ( $F_{(1,23,11)} = 17.159$ ;  $P < 0.05$ ) better than *Grin1-vΔ<sup>MCx</sup>* mice (Fig. 4d), again indicating that NMDAR function in motor cortex circuits is necessary for the acquisition of this type of associative learning task.

## Discussion

In the current study, we have developed a combinatorial genetic approach utilizing rAAVs equipped with tet-controlled genetic switches and *loxP*-engineered knock-in mice for Dox-induced,

cell-type-specific *Grin1* gene knockout, selectively in the M1 cortex of mice. We provide here very strong evidence that functional loss of the NMDA receptor abolished *in vivo* LTP in the cortex. We also found that synaptic strengthening of synapses between somatosensory and motor cortices was impaired during associative learning. Importantly, in the same mice, there was strong impairment of conditioned-evoked behavioural responses and learning was significantly reduced in the Skinner-box test.

Interestingly, we observed that the *Grin1-vΔ<sup>MCx</sup>* mice showed some residual learning, both in the classical EBC task and the instrumental conditioning. We anticipate two possible explanations for this interesting observation. First, with  $\sim 80\%$



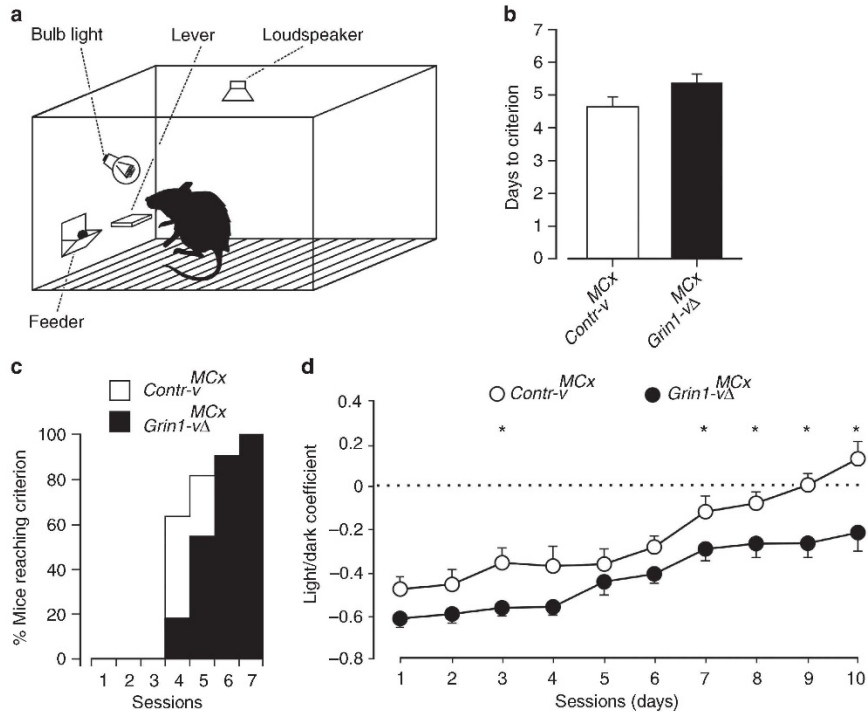


**Figure 4 | Performance during operant conditioning tasks.** (a) Experimental set-up. Mice were trained in a Skinner box to press a lever to obtain a food pellet with a fixed-ratio (1:1) schedule. (b) Number of days necessary to reach criterion (mean  $\pm$  s.e.m.) for *Contr-v*<sup>MCx</sup> (white bar) and *Grin1-vΔ*<sup>MCx</sup> (black bar) mice. (c) Percentage of mice reaching criterion across training. Note in (b) and (c) those *Contr-v*<sup>MCx</sup> mice ( $n=10$ ) reached criterion before *Grin1-vΔ*<sup>MCx</sup> ( $n=11$ ) mice. (d) Performance of the light/dark test. After reaching criterion for a fixed (1:1) schedule, animals were presented with a more difficult task in which lever presses were rewarded only when a light bulb was switched on. In this situation, *Contr-v*<sup>MCx</sup> mice presented a significantly ( $*P \leq 0.05$ , two-way ANOVA) better performance than *Grin1-vΔ*<sup>MCx</sup> mice. The light/dark coefficient was calculated as: (number of lever presses during the light period – number of lever presses during the dark period)/total number of lever presses (mean  $\pm$  s.e.m.).

of neurons targeted by rAAVs<sup>40,41</sup>, and with redundancy in neuronal coding for the same behavioural task in the motor cortex<sup>7,42</sup>, possibly to improve behavioural performance<sup>43</sup>, it is possible that the remaining untargeted neurons in the M1 cortex (without the *Grin1* gene deletion) might have contributed in executing some residual learning function. Second, it is also possible that in *Grin1-vΔ*<sup>MCx</sup> mice, the cerebellar function, in part, might have participated in trace EBC<sup>44</sup>.

Although a simple EBC is a prototypical example of a non-declarative memory, trace and delay EBC are fundamentally different kinds of learning<sup>45</sup>. An introduction of a 'trace'<sup>46</sup> component in the EBC endows it with some common features shared with the declarative memory. With dynamic feedforward and top-down interactions between different cortical and subcortical brain regions, involving both localized<sup>15</sup> and widely distributed<sup>47</sup> neuronal networks, distinct cortical cell ensembles representing different experiences might be linked by learning to form unique memories. Our results provide convincing evidence that the memory of acquired trace eyeblink-conditioned responses is localized in the M1 cortex. Therefore, dissecting the mechanisms of trace EBC in the M1 cortex is bound to provide deeper insight into the molecular and cellular mechanisms of declarative memory<sup>48</sup>.

Curiously, in earlier studies, genetically modified mice with deletion of the *Grin1* gene in CA1 showed deficit in acquisition of both spatial<sup>49</sup> and temporal<sup>50</sup> memories. However, it was later

found that, over time (several months), the *Grin1* gene deletion in these mice had also spread to all cortical layers<sup>51</sup>, leaving open the possibility that a cortical component might be having a crucial role in forming associations between spatial cues<sup>49</sup> and between temporally separated events<sup>50</sup>. With an improved genetic mouse model, a recent study provides the best evidence thus far that the NMDAR in the dorsal CA1 subfield and dentate gyrus is not required for the acquisition of spatial memories, despite impaired hippocampal LTP in these mice<sup>52</sup>. Instead, hippocampal NMDARs are needed to resolve conflict between competing spatial cues<sup>52</sup>. Notably, deletion of the *Grin1* gene specifically in CA3 also did not interfere with trace EBC<sup>53</sup>. However, CA3-NMDARs tend to have a crucial role in the memory of adaptive CR timing<sup>53</sup>. It thus seems quite plausible that while the hippocampus is needed for organizing spatial computations, it is in the cerebral cortex, where spatial memories<sup>49</sup> and temporal associations<sup>50</sup> are acquired and, perhaps, even stored<sup>47,54,55</sup>, possibly involving both localized and widely distributed cortical cell assemblies<sup>54</sup>. Interestingly, it was found that during classical EBC, the CA3-CA1 synapses and the S1-M1 synapses were similarly strengthened<sup>16,18</sup>. As hippocampus lesion is known to impair eyeblink trace conditioning<sup>53,56</sup>, it is quite important to investigate the role of CA1-NMDAR function in this particular associative learning paradigm.

Our virus-based, chemically controlled genetic approach allows for inducible control of gene expression<sup>34,57</sup> and inducible gene

knockout in mouse brain. With these powerful tools, it is now possible to precisely manipulate the function of individual neuronal cell types, cortical layers and brain regions in different mammalian species. In our current study, the AAVs of hybrid serotype 1 and 2 targeted cortical neurons<sup>40,41</sup> of layer 2/3 and layer 5, thereby deleting in these cells the *Grin1* gene and impairing NMDAR function. In future studies, our virus-based inducible genetic approach should further help to investigate, in cortical layer- and cell-type-specific manner, whether motor cortex NMDAR function is required for consolidation and retrieval of the conditioned eyeblink response.

## Methods

**Motor cortex-specific *Grin1* gene knockout.** Homozygous *Grin1*<sup>2loxP</sup> mice or (*Grin1*<sup>tm1Rap</sup>)<sup>33</sup> were generated by mating heterozygous males with heterozygous females. Viruses equipped with tet-controlled genetic switches<sup>34,37</sup> were bilaterally injected in the primary motor cortex (M1) of adult homozygous *Grin1*<sup>2loxP</sup> male<sup>33</sup> mice or wild-type control (*Contr*) littermates, and abbreviated as *Grin1*-v<sup>MCx</sup> and *Contr*-v<sup>MCx</sup>, respectively. Three weeks after virus (v) injection, both groups of mice were similarly treated with Dox, enabling Cre-mediated deletion (Δ) of the *Grin1* gene in adult homozygous *Grin1*<sup>2loxP</sup> males<sup>33</sup> and leading to the generation of motor cortex (MCx)-specific *Grin1* gene knockout mice (here referred to as *Grin1*-v<sup>MCx</sup>Δ). These mice were analysed for Dox-induced gene expression, *Grin1* gene deletion by *in situ* hybridization and functional NMDAR activity. See Supplementary Methods for details on the combinatorial genetic approach applied for motor cortex-specific *Grin1* gene knockout in the mouse brain and for validating functional loss of *Grin1* gene expression by *in situ* hybridization, and NMDA receptor function by *in vitro* electrophysiology. All experiments were conducted according to German and Spanish animal welfare regulations.

**Surgery for chronic-recording experiments.** Animals were anesthetized with 0.8–3% halothane delivered from a calibrated Fluotec 5 (Fluotec-Olhmeda, Tewksbury, Massachusetts, USA) vaporizer at a flow rate of 1–2 l min<sup>-1</sup> oxygen. Animals were implanted with bipolar stimulating electrodes aimed at the facial area<sup>18</sup> of the right S1 region (1 mm posterior to bregma, 2.5 mm lateral and 1.2 mm from brain surface) and with two recording electrodes aimed at the facial<sup>18</sup> ipsilateral primary motor cortex (1 mm anterior to bregma, 1 mm lateral and 0.8 mm from brain surface). These electrodes were made of 50 μm, Teflon-coated tungsten wire (Advent Research Materials Ltd, Eynsham, UK). The final position of the recording electrodes was determined using as a guide the field potential depth profile evoked by paired (40 ms of interval) pulses presented at the S1 area<sup>18</sup>. A bare silver wire (0.1 mm) was affixed to the skull as a ground. Wires were connected to a four-pin socket and the socket was fixed to the skull with the help of two small screws and dental cement<sup>16</sup>.

**Recording and stimulation procedures.** Both the EMG activity of the orbicularis oculi muscle and fEPSPs were recorded with Grass P511 differential amplifiers (Grass-Telefactor, West Warwick, Rhode Island, USA), at a bandwidth of 0.1 Hz–10 kHz. A high-impedance probe (2 × 10<sup>12</sup> Ω, 10 pF) was used for fEPSP recordings. Electrical stimulus applied to the S1 region consisted of 100 μs, square, biphasic pulses presented alone, paired or in trains. Stimulus intensities ranged from 0.02 to 0.4 mA for the construction of the input/output curves. For paired-pulse facilitation, the stimulus intensity was set well below the threshold for evoking a population spike, usually 30–40% of the intensity (mA) necessary for evoking a maximum fEPSP response<sup>38</sup>. Paired pulses were presented at six (10, 20, 40, 100, 200 and 500 ms) different pulse intervals.

For LTP induction, the stimulus intensity was also set at ≈35% of peak fEPSP values. An additional criterion for selecting stimulus intensity for LTP induction was that a second stimulus, presented 40 ms after a conditioning pulse, evoked a synaptic field potential 20% larger than the first fEPSP<sup>59</sup>. After 15 min of baseline records (1 stimulus per 20 s), each animal was presented with an HFS protocol consisting of five trains (200 Hz, 100 ms) of pulses at a rate of 1 per s. This protocol was presented six times in total, at intervals of 1 min. Evolution of fEPSPs after the HFS protocol was followed for 30 min at the same stimulation rate (1 stimulus per 20 s). Additional recording sessions (15 min) were carried out for up to 5 days<sup>16,38</sup>.

**Classical EBC.** Experimental sessions were carried out with three animals at a time. Animals were placed in separate small (5 × 5 × 10 cm) plastic chambers located inside a larger (30 × 30 × 20 cm) Faraday box. Animals were classically conditioned using a trace paradigm. For this, a tone (20 ms, 2.4 kHz, 85 dB) was presented as CS, while the US consisted of a 500-μs, 3 × threshold, square, cathodal pulse applied to the supraorbital nerve 500 ms after the end of the CS. A total of two habituation and 10 conditioning sessions (one session per day) were carried out for each animal. A conditioning session consisted of 60 CS–US presentations, and lasted for ≈30 min. For a proper analysis of conditioned responses, the CS was presented alone in 10% of the cases. CS–US presentations

were separated at random by 30 ± 5 s. For habituation sessions, only the CS was presented, also for 60 times per session, at intervals of 30 ± 5 s. As a criterion, we considered a 'conditioned response', the presence, during the CS–US interval, of EMG activity lasting >20 ms and initiated >50 ms after CS onset. In addition, the integrated EMG activity recorded during the CS–US interval had to be at least 2.5 times greater than the averaged activity recorded immediately before CS presentation<sup>16,60</sup>.

During habituation and conditioning sessions, fEPSPs were evoked in the motor cortex area by single 100 μs, square, biphasic (negative–positive) pulses applied the S1 region 300 ms after CS presentation. As above-indicated, pulse intensity was set at 30–40% of the amount necessary to evoke a maximum fEPSP response (range, 0.05–0.15 mA). An additional criterion for selecting stimulus intensity was that a second stimulus, presented 40 ms later, evoked a larger (>20%) synaptic field potential than the first<sup>38,59</sup>.

**Instrumental conditioning.** Training and testing took place in five Skinner box modules measuring 12.5 × 13.5 × 18.5 cm (MED Associates, St Albans, Vermont, USA). The operant conditioning boxes were housed within independent sound-attenuating chambers (90 × 55 × 60 cm), which were constantly illuminated (19 W lamp) and exposed to a 45 dB white noise (Cibertec SA, Madrid, Spain). Each Skinner box was equipped with a food dispenser from which pellets (Noyes formula P; 45 mg; Sandown Scientific, Hampton, UK) could be delivered by pressing a lever. Before training, mice were handled daily for 7 days and food-deprived to 80% of their free-feeding weight. Training took place for 20 min during successive days, in which mice were allowed to press the lever to receive pellets from the feeder using a fixed-ratio (1:1) schedule. The start and end of each session was indicated by a tone (2 kHz, 200 ms, 70 dB) provided by a loudspeaker located in the isolating chamber. Animals were maintained on this 1:1 schedule until they reached the selected criterion—namely, until they were able to obtain ≥20 pellets for two successive sessions. Mice reached the criterion after 4–7 days of training. Once the criterion for the 1:1 schedule was reached, conditioning was carried out for 10 additional days using a light/dark protocol. In this protocol, only lever presses performed during the light period (20 s) were reinforced with a pellet. In contrast, lever presses performed during the dark period (20 ± 10 s) were not reinforced. Moreover, lever presses carried out during the dark period increased its duration in up to 10 additional seconds.

**Histology.** At the end of the recording sessions, mice were deeply anesthetized (sodium pentobarbital, 50 mg kg<sup>-1</sup>) and perfused transcardially with saline and 4% phosphate-buffered paraformaldehyde. Brains were dissected, postfixed overnight at 4 °C, and cryoprotected in 30% sucrose in PBS. Sections were obtained in a microtome (Leica, Wetzlar, Germany) at 50 μm. Some selected sections including motor and somatosensory cortices were mounted on gelatinized glass slides and stained using the Nissl technique with 0.1% toluidine blue to determine the location of stimulating and recording electrodes.

**Data analysis.** Field EPSPs, EMG and 1–V rectangular pulses corresponding to CS and US presentations were stored digitally on a computer via an analogue/digital converter (CED 1401 Plus, Cambridge, England) at a sampling frequency of 11–22 kHz and with an amplitude resolution of 12 bits. Data were analysed offline for quantification of conditioned responses and fEPSP slopes with the help of commercial (Spike 2 and SIGAVG from CED) and custom programs<sup>16,60</sup>. The slope of evoked fEPSPs was computed as the first derivative (V s<sup>-1</sup>) of fEPSP recordings (V). For this, five successive fEPSPs were averaged, and the mean value of the slope during the rise time period (that is, between the initial and final 10% of the fEPSP) was determined. Computed results were processed for statistical analysis using the Sigma Stat software package (SSI, San Jose, California).

Instrumental conditioning programs, lever presses and delivered reinforcements were controlled and recorded by a computer, using a MED-PC programme (MED Associates). Operant sessions were recorded with a synchronized video capture system (Sony HDR-SR12E, Tokyo, Japan) for offline analysis.

## References

- Sanes, J. N. & Donoghue, J. P. Plasticity and primary motor cortex. *Annu. Rev. Neurosci.* **23**, 393–415 (2000).
- Hubel, D. H. & Wiesel, T. N. Receptive fields of single neurones in the cat's striate cortex. *J. Physiol.* **148**, 574–591 (1959).
- Mountcastle, V. B. Modality and topographic properties of single neurons of cat's somatic sensory cortex. *J. Neurophysiol.* **20**, 408–434 (1957).
- Buonomano, D. V. & Merzenich, M. M. Cortical plasticity: from synapses to maps. *Annu. Rev. Neurosci.* **21**, 149–186 (1998).
- Rioult-Pedotti, M. S., Friedman, D., Donoghue, J. P. & Learning-induced, L. T. P. in neocortex. *Science* **290**, 533–536 (2000).
- Margolis, D. J. *et al.* Reorganization of cortical population activity imaged throughout long-term sensory deprivation. *Nat. Neurosci.* **15**, 1539–1546 (2012).
- Huber, D. *et al.* Multiple dynamic representations in the motor cortex during sensorimotor learning. *Nature* **484**, 473–478 (2012).

8. Hebb, D. O. *The Organization of Behavior: A Neuropsychological Theory* (Wiley and Sons, 1949).
9. Buzsáki, G. Neural syntax: cell assemblies, synapses, and readers. *Neuron* **68**, 362–385 (2010).
10. Callaway, E. M. Feedforward, feedback and inhibitory connections in primate visual cortex. *Neural Netw.* **17**, 625–632 (2004).
11. Aronoff, R. et al. Long-range connectivity of mouse primary somatosensory barrel cortex. *Eur. J. Neurosci.* **31**, 2221–2233 (2010).
12. Perezou, I. et al. Spatiotemporal dynamics of cortical sensorimotor integration in behaving mice. *Neuron* **56**, 907–923 (2007).
13. Larkum, M. E., Nevian, T., Sandler, M., Polsky, A. & Schiller, J. Synaptic integration in tuft dendrites of layer 5 pyramidal neurons: a new unifying principle. *Science* **325**, 756–760 (2009).
14. Xu, N. L. et al. Nonlinear dendritic integration of sensory and motor input during an active sensing task. *Nature* **492**, 247–251 (2012).
15. McCormick, D. A. & Thompson, R. F. Cerebellum: essential involvement in the classically conditioned eyelid response. *Science* **223**, 296–299 (1984).
16. Gruart, A., Muñoz, M. D. & Delgado-García, J. M. Involvement of the CA3-CA1 synapse in the acquisition of associative learning in behaving mice. *J. Neurosci.* **26**, 1077–1087 (2006).
17. Moyer, Jr J. R., Thompson, L. T. & Disterhoft, J. F. Trace eyeblink conditioning increases CA1 excitability in a transient and learning-specific manner. *J. Neurosci.* **16**, 5536–5546 (1996).
18. Troncoso, J., Munera, A. & Delgado-García, J. M. Learning-dependent potentiation in the vibrissal motor cortex is closely related to the acquisition of conditioned whisker responses in behaving mice. *Learn. Mem.* **14**, 84–93 (2007).
19. Weible, A. P., McEchron, M. D. & Disterhoft, J. F. Cortical involvement in acquisition and extinction of trace eyeblink conditioning. *Behav. Neurosci.* **114**, 1058–1067 (2000).
20. Karni, A. et al. The acquisition of skilled motor performance: fast and slow experience-driven changes in primary motor cortex. *Proc. Natl Acad. Sci. USA* **95**, 861–868 (1998).
21. Kleim, J. A. et al. Cortical synaptogenesis and motor map reorganization occur during late, but not early, phase of motor skill learning. *J. Neurosci.* **24**, 628–633 (2004).
22. Komiyama, T. et al. Learning-related fine-scale specificity imaged in motor cortex circuits of behaving mice. *Nature* **464**, 1182–1186 (2010).
23. Kleim, J. A., Lussnig, E., Schwarz, E. R., Comery, T. A. & Greenough, W. T. Synaptogenesis and Fos expression in the motor cortex of the adult rat after motor skill learning. *J. Neurosci.* **16**, 4529–4535 (1996).
24. Xu, T. et al. Rapid formation and selective stabilization of synapses for enduring motor memories. *Nature* **462**, 915–919 (2009).
25. Kleim, J. A. et al. Motor learning-dependent synaptogenesis is localized to functionally reorganized motor cortex. *Neurobiol. Learn. Mem.* **77**, 63–77 (2002).
26. Hess, G. & Donoghue, J. P. Long-term potentiation of horizontal connections provides a mechanism to reorganize cortical motor maps. *J. Neurophysiol.* **71**, 2543–2547 (1994).
27. Rioult-Pedotti, M. S., Friedman, D., Hess, G. & Donoghue, J. P. Strengthening of horizontal cortical connections following skill learning. *Nat. Neurosci.* **1**, 230–234 (1998).
28. Hess, G., Jacobs, K. M. & Donoghue, J. P. N-methyl-D-aspartate receptor mediated component of field potentials evoked in horizontal pathways of rat motor cortex. *Neuroscience* **61**, 225–235 (1994).
29. Iwasato, T. et al. Cortex-restricted disruption of NMDAR1 impairs neuronal patterns in the barrel cortex. *Nature* **406**, 726–731 (2000).
30. Kishimoto, Y. et al. Conditioned eyeblink response is impaired in mutant mice lacking NMDA receptor subunit NR2A. *Neuroreport* **8**, 3717–3721 (1997).
31. Takatsuki, K., Kawahara, S., Takehara, K., Kishimoto, Y. & Kirino, Y. Effects of the noncompetitive NMDA receptor antagonist MK-801 on classical eyeblink conditioning in mice. *Neuropharmacology* **41**, 618–628 (2001).
32. Kishimoto, Y., Kawahara, S., Mori, H., Mishina, M. & Kirino, Y. Long-trace interval eyeblink conditioning is impaired in mutant mice lacking the NMDA receptor subunit epsilon 1. *Eur. J. Neurosci.* **13**, 1221–1227 (2001).
33. Nieuwenhuis, B. et al. Impaired spatial working memory but spared spatial reference memory following functional loss of NMDA receptors in the dentate gyrus. *Eur. J. Neurosci.* **25**, 837–846 (2007).
34. Zhu, P. et al. Silencing and un-silencing of tetracycline-controlled genes in neurons. *PLoS One* **2**, e533 (2007).
35. Cambridge, S. B. et al. Doxycycline-dependent photoactivated gene expression in eukaryotic systems. *Nat. Methods* **6**, 527–531 (2009).
36. Mastakov, M. Y., Baer, K., Xu, R., Fitzsimons, H. & During, M. J. Combined injection of rAAV with mannitol enhances gene expression in the rat brain. *Mol. Ther.* **3**, 225–232 (2000).
37. Burger, C., Nguyen, F. N., Deng, J. & Mandel, R. J. Systemic mannitol-induced hyperosmolality amplifies rAAV2-mediated striatal transduction to a greater extent than local co-infusion. *Mol. Ther.* **11**, 327–331 (2004).
38. Madronal, N., Gruart, A. & Delgado-García, J. M. Differing presynaptic contributions to LTP and associative learning in behaving mice. *Front. Behav. Neurosci.* **3**, 7 (2009).
39. Zucker, R. S. & Regehr, W. G. Short-term synaptic plasticity. *Annu. Rev. Physiol.* **64**, 355–405 (2002).
40. Lutcke, H. et al. Optical recording of neuronal activity with a genetically-encoded calcium indicator in anesthetized and freely moving mice. *Front. Neural Circuits* **4**, 9 (2010).
41. Wallace, D. J. et al. Single-spike detection in vitro and in vivo with a genetic Ca<sup>2+</sup> sensor. *Nat. Methods* **5**, 797–804 (2008).
42. Rokni, U., Richardson, A. G., Bizzi, E. & Seung, H. S. Motor learning with unstable neural representations. *Neuron* **54**, 653–666 (2007).
43. Takiyama, K. & Okada, M. Maximization of learning speed in the motor cortex due to neuronal redundancy. *PLoS Comput. Biol.* **8**, e1002348 (2012).
44. Woodruff-Pak, D. S. & Disterhoft, J. F. Where is the trace in trace conditioning? *Trends Neurosci.* (2008); **31**, 105–112.
45. Clark, R. E., Manns, J. R. & Squire, L. R. Trace and delay eyeblink conditioning: contrasting phenomena of declarative and nondeclarative memory. *Psychol. Sci.* **12**, 304–308 (2001).
46. Cheng, D. T., Disterhoft, J. F., Power, J. M., Ellis, D. A. & Desmond, J. E. Neural substrates underlying human delay and trace eyeblink conditioning. *Proc. Natl Acad. Sci. USA* **105**, 8108–8113 (2008).
47. Fuster, J. M. Cortex and memory: emergence of a new paradigm. *J. Cogn. Neurosci.* **21**, 2047–2072 (2009).
48. Clark, R. E. Eyeblink conditioning and systems consolidation: an ironic yet powerful pairing. *Neurobiol. Learn. Mem.* **95**, 118–124 (2011).
49. Tsien, J. Z., Huerta, P. T. & Tonegawa, S. The essential role of hippocampal CA1 NMDA receptor-dependent synaptic plasticity in spatial memory. *Cell* **87**, 1327–1338 (1996).
50. Huerta, P. T., Sun, L. D., Wilson, M. A. & Tonegawa, S. Formation of temporal memory requires NMDA receptors within CA1 pyramidal neurons. *Neuron* **25**, 473–480 (2000).
51. Fukaya, M., Kato, A., Lovett, C., Tonegawa, S. & Watanabe, M. Retention of NMDA receptor NR2 subunits in the lumen of endoplasmic reticulum in targeted NR1 knockout mice. *Proc. Natl Acad. Sci. USA* **100**, 4855–4860 (2003).
52. Bannerman, D. M. et al. Dissecting spatial knowledge from spatial choice by hippocampal NMDA receptor deletion. *Nat. Neurosci.* **15**, 1153–1159 (2012).
53. Kishimoto, Y., Nakazawa, K., Tonegawa, S., Kirino, Y. & Kano, M. Hippocampal CA3 NMDA receptors are crucial for adaptive timing of trace eyeblink conditioned response. *J. Neurosci.* **26**, 1562–1570 (2006).
54. Osada, T., Adachi, Y., Kimura, H. M. & Miyashita, Y. Towards understanding of the cortical network underlying associative memory. *Philos. Trans. R Soc. Lond. B Biol. Sci.* **363**, 2187–2199 (2008).
55. Miyamoto, K. et al. Functional differentiation of memory retrieval network in macaque posterior parietal cortex. *Neuron* **77**, 787–799 (2013).
56. Moyer, Jr J. R., Deyo, R. A. & Disterhoft, J. P. Hippocampectomy disrupts trace eye-blink conditioning in rabbits. *Behav. Neurosci.* **104**, 243–252 (1990).
57. Sprengel, R. & Hasan, M. T. Tetracycline-controlled genetic switches. *Handb. Exp. Pharmacol.* **178**, 49–72 (2007).
58. Gureviciene, I. et al. Normal induction but accelerated decay of LTP in APP+PS1 transgenic mice. *Neurobiol. Dis.* **15**, 188–195 (2004).
59. Bliss, T. V. & Gardner-Medwin, A. R. Long-lasting potentiation of synaptic transmission in the dentate area of the unanesthetized rabbit following stimulation of the perforant path. *J. Physiol.* **232**, 357–374 (1973).
60. Porras-García, E., Cendelin, J., Domínguez-del-Toro, E., Vozeh, F. & Delgado-García, J. M. Purkinje cell loss affects differentially the execution, acquisition and prepulse inhibition of skeletal and facial motor responses in Lurcher mice. *Eur. J. Neurosci.* **21**, 979–988 (2005).

## Acknowledgements

This study was supported by grants from the Spanish Ministry of Science and Innovation (BFU2008-00899 and BFU2008-03390) and the Junta de Andalucía (Spain, BIO-122, CVI-02487 and P07-CVI-02686). The research leading to these results also received funding from the European Community's Seventh Framework Program (FP7/2007-2013) under grant agreement no. 201714 (DEVANX). This study was also supported in part by the Fritz Thyssen Stiftung, the Max Planck Society and NeuroCure Cluster of Excellence, Charité-Universitätsmedizin-Berlin. We thank María Sánchez-Enciso, Sabine Grunwald and Simone Hündemeyer for excellent technical assistance. We are grateful to Thomas Spletstoeser (info@scitystyle.com) for excellent graphics. We especially thank Rolf Sprengel and Peter H. Seeburg for providing the *Grin1<sup>tm1Esp</sup>* (*Grin1<sup>2lox</sup>*) mice and generous support.

## Author contributions

M.T.H., A.G. and J.M.D.-G. initiated, conceptualized and headed the project; M.T.H. and G.D. developed virus-delivered conditional genetic manipulation method and generated neuron-specific, motor cortex-targeted *Grin1* gene knockout mice; M.T. performed *in vitro* electrophysiology; I.B. performed *in situ* hybridization; S.H.-G., A.G., J.M.D.-G. performed *in vivo* electrophysiological and behavioural studies; M.T.H., A.G. and J.M.D.-G. wrote the paper with comments and contributions from all authors.

**Additional information**

**Supplementary Information** accompanies this paper at <http://www.nature.com/naturecommunications>

**Competing financial interests:** The authors declare no competing financial interests.

**Reprints and permission** information is available online at <http://npg.nature.com/reprintsandpermissions/>

**How to cite this article:** Hasan Mazahir T. *et al.* Role of motor cortex NMDA receptors in learning-dependent synaptic plasticity of behaving mice. *Nat. Commun.* 4:2258 doi: 10.1038/ncomms3258 (2013).



This work is licensed under a Creative Commons Attribution-NonCommercial-ShareAlike 3.0 Unported License. To view a copy of this license, visit <http://creativecommons.org/licenses/by-nc-sa/3.0/>



# A Cognition-Related Neural Oscillation Pattern, Generated in the Prelimbic Cortex, Can Control Operant Learning in Rats

Samuel Hernández-González,<sup>1</sup> Celia Andreu-Sánchez,<sup>2</sup> Miguel Ángel Martín-Pascual,<sup>2</sup> Agnès Gruart,<sup>1</sup> and José María Delgado-García<sup>1</sup>

<sup>1</sup>Division of Neurosciences, Pablo de Olavide University, 41013 Seville, Spain, and <sup>2</sup>Audiovisual Communication and Advertising Department, Universitat Autònoma de Barcelona, 08193 Bellaterra, Spain

The prefrontal (PrL) cortex constitutes one of the highest levels of cortical hierarchy dedicated to the execution of adaptive behaviors. We have identified a specific local field potential (LFP) pattern generated in the PrL cortex and associated with cognition-related behaviors. We used this pattern to trigger the activation of a visual display on a touch screen as part of an operant conditioning task. Rats learned to increase the presentation rate of the selected  $\theta$  to  $\beta$ - $\gamma$  ( $\theta/\beta$ - $\gamma$ ) transition pattern across training sessions. The selected LFP pattern appeared to coincide with a significant decrease in the firing of PrL pyramidal neurons and did not seem to propagate to other cortical or subcortical areas. An indication of the PrL cortex's cognitive nature is that the experimental disruption of this  $\theta/\beta$ - $\gamma$  transition pattern prevented the proper performance of the acquired task without affecting the generation of other motor responses. The use of this LFP pattern to trigger an operant task evoked only minor changes in its electrophysiological properties. Thus, the PrL cortex has the capability of generating an oscillatory pattern for dealing with environmental constraints. In addition, the selected  $\theta/\beta$ - $\gamma$  transition pattern could be a useful tool to activate the presentation of external cues or to modify the current circumstances.

**Key words:** behaving rats; brain-machine interaction; local field potentials; neural oscillations; operant conditioning; prefrontal cortex

## Significance Statement

Brain-machine interfaces represent a solution for physically impaired people to communicate with external devices. We have identified a specific local field potential pattern generated in the prefrontal cortex and associated with goal-directed behaviors. We used the pattern to trigger the activation of a visual display on a touch screen as part of an operant conditioning task. Rats learned to increase the presentation rate of the selected field potential pattern across training. The selected pattern was not modified when used to activate the touch screen. Electrical stimulation of the recording site prevented the proper performance of the task. Our findings show that the prefrontal cortex can generate oscillatory patterns that rats can use to control their environment for achieving specific goals.

## Introduction

The use of the neural cortical activity for operant conditioning tasks goes back to the 1970s, with the innovative approaches of Fetz and colleagues (Fetz, 1969; Fetz and Finocchio, 1971, 1972).

Fetz's group used awake monkeys to demonstrate the conditioning of single neurons by reinforcing a high rate of neuronal activity with the delivery of a reward. Latterly, it was also shown that the information contained in local field potentials (LFPs) possesses features suited (Pesarin et al., 2002; Mehring et al., 2003) for use as brain-machine interfaces (BMIs; Flint et al., 2013; So et al., 2014). LFPs are more stable than unitary recordings and present higher spatial resolution and signal amplitudes than electroencephalographic recordings (Freeman et al., 2003; Shain et al., 2003).

Many studies have used the neural activity recorded in the MI and/or the posterior parietal cortices for different experimental designs, including the activation of external devices (Lebedev and Nicolelis, 2006; Bouton et al., 2016). But, in the past few years, the appearance of noninvasive techniques has allowed the use of deep brain regions, such as the prefrontal cortex, for BMIs controlled by cognitive activities (Schudlo et al., 2013; Hong et al., 2015). BMIs have been largely explored from the point of view of inter-

Received Nov. 28, 2016; revised March 23, 2017; accepted April 2, 2017.

Author contributions: AG and JMD-G designed research; SH-G performed research; CA-S and MAM-P contributed unpublished reagents/strategies; SH-G, CA-S, MAM-P, and AG analyzed data; SH-G, AG, and JMD-G wrote the paper.

This work was supported by grants from the Spanish Ministerio de Economía Industria y Competitividad (MINECO) (BFU2014-50022-BI-I0) and the Junta de Andalucía (B122-CV-2887 and B17-CV-2388), and the Spanish Ministerio de Sanidad Consumo y Bienestar Social (AG and JMD-G). SH-G was supported by a fellowship from the Spanish MINECO (BS-2012-052039). We thank JA Santos-Niherro for his help in instrumental design and the MUPAC-oxides research Center for providing.

The authors declare no competing financial interests.

Correspondence should be addressed to Professor José María Delgado-García, División de Neurociencias, Universidad Pablo de Olavide, 41013 Seville, Spain. E-mail: jmdg@upo.es.

DOI:10.1523/JNEUROSCI.3651-16.2017

Copyright © 2017 the authors 0270-6474/17/370301-11\$15.00/0

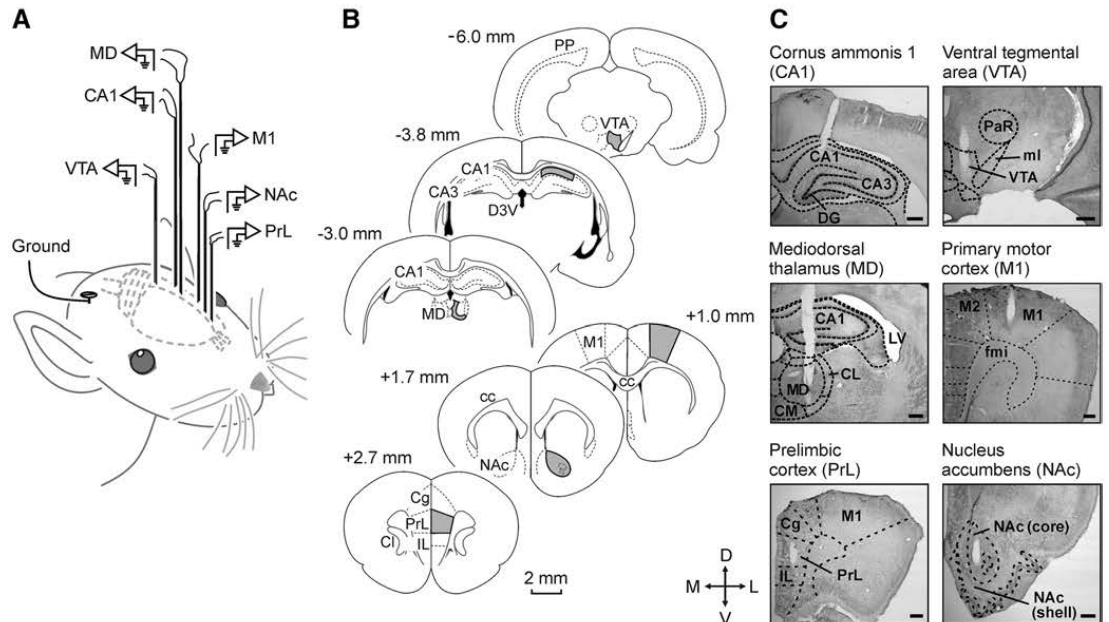


**Figure 1.** Experimental design for brain stimulation and LFP recordings. **A**, Schematic representation of the location of stimulating and recording electrodes. **B**, Diagrams of brain sagittal sections illustrating in gray the implanted cortical and subcortical areas. Coordinates with respect to bregma are indicated. **C**, Representative photomicrographs illustrating the location of implanted electrodes. Cg, Cingulate cortex; IL, infralimbic cortex; CC, corpus callosum; Cl, claustrum; CL, central lateral thalamic nucleus; CM, central medial thalamic nucleus; D3V, dorsal third ventricle; DG, dentate gyrus; fmi, forceps minor of the corpus callosum; LV, lateral ventricle; ml, medial lemniscus; PaR, parabrachial nucleus; PP, perforant pathway; D, dorsal; L, lateral; M, medial; V, ventral.

face design, including algorithms, motor imagery, and adapted electronic devices, but rarely from an electrophysiological approach, specifically a learning process where two events—a specific cortical activity pattern and a subsequent response generated in an external device—are progressively associated. In this regard, recent papers have been focused on the study of neural mechanisms underlying motor and cognitive processes using these sorts of interfaces (Koralek et al., 2012; Rouse et al., 2013; Wander et al., 2013). These types of study could help identify some of the physiological processes related to the actual motor and cognitive learning tasks (O'Doherty et al., 2011; Schafer and Moore, 2011; Hiremath et al., 2015).

Although they present many experimental (extended laboratory use, adequate brain size, easy acquisition of operant condition tasks) and ethical advantages, rats have not often been used in studies related to BEMs. In our approach, we have used a well defined LFP [ $\alpha$  to  $\beta$ - $\gamma$  ( $\theta$ / $\beta$ - $\gamma$ )] transition pattern recorded at the rostral prefrontal (PrL) cortex of rats to trigger the presentation of a visual display on an iPad tablet. The rat was rewarded with a pellet of food when touching the iPad screen. This operant conditioning design has the advantage of using a LFP pattern generated in a brain area not directly related to motor control commands (Khanna and Carmena, 2015), but to volitional and valuation processes (Kable and Glimcher, 2009; Graybeal et al., 2011; Fuster, 2015). We also studied the putative changes in the profiles of the LFPs used to activate the touch screen as well as the firing activities of putative PrL pyramidal cells to determine their contribution to the generation of the selected LFP pattern. In addition, we checked the cognitive nature of the selected LFP pattern by determining each animal's behavior associated with it and the behavioral effects of PrL cortex stimulation during the

pattern's spontaneous appearances. In this regard, it has been recently described that the electrical stimulation of the PrL cortex recording sites prevent the proper performance of acquired operant conditioning tasks (Jurado-Parras et al., 2012). In summary, present results indicate that PrL cortex circuits seem to evoke specific oscillatory patterns probably related to attentional and cognitive processes that can be safely used to trigger external cues and/or to deal with specific environmental constraints.

## Materials and Methods

**Experimental animals.** Experiments were performed on male Lister hooded rats (5–6 months old) provided by an authorized supplier (Charles River Laboratories). Upon arrival at the Pablo de Olavide Animal House (Seville, Spain), animals were housed in individual cages until the end of the experiment. Rats were kept on a 12 h light/dark cycle with constant ambient temperature ( $21.5 \pm 1^\circ\text{C}$ ) and humidity ( $55 \pm 8\%$ ), with food and water available *ad libitum*. All experiments were performed in accordance with the guidelines of the European Union Council (2010/276/33-79/EU) and Spanish regulations (BOE 34:11370-421, 2013) for the use of laboratory animals in chronic studies, and approved by the local Ethics Committee of the Pablo de Olavide University.

**Surgery.** Animals were anesthetized with 1–2.5% isoflurane delivered by a rat anesthesia mask (David Kopf Instruments). The anesthetic gas was supplied from a calibrated Fluotec 5 (Fluotec-Ohmeda) vaporizer, at a flow rate of 1–3 l/min oxygen (AstraZeneca). For LFP recordings (Fig. 1B, C) and following the Paxinos and Watson atlas (1998; RRID: SCR\_006369), animals ( $n = 10$ ) were chronically implanted with recording electrodes aimed at the PrL cortex (2.7 mm anterior to bregma, 0.8 mm lateral to bregma, and 3.6 mm below the brain surface), the nucleus accumbens (1.7 mm anterior to bregma, 1.4 mm lateral to bregma, and 7.6 mm below the brain surface), the primary motor cortex (1.0 mm anterior to bregma, 2.3 mm lateral to bregma, and 2.0 mm below the brain surface), the mediodorsal thalamic nucleus (3.0 mm posterior to

bregma, 0.5 mm lateral to bregma, and 5.3 mm below the brain surface), the hippocampal CA1 area (3.8 mm posterior to bregma, 2.0 mm lateral to bregma, and 2.5 mm below the brain surface), and the ventral tegmental area (6.0 mm posterior to bregma, 0.5 mm lateral to bregma, and 7.8 mm below the brain surface). These electrodes were made from 50  $\mu$ m, Teflon-coated, tungsten wire (Advent Research). Each electrode consisted of three individual tungsten wires with their tips spaced 300  $\mu$ m apart along the extent of the electrode. With the aim of recording the unitary activity present in the PrL cortex during the appearance of the selected  $\theta/\beta\text{-}\gamma$  transition pattern, five additional animals were implanted in the PrL cortex with the same recording electrode but with the addition of a home-made multielectrode. The multielectrode was composed of six 25  $\mu$ m, Teflon-coated, tungsten wires (Advent Research).

To determine whether vibrissal movements were related to LFPs recorded at the PrL cortex, a pair of recording electrodes was implanted in the center of the contralateral whisker pad in the above-mentioned animals. Vibrissal electrodes were made from 50  $\mu$ m, Teflon-coated, annealed stainless steel wire (A-M Systems). A bare silver wire was affixed to the bone as ground. All the implanted wires were soldered to three six-pin sockets (RS Amidata) and fixed to the skull with dental cement (Fig. 1; Gruart et al., 2006).

Since the presence of recording wires could represent a significant impairment for the proper acquisition of the pattern-triggered tasks, an additional group ( $n = 5$ ) of rats were chronically implanted with five 50  $\mu$ m tungsten recording electrodes aimed at the PrL cortex. These electrodes, plus a ground wire, were connected to a Bakelite integrated circuit (Cibertec) equipped with an eight-pin Omnetics socket (RS Amidata).

**Recording and stimulating procedures.** LFP and electromyographic recordings were performed using Grass P511 differential amplifiers with a bandwidth of 0.1–10 kHz (Grass-Telefactor). Wireless recordings were performed with the help of a five-channel TBSI head-stage system (Harvard Bioscience). Unitary recordings were performed with high-impedance probes ( $2 \times 10^{12} \Omega$ , 10 pF) and filtered between 450 and 4500 Hz, with the help of a finite impulse response filter.

For the electrical stimulation of the PrL cortex region during operant conditioning, we used a 200 Hz train of pulses (50  $\mu$ s negative-positive) lasting 200 ms. The train was triggered, with a delay of <0.5 ms, by a touch of a square virtual button on the iPad screen. To avoid excessive stimulations of the experimental animal, subsequent iPad touches within a 6 s window did not trigger any stimulus. Stimulus intensities ranged from 0.5 to 1 mA. For each animal, we selected the minimum intensity evoking a short disruption in the expected behavioral sequence (touch the visual display, go to the feeder, eat the pellet; Jurado-Paras et al., 2012).

**Instrumental conditioning.** In a preliminary series of experiments, a group of rats ( $n = 5$ ) were trained for operant conditioning in a basic Skinner box module measuring 29.2  $\times$  24.1  $\times$  21 cm (MED Associates). The operant chamber was housed within a sound-attenuating chamber (90  $\times$  55  $\times$  60 cm), which was constantly illuminated (19 W lamp) and exposed to a 45 dB of white noise (Cibertec). The Skinner box was equipped with a food dispenser from which pellets (Noyes formula P; 45 mg; Sandown Scientific) could be delivered by pressing a lever. Before training, rats were handled daily for >7 d and food-deprived to 80–85% of their *ad libitum* feeding weight. Once the desired weight was reached, animals were placed in the Skinner box for 20 min and allowed to press the lever to receive pellets from the food tray using a fixed-ratio (FR 1:1) schedule, until reaching criterion. Criterion was to press the lever >80 times/session for 2 consecutive days (Fig. 2; Hasan et al., 2013). Another group of rats ( $n = 5$ ) were trained in a modified Skinner box module of similar dimensions (MED Associates) equipped with an iPad tablet computer and the same food dispenser from which pellets could be delivered by touching a square (200  $\times$  200 pixels; i.e.,  $\approx 3.4 \times 3.4$  cm) virtual button displayed on the screen. In this case, rats were pretreated and trained as indicated above. Collected results of this comparative study are illustrated in Figure 2B, C.

**Conditioning programs.** LFP pattern detections, lever presses, screen touches, and delivered reinforcements were monitored and recorded with a computer, using a MED-PC program (MED Associates; RRID: SCR\_012156). All operant sessions were recorded with a video capture system (Sony HDR-SR12E) synchronized to LFP recordings.

**Activation of the touch screen by LFPs recorded in the PrL cortex.** In the next experiments, rats implanted with recording electrodes were trained to activate the visual display on the touch screen by LFP patterns recorded from the PrL cortex. For this, a capacitive multitouch-screen device (iPad 2, Apple) with a 9.7 inch LED-back-lit glossy widescreen display with in-plane switching technology (Leising et al., 2013) was used. It had 1024  $\times$  768 pixel resolution at 132 pixels per inch.

First, rats were trained to touch the square virtual button in the modified Skinner box until reaching the above-specified criterion. Then, they had to learn to trigger the appearance of the square button on the touch screen by the generation of a  $\theta/\beta\text{-}\gamma$  transition pattern. This LFP pattern was identified in previous recordings of PrL cortex activities as being related to the presentation of behaviors, such as remaining still (motionless) in the cage, observing the feeder, or rearing (Figs. 3, 4). This specific LFP pattern was characterized by a significant decrease in power in the  $\theta$  band (Fig. 3A, B) accompanied by smaller changes in the power of both  $\beta$  and  $\gamma$  bands (Fig. 3E). The detection of this  $\theta/\beta\text{-}\gamma$  transition pattern was based on the instantaneous calculation of the power in a wide band of frequencies between 3 and 150 Hz that included the three mentioned oscillation bands ( $\theta$ ,  $\beta$ , and  $\gamma$ ). This spectral analysis was performed with the help of a home-made program implemented with Spike2 software (CED 1401 Plus, Cambridge Electronics Design, RRID: SCR\_000903). Power was calculated using the fast Fourier transform with a raised cosine window. In addition to the above, a spectral power threshold was calculated from LFPs recorded during preliminary baseline and training sessions and maintained during the whole experiment. According to the intrinsic characteristics of the LFP recordings from each experimental rat, the criterion values assigned to the threshold ranged from 0.00125 to 0.00215  $V^2$ . Thresholds were calculated as the average of the minimum values of power between 3 and 150 Hz plus 3  $\times$  SD. The detections of the selected  $\theta/\beta\text{-}\gamma$  transition pattern generated a new event channel in Spike2, which was translated into a command system to display the visual stimulus on the touch screen (Fig. 5A).

For the command system, we developed an ad hoc software (RatButton 21.3, for iC6 8.4) for stimulus presentation on the touch screen triggered by the selected  $\theta/\beta\text{-}\gamma$  transition pattern. The RatButton system was activated when power for the three bands fell below the established power threshold. The same software also activated the feeder to supply the reward and quantify the number and time of correct screen touches. The RatButton software was developed with X-Code in object-oriented programming language Objective-C. Stimulus color (sRGB IEC61966-2.1: 0, 240, 100 — a green square) and luminance (150  $cd/m^2$  at 20 cm distance) were adapted to rats' vision with the help of a colorimeter (Minolta Chroma Meter xy-1, Minolta Camera) and a photometer (Sekonic DualMaster L-558/L; Sekonic; Jacobs et al., 2001).

**Electrical stimulation of the PrL cortex.** To determine whether the PrL area—from which the selected  $\theta/\beta\text{-}\gamma$  transition pattern was recorded—was related to cognitive processes involved in the operant conditioning paradigm, we checked the effects of its electrical stimulation on the ongoing behavioral sequence of touching the iPad and going to collect the rewarded pellet. The PrL cortex was stimulated at the precise moment of each correct touch on the screen.

**Histology.** At the end of the experiments, rats were deeply reanesthetized with a mixture of ketamine (100 mg/kg) and medetomidine (0.1 mg/kg) and perfused transcardially with saline and 4% paraformaldehyde in PBS (0.1 M, pH 7.4). Brains were cryoprotected with 30% sucrose in PB, and coronal sections (50  $\mu$ m) were obtained with a sliding freezing microtome (Leica, SM2000R) and stored at  $-20^\circ C$  in 30% glycerol and 30% ethylene glycol in PB until used. Selected sections, including the implanted sites, were mounted on gelatinized glass slides and stained using the Nissl technique with 0.1% toluidine blue to determine the location of stimulating and recording electrodes (Fig. 1C).

**Data collection and analysis.** LFP,  $\theta/\beta\text{-}\gamma$  transition pattern detections, 5 V rectangular pulses corresponding to lever presses, iPad touches, pellet delivery and video recordings were stored digitally on a computer through an analog-to-digital converter (CED 1401 Plus, Cambridge Electronics Design). Collected data were sampled at 25 kHz for unitary recordings or at 20 kHz for LFPs, with an amplitude resolution of 16 bits. Data were analyzed off-line with the Spike2 software (Cambridge



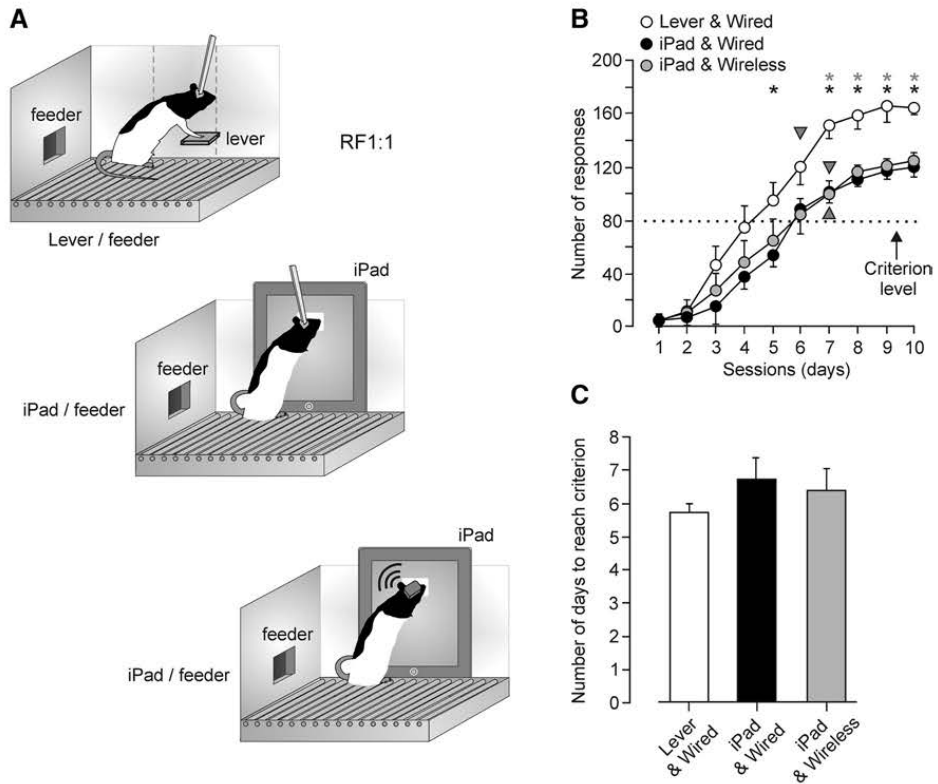


**Figure 2.** Validation of the touch-screen system compared with a classic lever one using the same instrumental conditioning paradigm. **A**, A group ( $n=5$ ) of rats were trained in a Skinner box to press a lever to obtain a pellet of food at a fixed 1:1 ratio while the other two groups (wire and wireless;  $n=5$  each) were trained in a modified Skinner box to touch a square virtual button displayed on an iPad screen to obtain a pellet at the same ratio. Rats were trained for 10 successive sessions of 20 min each. **B**, Learning curves corresponding to the three groups of rats. The selected criterion was to obtain >80 pellets for two successive sessions (gray triangles). Asterisks indicate significant differences ( $F_{(2,28,147)} = 5.496, p = 0.028$ , 2-way ANOVA) between the group trained in the conventional Skinner box (Lever & Wired) and the other two (iPad & Wired and iPad & Wireless) groups. **C**, The two touch-screen groups reached the selected criterion after the lever group, but without significant differences ( $F_{(2,28,12)} = 0.634, p = 0.547$ , 1-way ANOVA).

Electronics Design, RRID:SCR\_000903) for quantification of animal performance in the Skinner box,  $\theta/\beta$ - $\gamma$  pattern presentations and characteristics, power ratio indices of the  $\theta/\beta$ - $\gamma$  pattern, and power spectra of selected LFP recordings. Unitary activity was identified and computed with the help of specific Spike2 programs. These computed results were processed for statistical analysis using Sigmaplot 10 (Systat Software, RRID:SCR\_003210). Unless otherwise indicated, data are always represented as the mean  $\pm$  SEM. Acquired data were analyzed using one-way or two-way repeated-measures ANOVA. The Friedman repeated-measures ANOVA on ranks (nonparametric) statistical test was used if normality or equal variance tests failed. All of them were followed by Holm-Sidak or Tukey's *post hoc* testing depending on the previous statistical test. The Student's *t* test was applied when necessary. The corresponding degrees of freedom were reported accompanying the  $F$ ,  $\chi^2$ , or *t* statistic values. The analytical procedures of the LFP recordings to obtain the time-frequency representation (spectrogram) and the coherence between pairs of different brain regions (coherograms) were developed with the help of the Chronux toolbox (Matlab, MathWorks, RRID:SCR\_005547). In most representations, we selected the following frequency bands:  $\theta$ , 3–12 Hz;  $\beta$ , 12–30 Hz; low  $\gamma$ , 30–50 Hz, and high  $\gamma$ , 50–150 Hz. Comparisons between spectrograms of two different groups of data (Fig. 3 E, F) were processed for statistical analysis using the EEGLAB Statistics toolbox (Matlab, MathWorks, RRID:SCR\_010501) and Sigmaplot 10 (Systat Software, RRID:SCR\_003210).

## Results

### How the $\theta/\beta$ - $\gamma$ transition pattern was selected

Animals were implanted with recording electrodes in PrL and M1 cortices, the hippocampal CA1 area, the mediocaudal thalamic nucleus, nucleus accumbens septi, and the ventral tegmental area (Fig. 1A–C). In a preliminary series of experiments, animals were divided in three groups ( $n = 5$  each) and trained until reaching criterion (obtaining >80 pellets for two consecutive sessions; see Materials and Methods) in a conventional Skinner box, and in a modified box including a multi-touch (iPad) screen, using in both cases a fixed 1:1 rewarding ratio. Animals in the conventional Skinner box were equipped with a wired recording system, while animals belonging to the groups located in the modified Skinner box were implanted with either recording wires or a wireless system (Fig. 2). Although performance with the touch screen was significantly lower than with the lever ( $F_{(2,23,147)} = 5.496, p = 0.028$ , two-way ANOVA), the three groups of animals reached the selected criterion at similar times ( $F_{(2,23,12)} = 0.634, p = 0.547$ , one-way ANOVA). The analysis of LFPs recorded during those operant conditioning sessions, performed in the box equipped with the touch screen, showed the presence of short time periods (<1 s) characterized by a marked decrease in spectral power, mostly in the  $\theta$

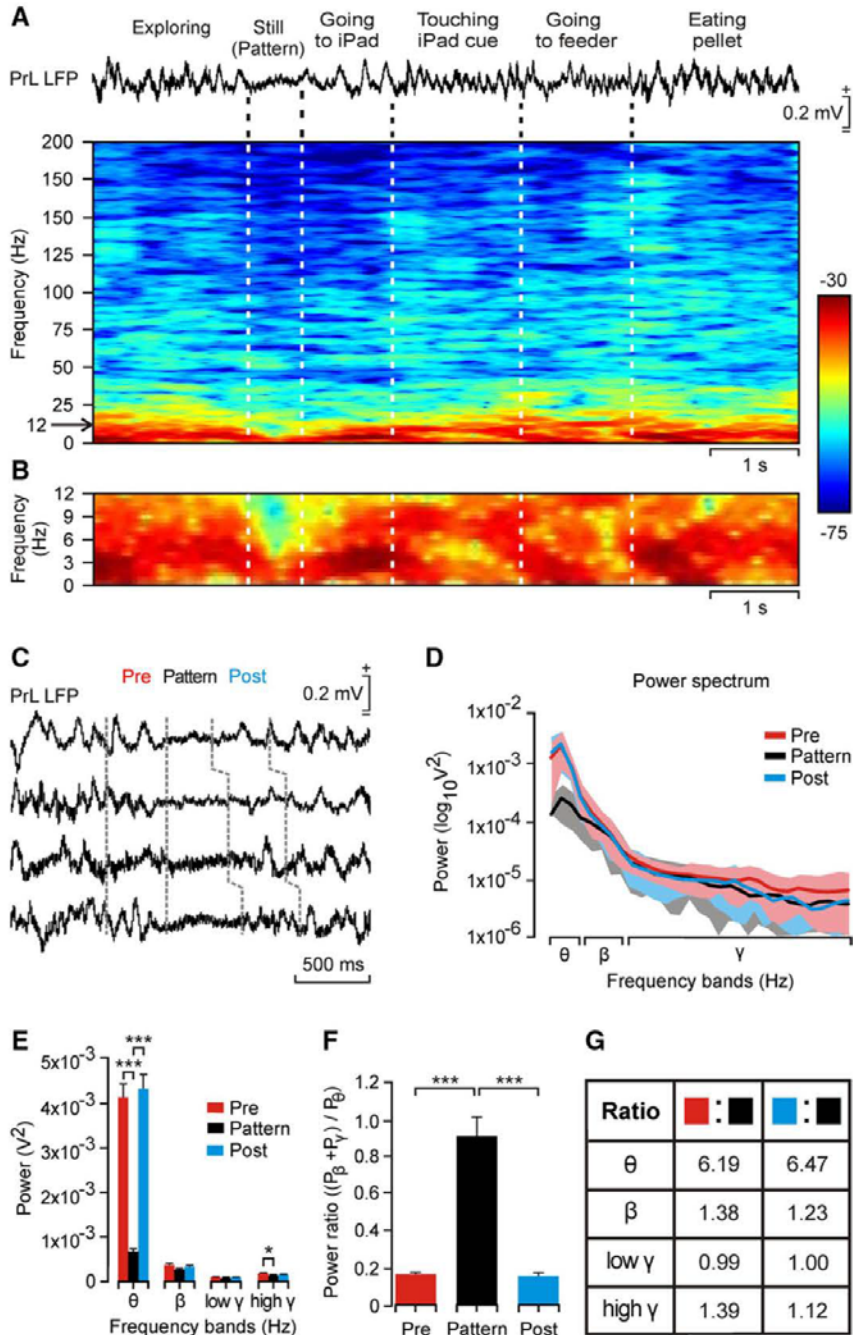


**Figure 3.** Dynamic changes in LFP activity recorded in the PrL cortex during a sequence of behaviors performed during operant conditioning tasks. **A**, Functional characteristics of the selected  $\theta/\beta$ - $\gamma$  transition pattern during a single operant conditioning sequence. From top to bottom are illustrated the behaviors and LFPs recorded in the PrL cortex during this time window. The time–frequency representation of this LFP activity is included below. Note the dominant spectral power (in dB; see the calibration bar) in the  $\theta$  band across the whole behavioral sequence, but its decrease during the moment ( $>1$  s) when the rat was still (motionless) before approaching the touch screen. **B**, An enlargement of the time–frequency display corresponding to the band of 0–12 Hz. **C**, Four examples of the selected  $\theta/\beta$ - $\gamma$  transition pattern. Pre and Post indicate the LFP activity during the 350 ms preceding and following the decrease in spectral power in the  $\theta$  band. **D**, Averaged ( $n=40$  samples; mean  $\pm$  SD) power spectra of each of the three periods (Pre, Pattern, Post) delimited in **C**. Note the large difference in the power for the  $\theta$  band during the pattern. **E**, Analysis of the spectral power of the  $\theta$ ,  $\beta$ , low- $\gamma$ , and high- $\gamma$  bands for data illustrated in **D** ( $\chi^2=150.32$ ; degrees of freedom, 2;  $p \leq 0.001$  for the  $\theta$  band;  $\chi^2=18.98$ ; degrees of freedom, 2;

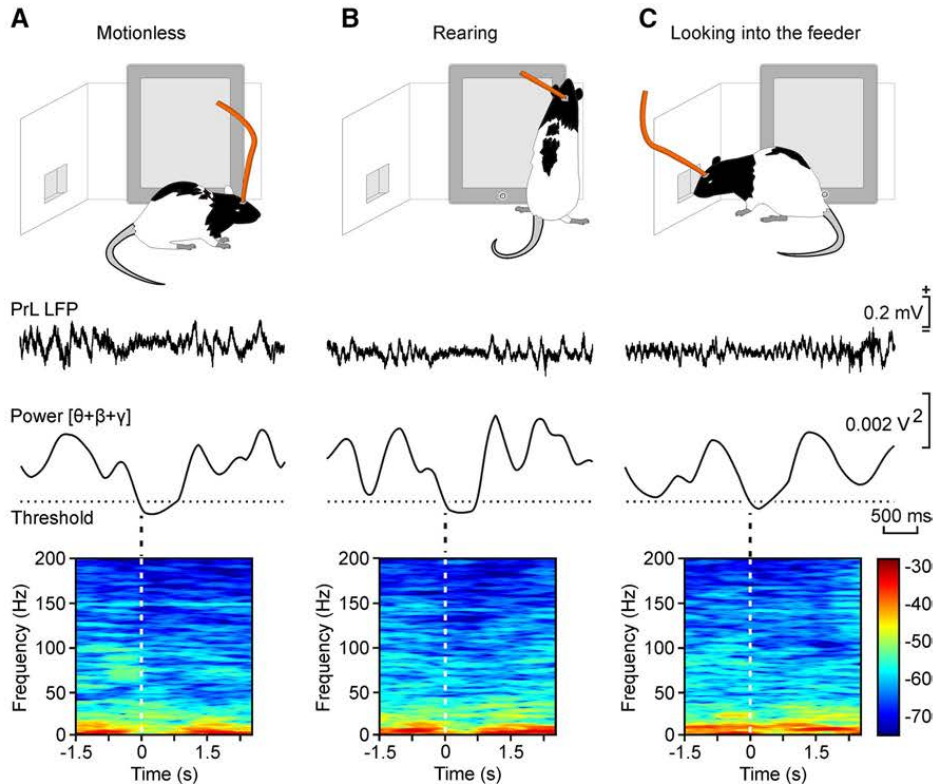


**Figure 4.** Different behaviors during which the selected  $\theta/\beta\text{-}\gamma$  transition pattern was recorded in the PrL cortex. **A–C**, Representative examples of LFPs recorded in the PrL cortex during the performance of the illustrated behaviors: **A**, motionless; **B**, rearing; **C**, looking into the feeder. For **A–C** and from top to bottom are illustrated the selected behavior, the corresponding LFP pattern, the evolution of the added spectral power for the  $\theta + \beta + \gamma$  bands across the recorded LFP, and the time–frequency representation of the LFP illustrated above. Note the decrease of power of the  $\theta$  band during the pattern. Analyses illustrated here were performed with the help of the Chronux application programmed in Matlab.

band (Fig. 3A–D). This peculiar pattern appeared during performance of specific behaviors, such as remaining still (i.e., motionless) in the cage, and during rearing or looking into the feeder (Fig. 4). The power in the  $\theta$  band was decreased significantly ( $\chi^2 = 150.32$ ; degrees of freedom, 2;  $p \leq 0.001$ , Friedman test) from that present during the periods of time immediately before (Pre) and after (Post; Fig. 3D,E). Smaller but significant differences ( $\chi^2 = 18.98$ ; degrees of freedom, 2;  $p \leq 0.05$ , Friedman test) were found for the high- $\gamma$  band between Pre and Pattern periods (Fig. 3E).

At this stage, we wondered whether this peculiar  $\theta/\beta\text{-}\gamma$  transition pattern could be used to trigger the presentation of the selected visual display on the touch screen. In this way, the experimental animal would be able to control the iPad with a specific LFP pattern generated in its PrL cortex. To facilitate this task, we quantified two parameters: the spectral power for the  $\theta + \beta + \gamma$  bands (Fig. 5A) and the power ratio  $[(P_\beta + P_\gamma)/P_\theta]$  during the Pre, Pattern, and Post periods (Fig. 3F, G), but only the first

$p \leq 0.05$  for the high- $\gamma$  band, Friedman test). **F**, Power ratio of  $\beta + \gamma$  bands with respect to

the  $\theta$  band [power ratio:  $(P_\beta + P_\gamma)/P_\theta$ ] for each of the three regions ( $n = 100$  samples collected from 5 animals;  $\chi^2 = 136.82$ ; degrees of freedom, 2;  $p \leq 0.001$ , Friedman test). **G**, Ratio between the spectral powers of each frequency band corresponding to LFPs recorded before and during the pattern (Pattern/Pre, second column) and after and during the pattern (Pattern/Post, third column). These ratios were computed for data illustrated in E.

parameter was used as an iPad trigger. Pre and Post periods presented similar power ratio values (0.17 and 0.16, respectively;  $\chi^2 = 136.82$ ; degrees of freedom, 2;  $p > 0.05$ ; Tukey's *post hoc* test for Friedman test). In contrast, the power ratio for the Pattern period reached a value significantly larger (0.91;  $\chi^2 = 136.82$ ; degrees of freedom, 2;  $p \leq 0.001$ , Tukey's *post hoc* test for Friedman test). Quotients between Pre/Pattern and Post/Pattern periods for each of the mentioned ( $\theta$ ,  $\beta$ , and  $\gamma$ ) power spectral bands yielded similar values (Fig. 3G). The quotient for the  $\theta$  band was  $>6$  times larger for the Pre/Pattern (6.19) and Post/Pattern (6.47) periods, but the other frequency bands presented minor differences (Fig. 3G). On the whole, these analyses indicate that the selected  $\theta/\beta\text{-}\gamma$  transition pattern was mainly characterized by a notable decrease in the  $\theta$  band during the Pattern period.

#### Use of the selected $\theta/\beta\text{-}\gamma$ transition pattern to trigger the appearance of a visual display on the touch screen

In a second series of experiments, a group of implanted rats were trained to touch a visual display that appeared automatically on the touch screen (Automatic cue; Fig. 5B–D). In this situation, they reached criterion between the fifth and the ninth conditioning sessions. Rats were maintained with this operant task for  $\leq 11$  sessions and then they were trained to activate the appearance of the same visual display with the generation of the selected  $\theta/\beta\text{-}\gamma$  transition pattern (Pattern-evoked cue; Fig. 5B–D). To trigger

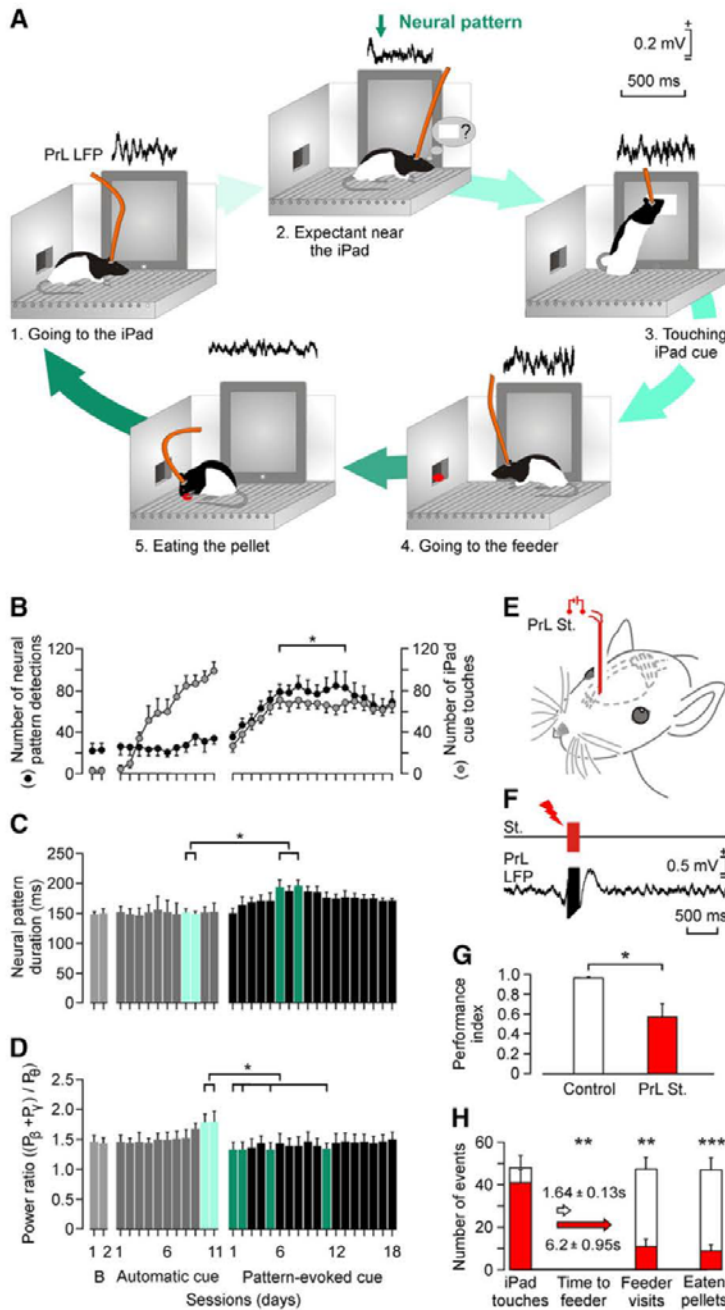


**Figure 5.** Evolution of the selected  $\theta/\beta\text{-}\gamma$  transition pattern across training with the touch-screen task. **A**, A diagram of behaviors performed by the experimental animal during a complete sequence of operant conditioning with the touch screen. The corresponding LFP evoked in the PrL cortex during the corresponding behavior is illustrated above each sketch. **B**, Evolution of the number of screen touches during baseline recordings, when the square virtual button display appeared spontaneously on the touch screen (Automatic cue) and when its appearance was triggered by the  $\theta/\beta\text{-}\gamma$  transition pattern recorded in the PrL cortex (Pattern-evoked cue). Data collected and averaged from 10 animals. Note that pattern presentation showed no significant ( $p > 0.05$ ) changes during automatic cue sessions, but increased significantly ( $F_{(1, 8.338)} = 30.096, p \leq 0.001$ , 2-way ANOVA) for pattern-evoked cue sessions. **C**, Evolution of pattern duration across training sessions illustrated in **B**. Note the slight increase in

the appearance of a visual display on the touch screen, a program was implemented to detect the Pre-to-Pattern transition with a delay of  $<0.25$  s (Fig. 5A). In this situation, rats presented a constant increment in the number of  $\theta/\beta\text{-}\gamma$  transition patterns during the first eight sessions, followed by a stabilization ( $\approx 80$  patterns and  $\approx 60$  touches) from the ninth to the 18th training sessions. Although the number of evoked patterns reached criterion, the number of screen touches did not. This lower performance was not due to the presence of recording wires, since wireless recordings performed in an additional group of rats produced similar results (Fig. 2B, C).

As illustrated in Figure 5B, there were no significant changes in the number of  $\theta/\beta\text{-}\gamma$  transition patterns for the two baseline and 11 training sessions in which the visual display was presented automatically ( $p > 0.05$ ). In contrast, during the sessions in which the visual display was triggered by the  $\theta/\beta\text{-}\gamma$  transition pattern, the number of screen touches progressed in parallel with a significant ( $F_{(8, 27.0310)} = 9.007, p \leq 0.001$ , one-way ANOVA) increase in the number of pattern detections from the sixth to the 13th conditioning sessions.

We checked whether the use of the  $\theta/\beta\text{-}\gamma$  transition pattern to trigger the iPad modified its properties regarding duration and the values reached by the power ratio index. As shown in Figure 5C, when used to trigger the iPad (Pattern-

duration across the first sessions in which the pattern was used to trigger the visual display on the touch screen. Significant differences are indicated ( $\chi^2 = 47.098$ ; degrees of freedom, 30;  $p \leq 0.05$ , Friedman test). This increase in pattern duration disappeared after the first 10 pattern-evoked cue sessions. **D**, Evolution of the power ratio  $[(P_{\theta} + P_{\gamma})/P_{\beta}]$  across training sessions. Power ratio was larger for automatic than for pattern-evoked cue sessions. Significant differences are indicated ( $\chi^2 = 55.423$ ; degrees of freedom, 30;  $p \leq 0.05$ , Friedman test). **E, F**, Experimental design for animal stimulation in the PrL cortex. The experimental animal was stimulated for 200 ms (50  $\mu\text{s}$  pulses at 200 Hz) the moment it touched the screen. A total of five rats/group was used. **G**, Differences in the performance index [index:  $(N_{\text{control}} + N_{\text{stim}})/(N_{\text{control}} + N_{\text{stim}})$ , where  $N$  = number of events]. Control rats reached an index of  $0.97 \pm 0.01$  (white bar), while stimulated rats reached significantly lower values ( $0.58 \pm 0.15, t_{(8, 0.02)} = 2.586, p \leq 0.05$ , Student's  $t$  test). **H**, Other quantitative differences in operant conditioning performance between the control and the stimulated groups. Although the number of screen touches was similar for the two groups ( $t_{(8, 0.02)} = 1.043, p = 0.328$ , Student's  $t$  test), the stimulated group spent a significantly longer time reaching the feeder ( $p = 0.001$ , Mann-Whitney rank sum test), paid fewer visits to the feeder ( $t_{(8, 0.02)} = 5.008, p < 0.001$ , Student's  $t$  test), and ate fewer pellets ( $t_{(8, 0.02)} = 5.334, p < 0.001$ , Student's  $t$  test).

evoked cue), the duration of the pattern increased steadily from the first to the eighth training sessions (from 150 to 197 ms;  $\chi^2 = 47.098$ ; degrees of freedom, 30;  $p \leq 0.05$ , Friedman test), decreasing afterward to intermediate values (from 186 to 160 ms). In contrast, the power ratio reached peak values at the end of the automatic cue sessions, being significantly smaller during pattern-evoked cue sessions ( $\chi^2 = 55.423$ ; degrees of freedom, 30;  $p \leq 0.05$ ; Friedman test; Fig. 5D). Thus, the use of the  $\theta/\beta\text{-}\gamma$  transition pattern to trigger the touch screen introduces small but significant changes in its duration and spectral power characteristics.

### The electrical stimulation of the PrL cortex prevented the proper performance of the operant conditioning task

It is well known that the PrL cortex from which the  $\theta/\beta\text{-}\gamma$  transition pattern was recorded is involved in cognitive, volitional, and valuation processes (Fuster, 2009; Kable and Glimcher, 2009; Graybiel et al., 2011). Specifically, its electrical stimulation seems to prevent the proper performance of an operant conditioning task (Jurado-Parras et al., 2012). In this regard, we checked whether the recorded area was also involved in these volitional processes. For this, we stimulated (a train of 200 Hz for 200 ms) the PrL cortex in animals trained to touch the visual display to obtain a pellet as a reward (Fig. 5E–H).

Control rats performed the task consistently, visiting the feeder and getting the pellet after each screen touch, with a performance index close to 1 ( $0.97 \pm 0.01$ ; Fig. 5C). In contrast, electrical stimulation of the PrL cortex (Fig. 5F) disturbed this sequential behavior because, although cortically stimulated rats touched the screen as many times as controls ( $t_{(30,05)} = 1.043$ ,  $p = 0.328$ , Student's  $t$  test), they either did not visit the feeder ( $t_{(30,05)} = 5.008$ ,  $p = 0.001$ , Student's  $t$  test) or they tried to visit it but returned to the touch screen without eating the reward ( $t_{(30,05)} = 5.334$ ,  $p \leq 0.001$ , Student's  $t$  test). In addition, the time elapsed before visiting the feeder was significantly increased ( $U_{(30,05)} < 0.001$ ,  $p = 0.008$ , Mann-Whitney rank sum test; Fig. 5H). Rats with stimulated PrL cortices produced a significantly ( $t_{(30,05)} = 2.586$ ,  $p = 0.032$ , Student's  $t$  test) lower performance index ( $0.58 \pm 0.15$ ) than rats in the control group (Fig. 5C), indicated that the stimulated rats did not visit the feeder and get the pellets delivered as effectively as controls did (Fig. 5H). These results suggest that the electrical stimulation of specific behavioral sequences related to the operant task.

### Unitary activity in the PrL cortex in presence of the $\theta/\beta\text{-}\gamma$ transition pattern

Particular attention was paid to the firing activities of PrL cortex neurons recorded simultaneously with the spontaneous appearance of the selected  $\theta/\beta\text{-}\gamma$  transition pattern (Automatic cue; Fig.

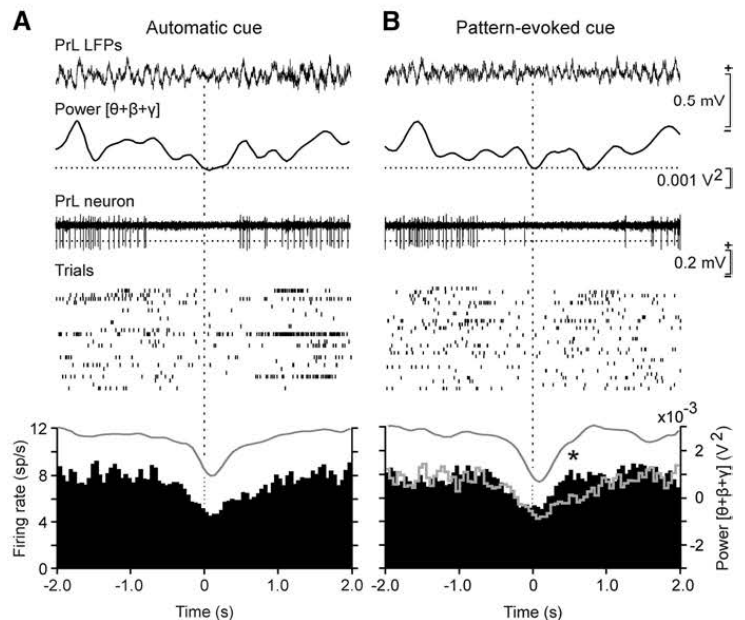


**Figure 6.** Unitary activity in the PrL cortex when the selected  $\theta/\beta\text{-}\gamma$  transition pattern was generated spontaneously and when used to trigger touch-screen cues. **A**, Unitary activity recorded in the PrL cortex coincided with the spontaneous appearance of the  $\theta/\beta\text{-}\gamma$  transition pattern during the automatic presentation of the visual (square virtual button) cue on the touch-screen (Automatic cue). From top to bottom are illustrated a representative example of LFPs, including the presence of a  $\theta/\beta\text{-}\gamma$  transition pattern, the evolution of the added spectral power for the  $\theta+\beta+\gamma$  bands across the recorded LFP, the firing activity of a PrL neuron, the raster plot of  $\geq 25$  successive trials of the same neuron, and the averaged firing rate (spikes/s) of PrL pyramidal neurons recorded during the same number of spontaneous transition patterns (the gray line indicated the averaged  $\theta+\beta+\gamma$  power, in  $V^2$ ). **B**, Same neurons as in **A** recorded during pattern-evoked cue sessions (Pattern-evoked cue). The gray line profile corresponds to the mean firing rate collected during the Automatic cue period. The statistical analysis of collected data indicated that there was a depression in the firing rate of the recorded neurons ( $n = 36$ ) during the transition pattern ( $F_{(78,320,399)} = 6.394$ ,  $p < 0.05$ , 1-way ANOVA) and that this depression was recovered significantly ( $t_{(19,05)} = -6.552$ ,  $p < 0.001$ , paired Student's  $t$  test) before, by the same neuronal group, during Pattern-evoked cue trials.

6A) or during its use to trigger the visual display in the iPad (Pattern-evoked cue; Fig. 6B). Most (80%) of the recorded units (36 of 45) were considered as putative PrL pyramidal neurons, based on the duration of the recorded spikes ( $>0.5$  ms) and on their spontaneous mean firing rates (2–15 spikes/s). These PrL neurons presented sustained tonic firings interrupted sometimes by short bursts of activity. Because of their firing properties, they appeared to be similar to the regular-spiking, slow-adapting pyramidal cells recorded by Dégenétais et al. (2002) in anesthetized rats and by Leal-Campanario et al. (2013) in alert behaving rabbits. In accordance with the collected results, averaged PrL pyramidal neurons presented a significant ( $F_{(78,320,399)} = 6.994$ ,  $p < 0.05$ , one-way ANOVA) decrease in their mean firing rate coinciding with the spontaneous appearance of the  $\theta/\beta\text{-}\gamma$  transition pattern (Fig. 6A) or during its use as Pattern-evoked cue (Fig. 6B). Nevertheless, the same set of neurons recovered their firing rates significantly ( $t_{(19,05)} = -6.552$ ,  $p < 0.001$ , paired Student's  $t$  test) faster following  $\theta/\beta\text{-}\gamma$  transition patterns used as a cue than during their spontaneous presentations.

In addition, and as illustrated in Figure 7, the selected  $\theta/\beta\text{-}\gamma$  transition pattern appeared to coincide with a small ( $\approx 50\%$ ) decrease in vibrissal activity, suggesting that this specific activity of the PrL cortex was not related to somatosensory information or exploratory behaviors, contrary to what has been described for the S1 and M1 cortical areas (Zagha et al., 2013).

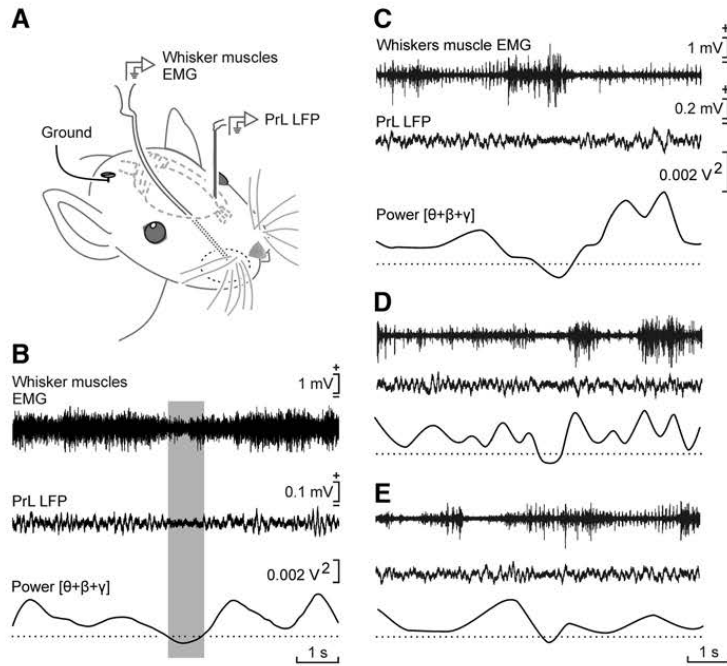


**Figure 7.** The selected  $\theta/\beta\text{-}\gamma$  pattern was not related to whisker motor responses. **A**, Experimental design. The electromyographic (EMG) activity of whisker muscles and the LFPs generated in the PrL cortex were recorded simultaneously in alert behaving rats during operant conditioning sessions in which the iPad was triggered by the  $\theta/\beta\text{-}\gamma$  pattern. **B**, Averaged ( $n = 175$  traces collected from 3 animals) EMG recordings collected from whisker muscles and LFPs collected from the PrL cortex. The average was triggered when the summed power of  $\theta + \beta + \gamma$  bands reached the selected minimum value. Although the averaged EMG activity of whisker muscles presented a minimum value during the presence of the selected pattern, no linear relationship was observed between the two variables ( $r = 0.073$ ; degrees of freedom, 348;  $p = 0.336$ , Pearson's  $r$ ). **C–E**, Three representative examples of LFPs recorded during the presence of the selected pattern in the PrL cortex accompanied by different levels of activity in whisker muscles. These results suggest that the two neural and muscle activities were not correlated.

#### Effects of the use of the $\theta/\beta\text{-}\gamma$ transition pattern as a trigger of the touch screen on the power spectra of LFPs recorded in the PrL cortex

We were interested in determining whether the use of the LFP pattern as a trigger modified its spectral characteristics. As mentioned above, rats already trained to touch the screen to obtain a reward generated spontaneously the  $\theta/\beta\text{-}\gamma$  transition pattern when looking toward the feeder, remaining motionless in the cage, or rearing (Figs. 4A–C, 8A). In this situation, the pattern was present  $24 \pm 1.5$  times per recording session (Fig. 5B). When the pattern was used to activate the touch screen, the rat usually generated it by standing still near the iPad (Figs. 4A, 8C). Figure 8B,D shows an averaged (150 times) time–frequency representation (1250 ms) triggered by the  $\theta/\beta\text{-}\gamma$  transition pattern during the two different experimental situations illustrated in Figure 8A,C. As illustrated in Figure 8G–I, a quantitative analysis of collected data indicated that, when the LFP pattern was used as a trigger, it presented a lower power in the  $\beta$  band ( $t_{(28005)} = 5.949$ ,  $p = 0.001$ , Student's  $t$  test) during Pre, Pattern, and Post periods and in the low- $\gamma$  band ( $t_{(28005)} = 7.863$ ,  $p < 0.001$ , Student's  $t$  test) during the Pattern and Post periods. Finally, there was a decrease ( $p \leq 0.05$ ) in the high- $\gamma$  band during the Post period. Interestingly, there was no significant change in the  $\theta$  band for any of these three periods ( $t_{(28005)} \leq -1.444$ ,  $p \geq 0.150$ , Student's  $t$  test).

A precise study of the high- $\gamma$  band revealed a significant decrease ( $p \leq 0.05$ ) of the power in a narrow range of frequencies (115–122 Hz;

Fig. 8F) that coincided with the detection of the LFP pattern when it was used to activate the touch-screen cue. Similar results were obtained for the low- $\gamma$  band and, particularly, in the range of frequencies between 32 and 41 Hz ( $p \leq 0.05$ ). Interestingly, these frequencies did not change their spectral powers before and after the Pattern period. The opposite alternation in the presence ( $p \leq 0.05$ ) or absence ( $p > 0.05$ ) of differences between the two experimental phases in the three different time periods (Pre: –250 to 0 ms; Pattern: 0–250 ms; Post: 250–500 ms) was observed in some frequencies of the  $\theta$ ,  $\beta$ , and low- $\gamma$  bands (Fig. 8E).

#### Analysis of coherence between the six recording sites across training

An interesting question was to determine whether the selected  $\theta/\beta\text{-}\gamma$  transition pattern was originated in a neural area other than the PrL cortex or was propagated from it to other cortical and subcortical areas. In Figure 9A are illustrated the LFPs recorded in the six selected areas during a complete operant conditioning sequence from going to the iPad to touch the visual display until eating the provided pellet. As illustrated in Figure 9B, there was a very low coherence for the  $\theta$  band ( $0.06 \leq C \leq 0.19$ ) and a slightly higher one for the 1 band ( $0.29 \leq C \leq 0.51$ ) when the PrL cortex was compared with the other five regions. Only the  $\gamma$  band (especially at high frequencies) presented a high coherence ( $C \leq 0.62$ ) between the PrL and M1 cortices. A detailed analysis of coherence between these six regions revealed peaks of

coherence in some frequencies, with values close to 0.6 during the generation of the  $\theta/\beta\text{-}\gamma$  transition pattern. When LFPs recorded in the PrL cortex were compared with those recorded in the M1 cortex, three peaks of medium-level coherence were found in low- $\gamma$  and high- $\gamma$  frequencies (42–65, 109–122, and 139–150 Hz;  $0.60 \leq C \leq 0.67$ ; Fig. 9C). Coherograms for LFPs recorded from PrL–mediodorsal thalamic nucleus and PrL–ventral tegmental area showed a generalized low coherence in most of the bands, apart from the low- $\gamma$  band (43–63 and 45–51 Hz respectively;  $0.60 \leq C \leq 0.67$ ; Fig. 9C,D), mostly during the Pre and the beginning of the Pattern periods. As illustrated in Figure 4D, the nucleus accumbens septi and the hippocampal CA1 area presented the lowest coherence in the  $\theta$ ,  $\beta$ , and low- $\gamma$  bands ( $0.06 \leq C \leq 0.37$ ), even though a narrow range of frequencies (between 146 and 150 Hz) reached coherence values from 0.60 to 0.62 for PrL and nucleus accumbens septi LFPs.

#### Discussion

Present results indicate that the use of definite LFP patterns generated in the PrL cortex can be safely used as an alternative for functional studies associated with EMIs and other neural processes related to neurofeedback procedures. As already described, and further confirmed here, the PrL cortex is involved in volitional and valuation processes (Vertes, 2004; Hoover and Vertes, 2007; Kable and Glimcher, 2009; Graybiel et al., 2011; Fuster, 2015),

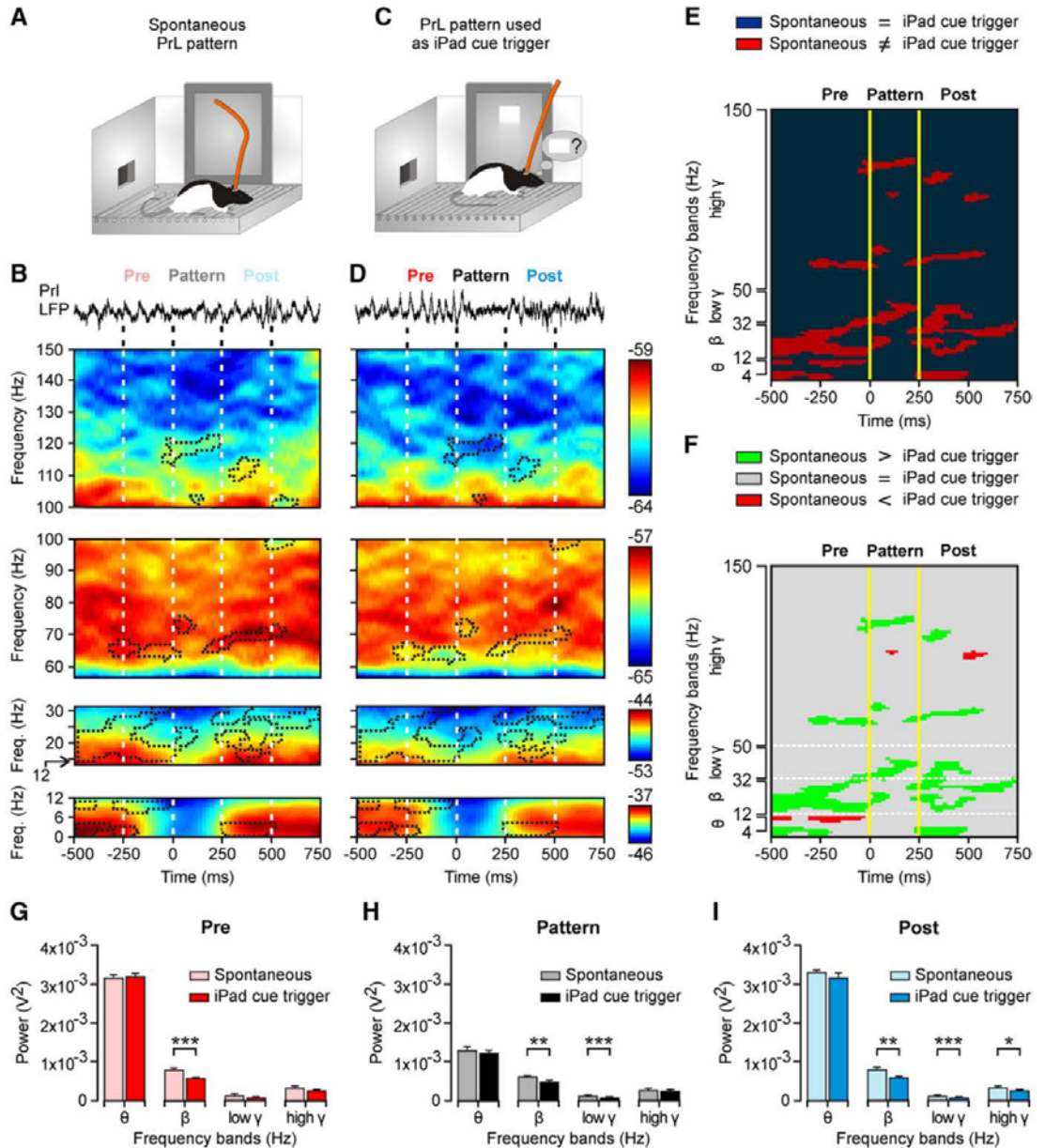


**Figure 8.** Differences in the spectral properties of the selected  $\theta/\beta$ - $\gamma$  transition pattern when generated spontaneously and when used to trigger touch-screen cues. **A**, As illustrated in Figure 5B–D, the spontaneous presentation of the  $\theta/\beta$ - $\gamma$  transition pattern during the automatic presentation of the visual (square virtual button) cue on the touch screen was recorded. **B**, At the top is illustrated a representative example of LFPs, including the presence of the  $\theta/\beta$ - $\gamma$  transition pattern evoked spontaneously. Below are illustrated time–frequency representations averaged from 150 traces ( $n = 5$  rats), including the selected pattern recorded from automatic cue sessions. **C**, **D**, The same as for **A** and **B**, but corresponding to LFPs recorded during pattern-evoked cue operant conditioning sessions (150 traces collected from 10 rats). Areas surrounded by dots correspond to observed differences between the two time–frequency displays. **E**, Significant differences ( $p \leq 0.05$ ) between the averaged time–frequency displays illustrated in **B** and **D**. **F**, Same as in **E**, but indicating when the spectral power was larger for  $\theta/\beta$ - $\gamma$  patterns evoked spontaneously (green areas) versus those cases in which the spectral power was larger for patterns used to trigger the visual cue (red areas). **G–I**, Spectral analysis for LFPs collected before (Pre, **G**), during (Pattern, **H**), and after (Post, **I**) for data illustrated in **B** and **D**. Significant differences are indicated. \* $p < 0.05$ ; \*\* $p < 0.01$ ; \*\*\* $p < 0.001$ , Student's *t* test.

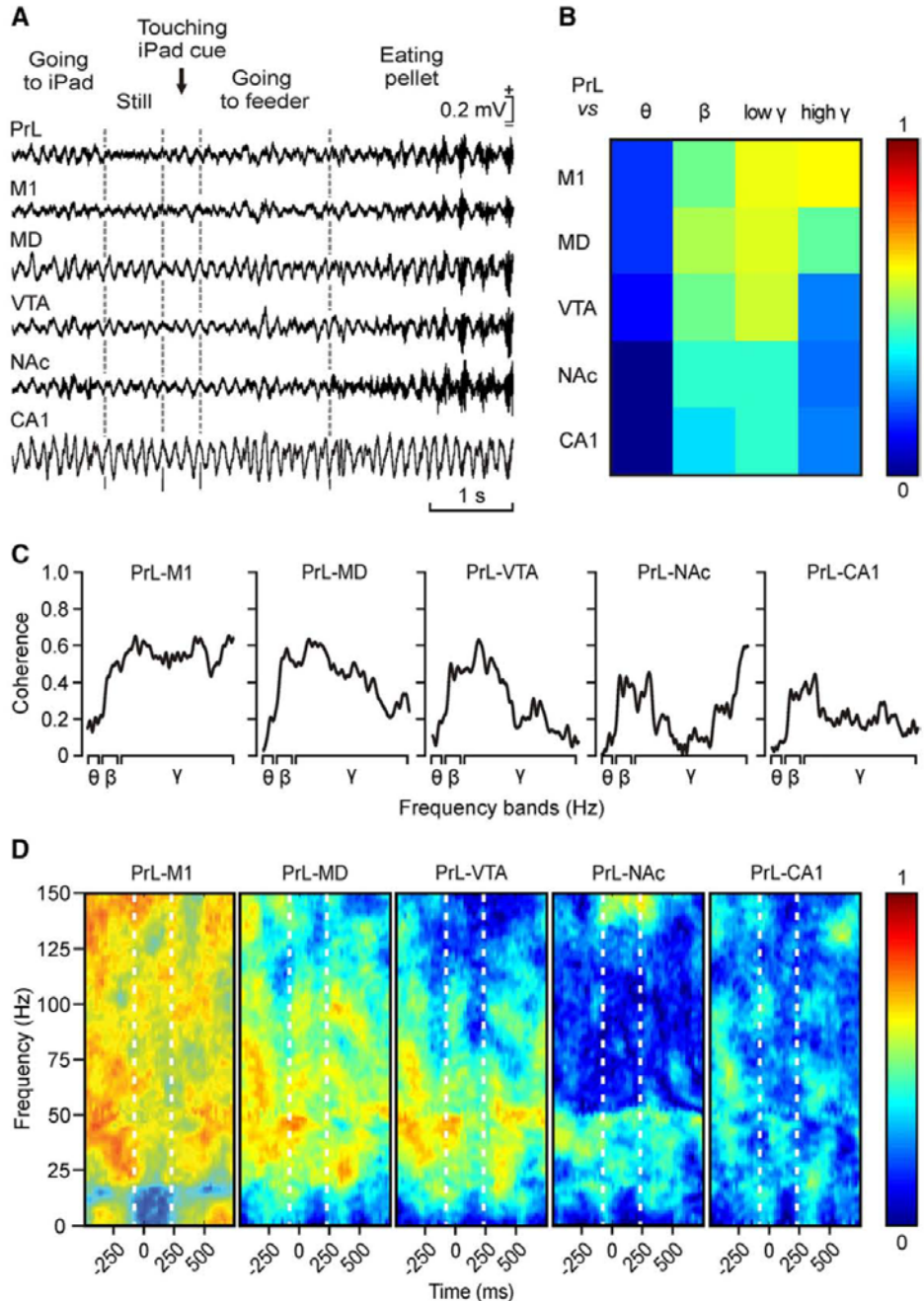


**Figure 9.** The selected  $\theta$ - $\beta$ - $\gamma$  transition pattern is restricted to the PrL cortex. **A**, LFPs recorded simultaneously in six different cortical and subcortical sites during a sequence of the touch-screen operant conditioning task. **B**, Analysis of coherence between the  $\theta$ - $\beta$ - $\gamma$  transition patterns recorded in the PrL cortex and the other five recording sites for the  $\theta$ ,  $\beta$ , low- $\gamma$ , and high- $\gamma$  bands. Note that the highest coherence (0.62, see color scale) was between the PrL and the M1 area of the motor cortex for the high- $\gamma$  band. **C**, Coherence profiles for the activity of  $\theta$ ,  $\beta$ , low- $\gamma$ , and high- $\gamma$  bands in the PrL cortex and the other five recording sites during the appearance of the  $\theta$ - $\beta$ - $\gamma$  transition pattern. **D**, Maps of time-frequency coherence between the Pre, Pattern, and Post periods for LFPs recorded in the PrL cortex and the other five recording sites. Illustrated maps correspond to the average of 100 samples collected from five different animals. Note the high coherence between recordings collected from PrL and M1 recording sites, mostly for the Pre and Post periods.



including classical and operant conditioning tasks (Leal-Campanario et al., 2007; Jurado-Parras et al., 2012). In particular, the effects of the electrical stimulation of the PrL cortex during the operant sequence used here suggest the involvement of this area in ongoing cognitive processes related to the association between touching the screen and getting the corresponding reward—a finding also reported in mice during a similar operant conditioning task (Jurado-Parras et al., 2012).

The behaviors (i.e., remaining motionless, rearing, and looking into the feeder; Fig. 4) during which the selected  $\theta/\beta\text{-}\gamma$  transition pattern was observed, as well as its intrinsic spectral characteristics (a significant decrease in power of the  $\theta$  band associated with smaller changes in the  $\beta$  and  $\gamma$  bands), could be related to the proposal that LFPs presenting low amplitudes and high- $\gamma$  frequencies are involved in attentive processes (Moruzzi and Magoun, 1949; Fries et al., 2001; Poulet and Petersen, 2008; Zagha et al., 2013) and with specific hypervigilance rhythms associated with immobility and focused attention (Bouyer et al., 1981; Wang, 2010; Koralek et al., 2012). Interestingly, an LFP pattern similar to the one described here has been reported to be present in neocortical SI and M1 areas during whisking conditions (Zagha et al., 2013). Nevertheless, apart from this similarity, the present  $\theta/\beta\text{-}\gamma$  transition pattern was more closely related to a significant decrease in the activity of whisker motor responses (Fig. 7). In fact, coherence in LFPs recorded simultaneously in PrL and M1 cortices decreases during the presentation of the  $\theta/\beta\text{-}\gamma$  transition pattern (Fig. 9). Thus, this pattern seems not to be related to specific  $\beta$  activities present in the M1 cortex during selected motor responses (Zagha et al., 2013; Khanna and Carmena, 2015).

The learning curve generated by the pattern-evoked cue presented a sigmoidal shape similar to (although with a slower evolution than) that generated by experimental animals during the automatic presentation of the cue on the touch screen (Fig. 6B) or during rewarded lever pressing in the Skinner box (Karni et al., 1998; Buitrago et al., 2004; Jurado-Parras et al., 2012). These results suggest that the use of an LFP pattern generated in the PrL cortex to activate an operant conditioning task does not represent an unviable burden for the experimental animal.

Pattern-evoked cue sessions generated some minor changes in the selected  $\theta/\beta\text{-}\gamma$  transition pattern, including a progressive increase in pattern duration, a decrease in the power ratio [ $(P_\beta + P_\gamma)/P_\theta$ ; Fig. 5C,D; resulting from faster recovery in the firing rate of PrL neurons], and a significant decrease in the spectral power of  $\beta$  and  $\gamma$  bands (Fig. 8F). In fact, these changes increased the probability of activating the touch screen, since a decrease in  $\theta + \beta + \gamma$  powers facilitated reaching the selected threshold (Fig. 4). Interestingly, these changes were not observed during the training period in which the cue was presented automatically, a fact suggesting that changes in the selected  $\theta/\beta\text{-}\gamma$  transition pattern were not due to the association between the cue (square virtual button) and the reward, but by the association between the  $\theta/\beta\text{-}\gamma$  transition pattern and the activation of the cue on the touch screen. These results coincide with available reports on neuronal operant conditioning in which the reward is obtained with changes in the discharge rate of conditioned neurons (Opris et al., 2011; Arduin et al., 2013). It should be noted that the reported changes in the selected  $\theta/\beta\text{-}\gamma$  transition pattern observed during pattern-evoked cue sessions did not modify the main spectral characteristic of the pattern—namely, a significant decrease in  $\theta$  and high- $\gamma$  bands.

Interestingly, the selected  $\theta/\beta\text{-}\gamma$  transition pattern appeared simultaneously with a significant decrease in the mean firing rate of PrL cells (Fig. 6) putatively considered as pyramidal neurons because of their firing properties (Dégénétais et al., 2002; Povysheva et al., 2006; Leal-Campanario et al., 2013). In this regard, it

has been recently proposed that the rostromedial prefrontal cortex plays an active role in preventing the release of newly acquired motor responses until advanced stages of the acquisition process and, in general, in the control of the ongoing behavior, depending on environmental and social constraints (Leal-Campanario et al., 2007, 2013). The inhibition of PrL cortex neurons during the  $\theta/\beta\text{-}\gamma$  transition pattern suggests that this pattern corresponds to a time window for the release of specific behaviors involving cognitive processes (Fig. 4). In addition, the electrical stimulation of the recording area evoked disturbing effects on the animal's performance during the operant task not related to any visible deficit in its motor activities (Hamani et al., 2010). Thus, these results indicate that the stimulation of the PrL cortex disturbed specific cognitive processes underlying the expected behavioral sequences (Jackson et al., 2001; Jurado-Parras et al., 2012).

It is important to point out the low coherence values between LFPs recorded in the PrL cortex, including the selected  $\theta/\beta\text{-}\gamma$  transition pattern, and LFPs recorded simultaneously in the nucleus accumbens, the motor cortex, the mediodorsal thalamic nucleus, and the hippocampal CA1 and ventral tegmental areas. Apparently, the selected  $\theta/\beta\text{-}\gamma$  transition pattern was not generated in and/or propagated to the five mentioned areas, but is an activity restricted to the PrL cortex. In fact, we obtained higher ( $0.60 < R > 0.69$ ) levels of coherence between LFPs recorded in the PrL cortex compared with those recorded in the motor cortex, the nucleus accumbens, and the mediodorsal thalamic nucleus in the high- $\gamma$  band during the generation of the pattern. In this regard, an increase has been reported in functional interactions in the high- $\gamma$  band between the PrL cortex and the mediodorsal thalamic nucleus during the acquisition of an instrumental conditioning task (Yu et al., 2012), as well as between the nucleus accumbens and the PrL cortex during a similar learning task (Chang et al., 2000). The observation of increased coherence values for narrow frequency bands between different cortical and subcortical areas suggests the involvement of different learning and memory processes taking place at the same time in these different neural structures using the selected  $\theta/\beta\text{-}\gamma$  transition pattern as a brain–iPad interface.

Finally, it can be questioned whether the  $\theta/\beta\text{-}\gamma$  transition pattern was just a byproduct of the preferred behavior (sitting still or motionless) used by the experimental rats to activate the iPad. In this regard, and as illustrated in Figure 4, the same LFP pattern was present during the performance of other behaviors (as rearing or looking into the feeder) and, at the same time, was not always present when the animal remained motionless in the cage—immobility per se is not enough to generate this LFP pattern (Gervasoni et al., 2004). Although in early conditioning sessions, animals generated the LFP pattern in different locations within the Skinner box, the animal selected this behavior (sitting still near the iPad) across training because of its adaptive value. In addition, given their rather poor visual acuity (Prusky et al., 2002) being near the iPad will facilitate an early detection of the visual cue. Thus, it can safely be expected that a paralyzed animal should still be able to generate this (and related) LFP patterns without the need to associate it to a given behavior, involving movements or, at the least, postural adjustments.

## References

- Arduin PJ, Frégnac Y, Shulz DE, Ego-Stengel V (2013) "Master" neurons induced by operant conditioning in rat motor cortex during a brain–machine interface task. *J Neurosci* 33:8308–8320. [CrossRef Medline](#)
- Bouton CE, Shaikhouni A, Annetta NV, Bockbrader MA, Friedenberg DA, Nielson DM, Shamma G, Sederberg PB, Glenn BC, Mysiw WJ, Morgan AG, Deogaonkar M, Rezaei AR (2016) Restoring cortical control of functional movement in a human with quadriplegia. *Nature* 533:247–250. [CrossRef Medline](#)

- Bouyer JJ, Montaron MF, Rougeul A (1981) Fast fronto-parietal rhythms during combined focused attentive behaviour and immobility in cat: cortical and thalamic localizations. *Electroencephalogr Clin Neurophysiol* 51:244–252. [CrossRef Medline](#)
- Buitrago MM, Ringer T, Schulz JB, Dichgans J, Luft AR (2004) Characterization of motor skill and instrumental learning time scales in a skilled reaching task in rat. *Behav Brain Res* 155:249–256. [CrossRef Medline](#)
- Chang JY, Janak PH, Woodward DJ (2000) Neuronal and behavioral correlations in the medial prefrontal cortex and nucleus accumbens during cocaine self-administration by rats. *Neuroscience* 99:433–443. [CrossRef Medline](#)
- Dege'rais E, Thierry AM, Glowinski J, Gioanni Y (2002) Electrophysiological properties of pyramidal neurons in the rat prefrontal cortex: an in vivo intracellular recording study. *Cereb Cortex* 12:1–16. [CrossRef Medline](#)
- Fetz EE (1969) Operant conditioning of cortical unit activity. *Science* 163:955–958. [CrossRef Medline](#)
- Fetz EE, Finocchio DV (1971) Operant conditioning of specific patterns of neural and muscular activity. *Science* 174:431–435. [CrossRef Medline](#)
- Fetz EE, Finocchio DV (1972) Operant conditioning of isolated activity in specific muscles and precentral cells. *Brain Res* 40:19–23. [CrossRef Medline](#)
- Flint RD, Wright ZA, Scheid MR, Slutzky MW (2013) Long term, stable brain machine interface performance using local field potentials and multi-unit spikes. *J Neural Eng* 10:056005. [CrossRef Medline](#)
- Freeman WJ, Holmes MD, Burke BC, Vanhatalo S (2003) Spatial spectra of scalp EEG and EMG from awake humans. *Clin Neurophysiol* 114:1053–68. [CrossRef Medline](#)
- Fries P, Reynolds JH, Rorie AE, Desimone R (2001) Modulation of oscillatory neuronal synchronization by selective visual attention. *Science* 291:1560–1563. [CrossRef Medline](#)
- Fuster JM (2015) *The prefrontal cortex*. London: Academic.
- Gervasoni D, Lin SC, Ribeiro S, Soares ES, Pantoja J, Nicolelis MA (2004) Global forebrain dynamics predict rat behavioral states and their transitions. *J Neurosci* 24:11137–11147. [CrossRef Medline](#)
- Graybiel C, Feyder M, Schulman E, Saksida LM, Bussey TJ, Brigman JL, Holmes A (2011) Paradoxical reversal learning enhancement by stress or prefrontal cortical damage: rescue with BDNF. *Nat Neurosci* 14:1507–1509. [CrossRef Medline](#)
- Gruart A, Muñoz MD, Delgado-García JM (2006) Involvement of the CA3–CA1 synapse in the acquisition of associative learning in behaving mice. *J Neurosci* 26:1077–1087. [CrossRef Medline](#)
- Hamani C, Diwan M, Isabella S, Lozano AM, Nobrega JN (2010) Effects of different stimulation parameters on the antidepressant-like response of medial prefrontal cortex deep brain stimulation in rats. *J Psychiatr Res* 44:683–687. [CrossRef Medline](#)
- Hasan MI, Hernández-González S, Dogbevia G, Treviño M, Bertocchi I, Gruart A, Delgado-García JM (2013) Role of motor cortex NMDA receptors in learning-dependent synaptic plasticity of behaving mice. *Nat Commun* 4:2258. [CrossRef Medline](#)
- Hirreath SV, Chen W, Wang W, Folders S, Yang Y, Tyler-Kabara EC, Collinger JL, Boninger ML (2015) Brain computer interface learning for systems based on electrocorticography and intracortical microelectrode arrays. *Front Integr Neurosci* 9:40. [CrossRef Medline](#)
- Hong KS, Naseer N, Kim YH (2015) Classification of prefrontal and motor cortex signals for three-class fNIRS–BCL. *Neurosci Lett* 587:87–92. [CrossRef Medline](#)
- Hoover WB, Vertes RP (2007) Anatomical analysis of afferent projections to the medial prefrontal cortex in the rat. *Brain Struct Funct* 212:149–179. [CrossRef Medline](#)
- Jackson ME, Frost AS, Moghaddam B (2001) Stimulation of prefrontal cortex at physiologically relevant frequencies inhibits dopamine release in the nucleus accumbens. *J Neurochem* 78:920–923. [CrossRef Medline](#)
- Jacobs GH, Fenwick JA, Williams GA (2001) Cone-based vision of rats for ultraviolet and visible lights. *J Exp Biol* 204:2439–2446. [CrossRef Medline](#)
- Jurado-Parras MT, Gruart A, Delgado-García JM (2012) Observational learning in mice can be prevented by medial prefrontal cortex stimulation and enhanced by nucleus accumbens stimulation. *Learn Mem* 19:99–106. [CrossRef Medline](#)
- Kable JW, Glimcher PW (2009) The neurobiology of decision: consensus and controversy. *Neuron* 63:733–745. [CrossRef Medline](#)
- Karni A, Meyer G, Rey-Hipolito C, Jezard P, Adams MM, Tumer R, Ungerleider LG (1998) The acquisition of skilled motor performance: fast and slow experience-driven changes in primary motor cortex. *Proc Natl Acad Sci U S A* 95:861–868. [CrossRef Medline](#)
- Khanna P, Carmenta JM (2015) Neural oscillations: beta band activity across motor networks. *Curr Opin Neurobiol* 32:60–67. [CrossRef Medline](#)
- Koralek AC, Jin X, Long JD 2nd, Costa RM, Carmenta JM (2012) Corticostriatal plasticity is necessary for learning intentional neuroprosthetic skills. *Nature* 483:331–335. [CrossRef Medline](#)
- Leal-Campanario R, Faire'n A, Delgado-García JM, Gruart A (2007) Electrical stimulation of the rostral medial prefrontal cortex in rabbits inhibits the expression of conditioned eyelid responses but not their acquisition. *Proc Natl Acad Sci U S A* 104:11459–11464. [CrossRef Medline](#)
- Leal-Campanario R, Delgado-García JM, Gruart A (2013) The rostral medial prefrontal cortex regulates the expression of conditioned eyelid responses in behaving rabbits. *J Neurosci* 33:4378–4386. [CrossRef Medline](#)
- Lebedev MA, Nicolelis MA (2006) Brain-machine interfaces: past, present and future. *Trends Neurosci* 29:536–546. [CrossRef Medline](#)
- Leising KJ, Wolf JE, Rupprecht CM (2013) Visual discrimination learning with an iPad-equipped apparatus. *Behav Processes* 93:140–147. [CrossRef Medline](#)
- Mehring C, Rickett J, Vaadia E, Cardoso de Oliveira S, Aertsen A, Rotter S (2003) Inference of hand movements from local field potentials in monkey motor cortex. *Nat Neurosci* 6:1253–1254. [CrossRef Medline](#)
- Moruzzi G, Magoun HW (1949) Brain stem reticular formation and activation of the EEG. *Electroencephalogr Clin Neurophysiol* 14:55–473. [CrossRef Medline](#)
- O'Doherty JE, Lebedev MA, Ifft PJ, Zhuang KZ, Shokur S, Bleuler H, Nicolelis MA (2011) Active tactile exploration using a brain-machine-brain-in-terface. *Nature* 479:228–231. [CrossRef Medline](#)
- Opris I, Lebedev M, Nelson RJ (2011) Motor planning under unpredictable reward: modulations of movement vigor and primate striatum activity. *Front Neurosci* 5:61. [CrossRef Medline](#)
- Paxinos G, Watson C (1998) *The rat brain in stereotaxic coordinates*. San Diego: Academic.
- Pesaran B, Pezaris JS, Sahani M, Mitra PP, Andersen RA (2002) Temporal structure in neuronal activity during working memory in macaque parietal cortex. *Nat Neurosci* 5:805–811. [CrossRef Medline](#)
- Poulet JF, Petersen CC (2008) Internal brain state regulates membrane potential synchrony in barrel cortex of behaving mice. *Nature* 454:881–885. [CrossRef Medline](#)
- Povysheva NV, Gonzalez-Burgos G, Zaitsev AV, Krüner S, Bamionuevo G, Lewis DA, Krimer LZ (2006) Properties of excitatory synaptic responses in fast-spiking interneurons and pyramidal cells from monkey and rat prefrontal cortex. *Cereb Cortex* 16:541–552. [CrossRef Medline](#)
- Prusky GT, Harker KT, Douglas RM, Whishaw IQ (2002) Variation in visual acuity within pigmented, and between pigmented and albino rat strains. *Behav Brain Res* 136:339–348. [CrossRef Medline](#)
- Rouse AG, Williams JJ, Wheeler JJ, Moran DW (2013) Cortical adaptation to a chronic micro-electrocorticographic brain computer interface. *J Neurosci* 33:1326–1330. [CrossRef Medline](#)
- Schafer RJ, Moore T (2011) Selective attention from voluntary control of neurons in prefrontal cortex. *Science* 332:1568–1571. [CrossRef Medline](#)
- Schuldlo LC, Power SD, Chau T (2013) Dynamic topographical pattern classification of multichannel prefrontal NIRS signals. *J Neural Eng* 10:046018. [CrossRef Medline](#)
- Shain W, Spataro L, Dilgen J, Haverstick K, Retterer S, Isaacson M, Saltzman M, Tumer JN (2003) Controlling cellular reactive responses around neural prosthetic devices using peripheral and local intervention strategies. *IEEE Trans Neural Syst Rehabil* 11:186–188. [CrossRef Medline](#)
- So K, Dangi S, Osborn AL, Gastpar MC, Carmenta JM (2014) Subject-specific modulation of local field potential spectral power during brain-machine interface control in primates. *J Neural Eng* 11:026002. [CrossRef Medline](#)
- Vertes RP (2004) Differential projections of the infralimbic and prelimbic cortex in the rat. *Synapse* 51:32–58. [CrossRef Medline](#)
- Wander JD, Blakely T, Miller KJ, Weaver KE, Johnson LA, Olson JD, Fetz EE, Rao RP, Ojemann JG (2013) Distributed cortical adaptation during learning of a brain-computer interface task. *Proc Natl Acad Sci U S A* 110:10818–10823. [CrossRef Medline](#)
- Wang XJ (2010) Neurophysiological and computational principles of cortical rhythms in cognition. *Physiol Rev* 90:1195–1268. [CrossRef Medline](#)
- Yu C, Fan D, Lopez A, Yin HH (2012) Dynamic changes in single unit activity and  $\gamma$  oscillations in a thalamocortical circuit during rapid instrumental learning. *PLoS One* 7:e50578. [CrossRef Medline](#)
- Zagha E, Casale AE, Sachdev RN, McGinley MJ, McCormick DA (2013) Motor cortex feedback influences sensory processing by modulating network state. *Neuron* 79:567–578. [CrossRef Medline](#)